AN ABSTRACT OF THE DISSERTATION OF

Michael D. Boller for the degree of Doctor of Philosophy in Electrical and Computer Engineering presented on May 31, 2023.

Title: Power System Reliability and Power Quality Assessments with Grid-Connected Wave Energy Converters

Abstract approved: _____

Ted K.A. Brekken Eduardo Cotilla-Sanchez

Generating abundant, renewable energy from Earth's oceans is an attractive option for meeting increasing energy demand. Marine renewable energy also comes with the variability of renewable sources, which impact the reliability and power quality of the electrical grid. On a transmission-level, this dissertation looks at ensuring reliability of the power system with both reactive reserves and minimizing loop flows. Clustering of the power flow analysis with Voltage Control Areas (VCAs) simplifies analysis of reactive reserves and serves as the basis for quantifying the effects a wave energy converter (WEC) has on transmission system loop flows. Proper WEC placement can minimize loop flow effects. On a device-level, WEC can cause issues with the power quality at the point of connection to the grid. The author uses a hybrid-simulated WEC to measure electrical power quality phenomena in a laboratory setting with a numerically modeled WEC. This setup

ensures realistic power-quality results while reducing the expense necessary to test a grid-connected WEC.

Power System Reliability and Power Quality Assessments with Grid-Connected Wave Energy Converters

by

Michael D. Boller

A DISSERTATION

submitted to

Oregon State University

in partial fulfillment of
the requirements for the
degree of

Doctor of Philosophy

Presented May 31, 2023
Commencement June 2023

Doctor of Philosophy dissertation of Michael D. Boller presented on May 31, 2023.

APPROVED:

Co-Major Professor, representing Electrical and Computer Engineering

---

Co-Major Professor, representing Electrical and Computer Engineering

---

Head of the School of Electrical Engineering and Computer Science

---

Dean of the Graduate School

I understand that my dissertation will become part of the permanent collection of Oregon State University libraries. My signature below authorizes release of my dissertation to any reader upon request.

Michael D. Boller, Author

ACKNOWLEDGEMENTS

To start with I would like to thank both of my major professors, Dr. Ted Brekken and Dr. Eduardo Cotilla-Sanchez for the countless hours they have spent helping me re-frame tough problems and guiding me through my research. In addition, you have both have been excellent teachers and helped me grow in explaining concepts.

To the rest of my PhD committee, Dr. Bryony DuPont, Dr. Yue Cao and Dr. Nathan Gibson, thank you for providing me with advice on my research and being flexible with my research journey.

I would also like to say thank you to my my colleagues in the Energy Systems lab who I have thought through problems with, worked together on projects and setting up laboratory experiments, and enjoyed getting to know better over the years.

To my family: Thank you for supporting me through graduate school. Your encouragement has been essential in getting me through the ups and downs of research. To Nathan: Thank you for the constant support in this portion of my graduate work.

TABLE OF CONTENTS

TABLE OF CONTENTS (Continued)

LIST OF FIGURES

LIST OF FIGURES (Continued)

LIST OF FIGURES (Continued)

LIST OF FIGURES (Continued)

LIST OF TABLES

Chapter 1: Introduction

Voltage stability and security allow power systems to provide reliable power and avoid costly blackouts. The stability of a power system is linked to adequate reactive power within the grid. To provide sufficient reactive power so that the grid withstands contingencies, utility operators must access the adequacy of reserves within their operating regions and compensate with specialized devices such as synchronous condensers, shunt capacitors, and FACTS [1]. The meshed nature of wide-area power systems makes this assessment difficult, leading to many different solutions. Previous solutions include both on-line and static identification methods [2]–[5]. These tools use methods such as QV curves to determine adequacy of reserves. The complexity of the voltage control problem makes reducing the scale of the problem a necessity, which can be done using clustering techniques to group the network into zones [6]. Voltage Control Areas (VCAs) which use an electrical distance metric for clustering have limited power transfers between zones indicating that VCAs serve as an ideal way to break down complicated power system problems. This research proposes combining VCAs with reactive reserve adequacy calculations to reduce the computational complexity of finding the reactive reserve adequacy of a system.

Still, reactive reserve metrics are not the only problem facing modern grid researchers. As energy demand continues to increase, developers have looked to

new renewable energy sources to provide the missing energy from clean, renewable sources. The Earth's oceans have an immense amount of power that can be harnessed by ocean wave energy converters (WECs) to replace existing fossil fuel generation [7]. WEC developers have connected several prototypes to the electrical grid; despite this, there is limited research considering the variable effects of WEC generation on the electrical grid, with grid studies focusing primarily on voltage deviations and branch overloads [8]–[11]. The variability present in waves can be both a hindrance and a benefit to the electrical grid. WEC installations can mitigate impacts on the grid through WEC placement and could potentially benefit the grid by offsetting other variable renewable resources such as wind and solar [12]. Studies such as [13], have commented on the need for future work to combine the temporal analysis of WECs with power flow analysis to model more grid-specific effects of WEC integration.

While expected on a large meshed network such as the electrical grid, loop flows cause additional reliability problems. Loop flows occur when the shortest electrical path for power to flow from generation to demand nodes passes through a zone outside its contracted path. If the loop flow travels in the same direction as regular flows, it increases system losses and fault conditions while also lowering system reliability [14]. The long transmission lines and variable scheduling characteristics of renewable generation such as wind and hydro has increased loop flows in both Western United States and Central Europe grids [15]–[17]. With similar characteristics, WEC placement will affect the loop flows in an interconnected grid.

Similar to the reactive reserve calculation, VCAs can help researchers quantify

the effects of system changes on loop flows as flows between zones are minimized. To perform an analysis of the effects of WECs on power system loop flows, researchers need quality power flow cases that exhibit accurate characteristics of the interconnection. Synthetic cases, such as ACTIVSg2000, provide necessary detail and geographic specificity while remaining open access due to the fictitious nature of its grid topology [18]. The author combines WEC temporal information with a quasi-steady-state scenario analysis of loop flows in VCAs on the synthetic ACTIVSg2000 case to evaluate the effects of WEC placement on loop flows.

In addition to transmission-scale power-flow effects, the grid integration of WECs also requires mitigation of power-quality issues at the point of connection [19]. In order to solve these issues, WEC developers must implement both prototypes and simulations to experiment with new solutions. Still, despite decades of research, WEC technology is still developing, hampered by the harsh ocean constraints. The simulations and scaled physical prototypes of WECs present limitations to apply their results to grid-connection studies. Similar scaling and simulation issues in the field of seismic civil engineering led to the development of real-time hybrid simulation where testing includes both a computer-based numerical model and a connected physical system [20]. Previous testing at Oregon State University's Wallace Energy Systems and Renewables Facility (WESRF) has implemented a hybrid-simulation testbed for WECs [21]. The author extends this research to evaluate the power quality of the hybrid-simulated WEC. Hybrid-simulated WECs look to bridge the gap between computer simulations and physical prototype deployment, allowing WEC developers to better understand the power

quality effects of their devices without requiring the expense of a physical WEC prototype or the electrical modelling assumptions.

This dissertation starts with an introduction to VCAs and their use in analyzing zonal reactive reserves in Chapter 2. The author then extends the use of VCAs with an additional application in loop flow analysis. Chapter 3 investigates how the placement of WECs affect transmission-level loop flows. Still, loop flows are not the only way WEC integration affects the electrical grid and Chapter 4 assesses the power quality effects of WEC integration through the use of WESRF's hybrid-simulation testbed.

Chapter 2: Zonal Reactive Reserve Adequacy

2.1 Introduction

Power systems need adequate voltage stability and security to provide reliable power and avoid blackouts. A key component to maintaining this component of stability and security is adequate reactive power within the system. Long transmission lines and large active power transfers can impede a system's ability to transmit reactive power. To compensate for these characteristics, power system planners must design power systems with additional specialized devices such as synchronous condensers, shunt capacitors, and FACTS [1].

In the context of a utility-scale transmission system, determining if a system has sufficient reactive reserves to withstand contingencies is a complicated task due to the size and meshed nature of wide-area power systems. Thus, it is necessary to reduce the scale of the problem. One method to reduce the complexity is to divide the network analysis into zones using clustering techniques. Happ is among the pioneers of "tearing" large systems into sub-groups to aid in solving complex problems. He notes several applications of clustering to power systems including system stability and automatic generator control [6]. In this chapter, the author creates zones to give system operators a better understanding of the voltage stability of their system.

Previous work to identify the voltage stability of a system and potential critical components prone to voltage instability has included online methods with indicator factors for voltage instability [2], as well as static identification using load margin, QV curves, and system loss reduction [3], system loadability [4], and monitoring using a modified counter propagation neural network using clustering to reduce time [5].

This chapter builds on previous stability and security metrics by combining that analysis with Voltage Control Areas (VCAs). The VCA framework leverages cluster analysis techniques to find zones based on an electrical distance similarity metric so that clustering optimizes either active, or reactive power transfers, or both [22]. Previous voltage stability and security methods are often computationally complex and time-intensive. By combining VCAs with reactive reserve adequacy calculations we can reduce the computational complexity of finding the reactive reserve adequacy of a system.

This chapter contributes a zonal reactive reserve adequacy method and presents results from both small utility and large representative systems. The remainder of this chapter is organized as follows: Section 2.2 and Section 2.3 provides background on VCA clustering. Section 2.4 describes the combination of the metrics and the power-flow cases the author uses in these tests and Section 2.5 presents the stability and security analysis on both synthetic and real utility systems along with comparisons to existing methods.

2.2 Importance of Reactive Reserves

At any point in the day, the balance between load and generation must be met to avoid system failures and blackouts. Many different types of disturbances, including power line faults, renewable resource generation variability, and human error can threaten a the ability of a power system to provide reliable power. One way power system operators provide reliable power is by maintaining voltage stability and security. Over half of studied blackouts between 1965 to 2005 listed voltage instability as a major factor [1] including the 2003 US and Canada Northeast blackout [23], highlighting the importance of voltage stability. For the context of this dissertation, a stable system means that its power flow equations converge with assumptions of nominal frequency and balanced three-phase operation. A system that is voltage secure operates stably and also has an acceptable reserve margin which allows it to survive the next contingency [24]. In this case, the author does not account for dynamic transients in the power system.

Heavy system loading combined with reactive power shortages due to device failure or intermittent renewable resources often causes voltage instability in a system [25]. Additionally, the reactive power necessary to restore voltage stability may be constrained by line or generator limits [26]. Large power angles due to transmission line length or large active power transfers make a system unable to transmit reactive power, even with large voltage magnitude gradients [24]. Power system planners must design power systems with additional specialized devices such as synchronous condensers, shunt capacitors, FACTS, or other supporting

equipment to offset difficulties in transmitting reactive power [1].

2.2.1 The V-Q Curve

A V-Q curve, an example shown in Fig. 2.1, is one approach to analyze and ensure voltage stability. The fourth quadrant of the power-flow Jacobian relates reactive power and voltage as dQ/dV. When determining the reactive power of a system, this factor becomes the primary component. A plot of both reactive power and voltage conveys the relationship between these two quantities. To generate a V-Q curve, the operator places a fictional synchronous condenser at the bus under test and runs power flows for a range of voltage setpoints at the test bus. For each voltage setpoint, the V-Q analysis plots the reactive power injections [27], [28]. At the nose of the V-Q load curve, the system reaches its maximum reactive load while retaining voltage stability after a large disturbance [24].

The V-Q curve is particularly useful for analyzing potential voltage collapse points since it converges even on the unstable portions of the grid. The V-Q curve also directly provides the reactive power margin or VQ margin which researchers often use as a reliability index [29]. The WECC defines the VQ margin as the negative of the synchronous condenser output value at the minimum point of the V-Q curve which is also the difference between the operating reactive power and the critical point at the bottom of the V-Q curve [28]. A high VQ margin indicates a more secure bus [30]. Along with its advantages, the V-Q curve method also has a few drawbacks including its high computation requirements [31] and its limited

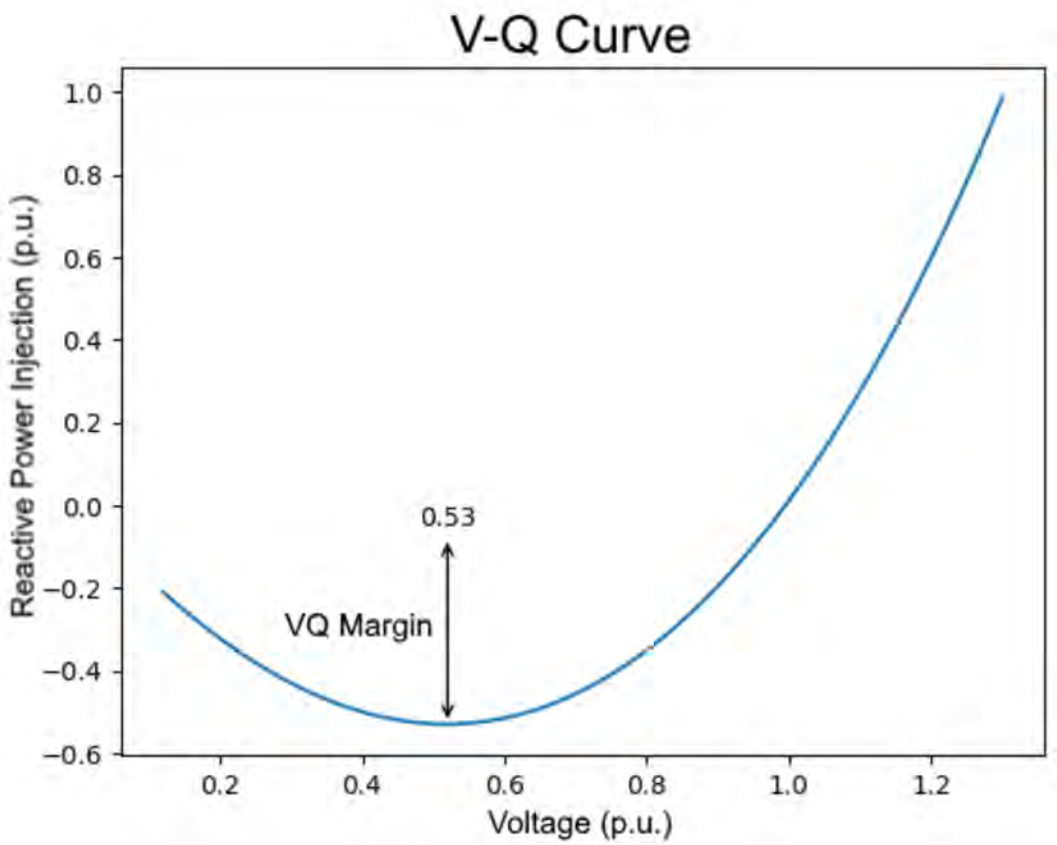

Figure 2.1: An example V-Q curve with the VQ margin labeled at the nose of the curve.

range of application to power systems covering a large area [29]. Pourbeik [32] demonstrates the usefulness of combining the V-Q curve with an optimal power flow to determine necessary reserves.

2.2.2 Voltage Sensitivity Factor

Also included in these stability metrics is the Voltage Sensitivity Factor (VSF). The sensitivity factor comes from the fourth quadrant of the power flow Jacobian, that is inverted to get the dV/dQ relationship. A higher value of dV/dQ corresponds to a weaker bus [30]. While the sensitivity may be found for any bus, VSF has a specific meaning for buses with generators. As the generator reaches the bottom of its V-Q curve, VSF increases and eventually changes sign, signaling unstable voltage conditions [26]. Additionally, a generator with a high sensitivity value can provide up to its maximum limit of reactive power [33]. Due to these factors, VSF is both an indication of voltage control and a measure of electrical distance. For this research, we use VSF for both its distance metric and as an indication of buses susceptible to voltage instability.

2.3 VCA Clustering

The results in this chapter use Voltage Control Areas (VCAs) created with the Electric Power Research Institute's (EPRI's) VCA Studio. VCAs are an application of clustering or partitioning. Partitioning of power system analysis looks to aid in power system understanding by breaking down complex problems into smaller areas for analysis. Previous research on clustering power systems includes identifying unstable regions [31],[34], finding critical contingencies [35], using reserves to aid in stability [36], and balancing generation for infrastructure resiliency [37].

There are several existing algorithms to create groups, including K-means, hier-

archical and spectral clustering. For this chapter, the author used spectral clustering to create zones in the power system analysis. Compared to K-means clustering, spectral clustering trades an increase in computational complexity for higher repeatability and often better results. Before splitting the data into clusters, spectral clustering first reduces the dimensions of the distance matrix of the system. Spectral clustering also makes no assumption of the final shape of clusters allowing it to find more complex groups than K-means [38]. Past research has applied spectral clustering to power systems [39], including applications to developing islanding schemes [40] and analyzing synchrophasor data [41].

All clustering algorithms perform clustering using a measure of distance between each node with a group of nodes that have similar distance from each other forming a zone. To apply clustering to the electrical grid, researchers need a measure of distance that accurately represents distance for electrical networks. VCA clustering uses electrical sensitivity, introduced in Section 2.2.2 to represent the electrical distance between nodes on the power system and accurately cluster the system such that it represents electrical rather than topological characteristics.

VCA Studio Consensus Clustering Tool developed by the Electric Power Research Institute (EPRI) integrates the stability and distance metrics with EPRI's clustering methods. This tool, which incorporates feedback from EPRI's member utilities, creates VCA partitions from a given power system case by using spectral clustering methods integrated with electrical distance from the power-flow Jacobian [42]. The author worked with EPRI to validate the concurrent development of VCA studio. This validation included the implementation various types of clus-

tering algorithms such as K-means and spectral clustering [43], computing critical contingencies for each zone, and implementing reactive reserve adequacy measurement per zone [42], [44]. When analyzing multiple cases that depict changes over time for a system, the author uses consensus clustering to produce a single VCA solution for all cases to allow for comparisons between the different cases for the system. VCA Studio uses a single clustering solution which has high similarity with the other solutions as the consensus VCA solution [42].

2.4 Methods

The proposed VCA reserve assessment integrates consensus VCA clustering with security metrics to help analyze the reserves within each zone. The VCA reserve assessment includes identifying critical contingencies and buses for each zone as well as determining the VQ margin for the critical bus. To illustrate the benefits of the VCA reserve assessment, we designed and ran experiments that compare entire-area and VCA reserve assessments and experiments that ascertain the security of the VCA zones. This study used a Texas synthetic case (ACTIVSg2000), a Polish Test System winter snapshot (2383wp), and a small real utility planning case.

2.4.1 Integrating Clustering with VQM

To show the usefulness of leveraging clustering techniques in power system analysis, the researchers integrated the VCA studio partitioning with the VQ margin

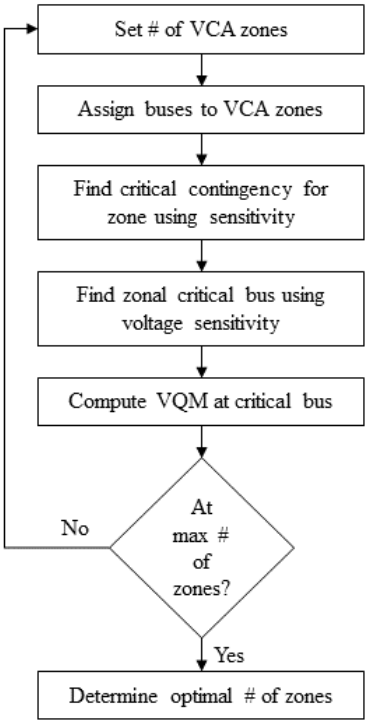

Figure 2.2: A flowchart of the integrated VQM and VCA zonal method. This methods computes critical contingencies, critical buses and VQM values for each zone. These results aid the user in determining the optimal number of zones.

(VQM) voltage stability metric. Although VQM is a very useful metric for determining the voltage stability of a single bus, it's computational intensity and poor generalization can keep it from being employed on a power system with a large number of buses. To solve these issues with VQM, this research finds a single representative bus for smaller areas within the power system, reducing the number of VQM calculations required while ensuring that the VQM metric still applies with enough specificity to provide useful results. Figure 2.2 illustrates the flowchart of the reserve methodology.

Since the VCA Studio's spectral clustering uses the Jacobian sensitivity between buses as a measure of electrical distance, the buses within the created clusters are close electrically. This allows the VQM of a single bus to be more representative of the voltage stability of the entire cluster. We now must choose a single representative bus for each zone. In finding VQM, we want to describe the voltage stability of the zone and a zone is only as secure as its weakest bus. Since a high value of VSF corresponds with a bus which has low voltage stability and can be found directly from the power-flow Jacobian, we use VSF to determine the critical bus at which to calculate VQM for a zone:

$$\mathrm{VSF}_i = \max\left(\left[\frac{\mathrm{d}Q_i}{\mathrm{d}V_i}\right]^{-1}\right) \tag{2.1}$$

where:

- VSF_i is the VSF at bus i,
- $\frac{\mathrm{d}Q_i}{\mathrm{d}V_i}$ is the fourth quadrant of the power-flow Jacobian.

While combining VSF with clustering methods allows us to quickly identify the VQM of a zone, the clustering of a power system requires several additional parameters to create the best analysis. The spectral clustering employed by the VCA Studio is unable to determine the best number of zones and relies on operator input to determine the optimal number of clusters for a power system. For this paper, we use a set of three criteria. When running clustering with varied numbers of partitions, one indicator of the optimal number of partitions is the point at

which adding an additional zone does not yield a cluster with a lower VQM value. Additionally, an optimal cluster must have relatively significant number of buses, additional zones which contain less than .01% of the buses in the system are often too small to be useful. Finally, if two solutions still meet both of these criteria, we choose the solution with generators present in each zone.

To provide an additional measure of security, this analysis also includes a critical contingency analysis. Prior to computing the reserves, the tool finds the critical contingency for each VCA zone. The critical contingencies come from a list of possible critical contingencies. EPRI's VCA Studio chooses the contingency that produces the largest absolute voltage sensitivity (dV/dQ) on any of the buses of a zone as the critical contingency [45]. For this paper, system contingencies consisted of a single generator or line outage. The location of the critical contingency does not have to be within the specific VCA zone under test.

2.4.2 Systems Under Test

We applied the VCA clustering methodology to three different types of systems, to show the ability of the VCA methodology to scale and produce interesting results for different types of cases. The three types of systems include two large benchmark cases and a utility planning case. Each type of system has its own benefits and challenges along with different properties and features. Specifically, this paper uses the 2000-bus synthetic case over Texas (ACTIVSg2000), the 2383-bus Polish Winter Peak Case (2383wp), and an anonymized planning case from a small utility.

2.4.2.1 ACTIVSg2000

The ACTIVSg2000 case is a synthetic 2000-bus power system based on statistical data from the Texas power grid. For security purposes, the case does not use any real-world data, but instead results from a methodology which places substations, loads, and generation based on both public data and realistic constraints. The resultant case power flow mirrors the Texas power grid without using Texas power flow case information [18]. We use this case to demonstrate the VCA methodology since its synthetic nature allows the case to be reproducible.

2.4.2.2 2383wp

By including the Polish Winter Peak Benchmark System, we allow for reproducible results to be scaled to a full-size utility system. The 2383wp case includes 2383 buses, 2896 branches, and 327 generators. In order to represent just the Polish 400, 220, and 110 kV networks within the larger, European UCTE system, Roman Korab replaced the tie lines to external networks with artificial load or generator buses. The number of components was further reduced by aggregating multiple generators at a single bus [46].

2.4.2.3 Small Utility Planning Case

The small utility planning case is an anonymized real-world planning case of a small utility which allows us to test with real-world data. This case contains 443

buses and 51 generators.

2.5 Results

We use the synthetic ACTIVSg2000 case to illustrate the process of finding reserve margin with VCA zones. After showing the process of finding zone-based VQM, we present these results along with results from small and large utility planning cases, comparing the computation time with a bus-by-bus validation.

2.5.1 Walkthrough

In this subsection we present the intermediate results using the methodology illustrated in Fig. 2.2. The ACTIVSg2000 or Texas2000 case serves as our test case for these steps. We start by creating electrically-close clusters and find critical contingencies for these clusters. We then find the critical buses by voltage sensitivity and compute a V-Q curve and VQ Margin at each critical bus.

Based on VCA results from similar sized cases, we started with a range of four to seven zones. Table 2.1 shows the range of clustering results by clustering the power flow buses into four to seven different zones. After splitting the case into more than four zones, most buses are part of three large zones, with the remaining zones containing very few buses.

As part of finding the zones, we also find critical contingencies for each zone. In this case we considered lines greater than 220 kV and generators greater than

Table 2.1: Quantity of Buses In Each Zone of ACTIVSg2000

VCA Zone	**4-Zone Buses**	**5-Zone Buses**	**6-Zone Buses**	**7-Zone Buses**
1	1794	38	892	878
2	40	13	13	877
3	14	903	883	159
4	152	887	17	13
5		159	159	28
6			36	28
7				17

50 MW as potential contingencies. Table 2.2 shows the seven critical contingencies picked. In runs with less than seven zones, the clustering used only a subset of these contingencies.

Table 2.2: Critical Contingencies for ACTIVSg2000

Contingency Name	**Contingency Type**	**Contingency Bus(es)**
'851'	Branch	7058, 7095
'364'	Gen	3074
'129'	Branch	8044, 8043
'3144'	Branch	1033, 3050
'305'	Gen	4177
'416'	Gen	1070
'406'	Gen	1088

With buses clustered into zones and critical contingencies applied, we then look for critical buses where we will compute reserve margin. Table 2.3 shows the critical bus numbers for each zone and each clustering solution.

Finally, we compute the VQM at each critical bus. We select our optimal

Table 2.3: Critical Buses In Each Zone of ACTIVSg2000

VCA Zone #	**4-Zone Crit. Bus #**	**5-Zone Crit. Bus #**	**6-Zone Crit. Bus #**	**7-Zone Crit. Bus #**
1	5062	1015	5460	5062
2	1015	3010	3010	5460
3	3010	5460	5062	4179
4	4179	5062	3132	3010
5		4179	4179	1068
6			1015	1015
7				3132

clustering solution by finding the last solution to find a critical bus with lower VQM than the largest VQM in the original 4-cluster set. Given the VQM values from the four different clustering solutions shown in Table 2.4, we chose the six-zone solution as our optimal clustering solution. The six-zone solution still finds all zones with VQM less than or equal to 79.28 MVAR, while the seven-zone solution finds a zone with VQM as high as 103.79 MVAR which is larger than the 79.28 MVAR largest VQM from the original 4-zone solution.

Table 2.4: VQ Margin At Critical Buses of ACTIVSg2000 (MVAR)

VCA Zone #	**4-Zone VQM**	**5-Zone VQM**	**6-Zone VQM**	**7-Zone VQM**
1	51.86	49.17	56.86	51.86
2	49.17	69.27	69.27	56.86
3	69.27	56.86	51.86	79.28
4	79.28	51.86	78.27	69.72
5		79.28	79.28	103.79
6			49.17	49.17
7				78.27

With the number of zones selected, we can visualize the clustered solution for ACTIVSg2000 on the map of Texas using the coordinates included in the power flow case. Figure 2.3 shows the geographic location of the Texas 2000 system, using color to differentiate the different zones. The starred buses represent the critical bus for each zone.

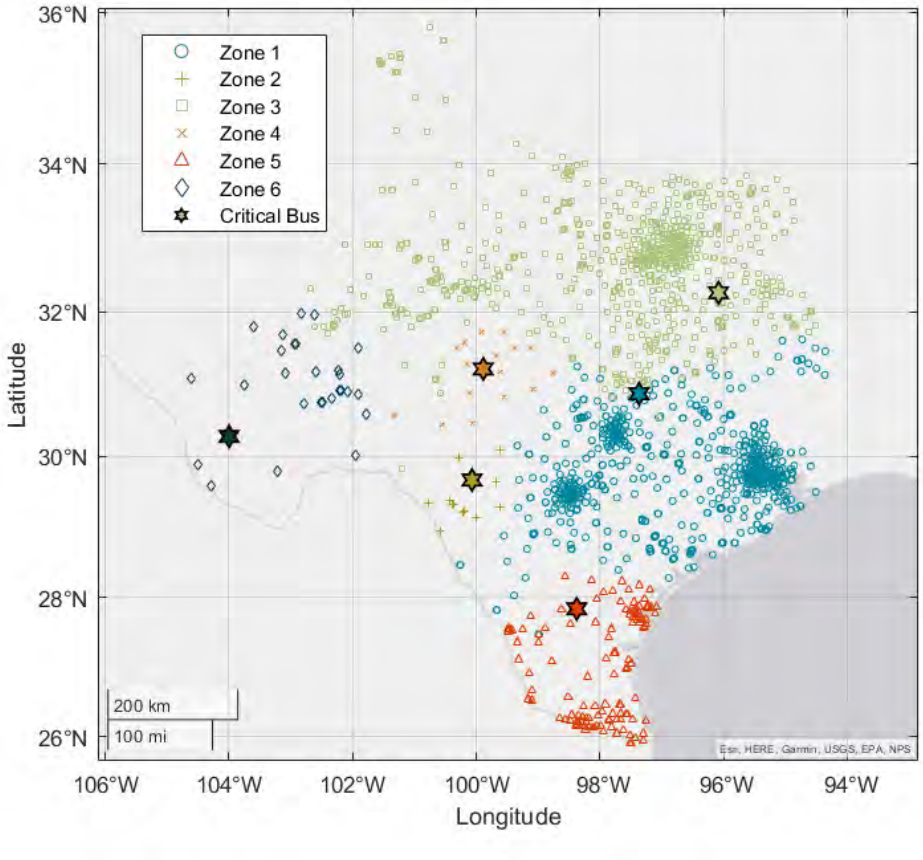

Figure 2.3: The buses of the ACTIVSg2000 system plotted geographically. The color and shape of the marker designates zone the bus belongs to. Starred buses indicate the critical bus for each zone.

The next subsection will compare the VQM analysis with a bus-by-bus method. As part of the comparison, we use a small utility system. This system has been anonymized and plotted on fictitious coordinates. Figure 2.4 shows the zones of the small utility. Clustering assigns many of the buses to a central zone representing the area with highest population density while the remaining buses are in peripheral zones.

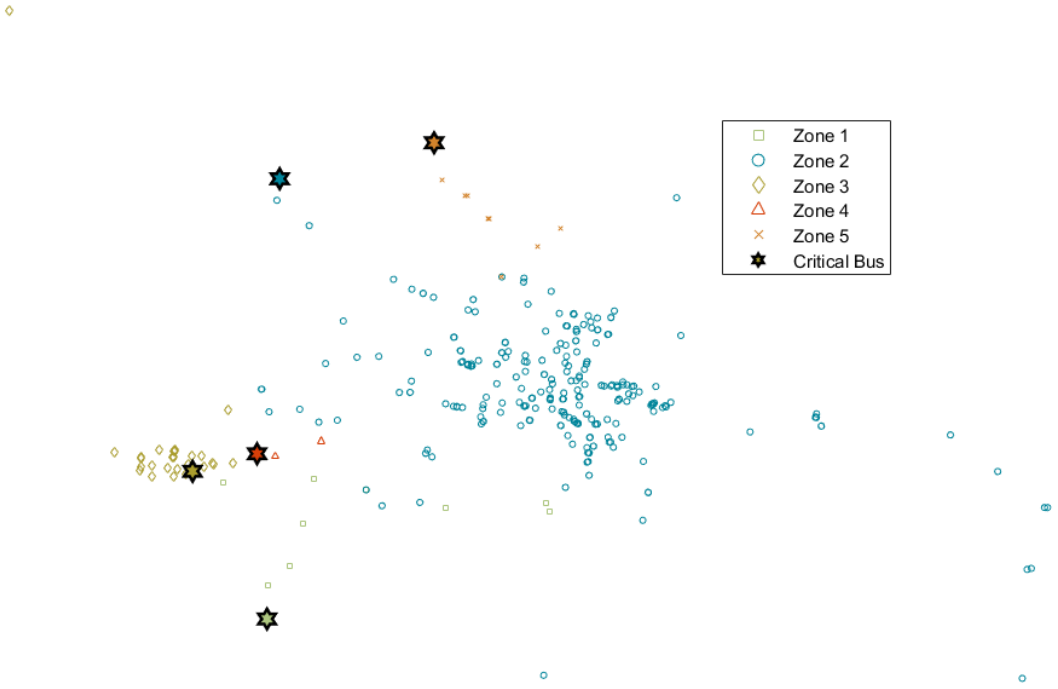

Figure 2.4: The buses of the small utility system plotted geographically. The color and shape of the marker designates zone the bus belongs to. Starred buses indicate the critical bus for each zone.

2.5.2 VQM Adequacy

By integrating the VCA clusters with VQM reserve analysis, we are able to quickly determine critical buses which represent the VQM levels in different sections of the power-flow case. To be useful for power-system analysis, the critical buses must be representative of their respective areas. We tested this by comparing the critical bus VQM results for each zone with the VQM results for each bus in the zone. For this methodology to be successful, the critical bus for each zone must have the lowest VQM or be close to the lowest VQM in the zone.

We compared VQM values for the small utility, and a larger reference utility. Table 2.5 includes a summary of the results from these two cases. For each case we note the total number of buses, the optimal number of zones, the average number of buses in each zone, and the normalized percent error. We found normalized percent error as follows,

$$\text{Norm\%Error} = \frac{1}{n} * \sum_{i=1}^{n} \left(\frac{|c_i - z_i|}{z_i} * 100 \right) \tag{2.2}$$

where:

- n is the number of VCA zones,
- c_i is the VQM of the critical bus in VCA i,
- z_i is the VQM of bus with the lowest VQM in VCA i.

As illustrated in final columns of Table 2.5, in both cases the overall normalized error is within one percent. Thus, the VCA methodology consistently finds buses

Table 2.5: VQM Adequacy Result Normalized Percent Error for a Small Utility, ACTIVSg2000, and 2383wp

Case	**Total # of Buses**	**Optimal # of Zones**	**Average # of Buses per Zone**	**Normalized % Error VQM (%)**
Small Utility	443	5	89	0.90
ACTIVSg2000	2000	6	333	0.00
2383wp	2383	5	476	0.26

with VQM adequacy close to the buses with the lowest VQM in each zone.

Table 2.6: Computation Time to find VQM Values using VCA and Bus-by-Bus Methods

Case	**Total # of Buses**	**VCA Time (min)**	**Bus-by-Bus Time (min)**
Small Utility	443	3	22
ACTIVSg2000	2000	34	2959
2383wp	2383	23	6310

The VCA and bus-by-bus methodologies can be compared in terms of time as well. Table 2.6 shows the computation time for finding VQM values using the VCA methodology compared to those found by determining the VQM value at every bus. These time values are for computations performed on a computer with an Intel Core i7-4700HQ 2.4 GHz processor, 8.00 GB of installed memory, and a 64-bit Windows 10 operating system.

Using the VCA methodology to reduce the number of VQM computations significantly reduces computation time with very similar results. Computation

time for the VCA methodology depends on both the number of buses and the number of potential contingencies. The ACTIVSg2000 case spent an additional 11 minutes compared to 2383 despite less buses due to higher number of potential critical contingencies. Computation time for the bus-by-bus method is significantly longer with the 2383wp case which is based on a historic Polish power-flow case compared to the synthetic Texas case.

2.6 Conclusion

Reactive reserves play a crucial role in ensuring that the electrical grid operates reliably. Combining reactive reserve analysis with VCAs allows researchers to quickly and accurately identify the critical buses with low VQ-margins. Since finding an optimal VCA clustering result depends on the chosen number of zones, this chapter outlines the process used to determine an optimal number of zones for VQ-margin analysis. When implemented, VCA clusters significantly reduce processing time required to compute VQ-margin at critical buses, especially for larger cases with 2000 or more buses. Additionally, the VCA methodology also adds reliablity through critical contingency analysis. With the techniques outlined in this paper, a power system operator can evaluate the reactive reserve security of a system. Future research in the allocation of reactive reserves when a VCA zone does not have enough reactive reserve to meet security constraints would allow this research to fill a valuable role in power-system planning and operation. EPRI continued on with this research with the final EPRI-VCA Optimal Reactive Power

Dispatch Tool [47].

Chapter 3: Evaluating Wave Energy Converter Farm Placement with Loop Flows

3.1 Introduction

Developers have connected several wave energy converters (WECs) and prototypes to the electrical grid; however, the area considering the effects of WECs on larger-system transmission dynamics is still an open topic. A few studies [8]–[11] have considered the effects of marine renewable energy (MRE) placement on the electrical grid. These studies consider system reliability aspects such as voltage deviations, branch overloads, voltage stability margin. While metrics such as voltage deviations and branch overloads give an immediate answer about the stability of the electrical system, there are other phenomena on the power grid that can effect the effectiveness of the electrical grid. Studies looking at the temporal characteristics of WECs note that MRE could complement existing renewable such as wind and solar and such explore the smoothing of WEC power with the spacing of WEC farms and combinations of multiple technologies. Studies such as [13], have commented on the need for future work to combine the temporal analysis of WECs with power flow analysis to model more grid-specific effects of WEC integration.

In particular, WEC developers should consider the grid connection early on - looking for ways to mitigate WEC impacts through placement and investigate

additional benefits that a WEC could have on the electrical grid [12]. One aspect of electrical grid that WEC developers can look at in addition to voltage deviations and branch overloads is loop flows. When the shortest electrical path for power to flow from generation to demand nodes passes through a zone outside its contracted path, this power transfer becomes a loop flow. While system operators expect a small amount of loop flow in their system as a trade-off for interconnection, loop flows that flow in the same direction as regular power flows lead to increased losses, higher fault conditions, and lower reliability [14]. In addition to these operation concerns, utilities also have economic incentives to limit loop flows traveling through their system as the non-contracted flows congest transmission lines without any payment from the organization causing the loop flow, thus the costing the utility transfer capacity without reimbursement. [48]. To control loop flows, utilities with use either pricing strategies or add power flow controlling equipment. While phase-shifting transformers or FACTS devices limit loop flows, they also increase system losses as power no longer flows on the shortest path between nodes [15].

Renewable energy technologies such as hydro and wind have had noticeable effects on loop flows in both Western United States and Central European grids. Long transmission lines due to the remote location of hydro generation combined with variability in the scheduling of hydro generation led to major loop flows in the WECC [15]. High penetrations of wind energy has similarly increased loop flows through neighboring countries as wind power flows long distances from northern Germany to reach load centers in southern Germany [16], [17]. MRE is a variable

renewable resource located along the coasts of countries often in areas of weak grids with limited transmission resources and lower load. The combination of dynamic scheduling and long transmission lines caused wind and hydro generation to increase loop flows when connected, with similar characteristics, MRE should exhibit similar loop-flow inciting patterns. Since utilities want to limit loop flows caused by integrating new generation, WEC siting will need to consider how WEC placement affects the loop flows in an interconnected grid and minimize the increased loop flows.

Loop flow calculations use sub-divisions of the larger electrical grid called areas or zones. In practice, areas on the transmission grid are composed of utility control areas. Since utilities historically were vertically integrated, these control zones are often defined by political and or geographical boundaries rather than the electrical topology. In these utility areas, loop flows are simply a result of power flowing by physical laws rather than financial contracts. If a researcher partitions the grid using Voltage Control Areas (VCAs), which constructs zones based on a bus's electrical proximity, then the ability better the clustering solution, the less loop flows or transaction leakage. Cotilla-Sanchez et al. [22] illustrated a link between quality electrical partitioning and loop flows. For several different sizes of cases, higher clustering quality resulted in lower loop flows. The optimal quality clustering solution resulted in the lowest level of loop flows for RTS-96 and IEEE-118 test cases, while for the large Polish case2382wp, the highest quality clustering solution did not exhibit the lowest level of loop flows; but, all well-clustered systems resulted in much lower levels of loop flows compared to random solutions.

To perform an analysis of the grid interconnection of WECs on the electrical grid, researchers need quality power flow cases that exhibit accurate characteristics of the interconnection. Additionally, for research to be validated and expanded, the research must be reproducible by outside parties. Current open-access power flow cases are often based on generalized versions of historical cases. These cases lack the geographic specificity and detail necessary to explore WEC interconnection since WECs are a coastal resource. Synthetic cases, such as ACTIVSg2000, provide necessary detail and geographic specificity while remaining open access due to the fictitious nature of its grid topology. As such, results from synthetic cases can be extrapolated to real-world cases. ACTIVSg2000 (also known as Texas 2000) models the interconnection managed by the Electric Reliability Council of Texas (ERCOT) with a 2000-bus power flow case [18].

In this chapter, the author proposes to investigate the effects of WEC integration on loop flows in the electrical grid by combining WEC temporal information with a quasi-steady-state scenario analysis of loop flows in VCAs on the synthetic Texas 2000 case. The low average loop flows between areas in a well-clustered VCA will serve to highlight the effects a WEC has on loop flow changes. Additionally, by using the ACTIVSg2000 test case, the author can evaluate a range of WEC placements with reproducible results. A spread of smaller WEC devices should have lower loop flow effects than a single farm with generation equal to the sum of smaller WEC generation.

This chapter is organized as follows: Section 3.2 highlights the effects of loop flows on the electrical grid with Section 3.3 introducing Wave Energy Converters

and the prior grid interconnection research. Section 3.4 provides background for the synthetic cases used as a foundation for the QSS scenarios in this chapter. Section 3.5 introduces the technical aspects involved in the investigation of loop flows including extending the ACTIVSg2000 case and adding WEC generation to a power flow. The results follow in Section 3.6 highlighting the specific loop effects caused by the introduction of a WEC farm with Section 3.7 concluding the chapter.

3.2 Loop Flows in Electrical Grids

In addition to maintaining proper reactive power, grid operators must also ensure that adequate power to supply demand flows through the transmission grid without overloading transmission lines. Interconnected grid effects such as loop flows can hinder the ability of a utility to operate the transmission grid within reliability margins [15]. At its core, loop flows (also know as parallel path, circulating, or unplanned flows) are defined as physical power flows that take a different path than the scheduled or contracted path [14]. For a more rigorous definition, one must consider breaking a meshed system such as a wide-area electrical grid into several areas or zones. In the case of the power system these areas are often independent system operators or utilities who control a portion of the entire electric grid.

In an simple, vertically integrated system the utility has its own generation and transmission system to provide all of the power for its customers. In reality, economic or emergency conditions can require a utility to either import or export electricity to other utilities which requires an interconnection with the larger

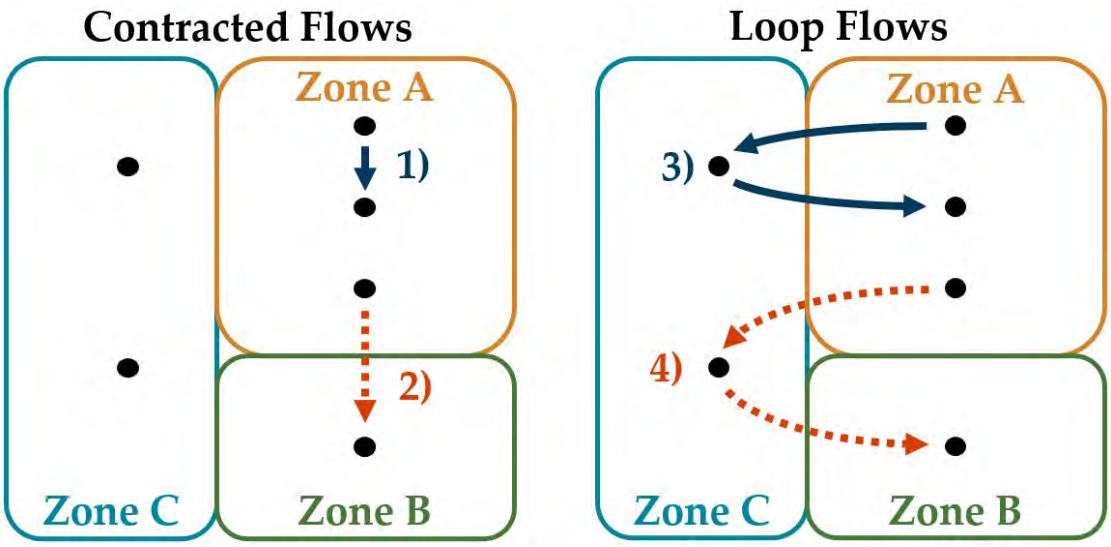

Figure 3.1: Transactions 1) and 2) in the contracted flow section represent electricity traveling as expected between demand and load nodes. Transactions 3) and 4) both represent loop flows where power passes through another zone to reach demand nodes. Transaction 4) can be further classified as wheeling since this transfer between two zones flows through a third zone.

electrical grid. Connecting to a larger system gives electricity new parallel paths through other zones by which it can travel from generation to demand nodes. At times the impedance of electrical lines may be such that the shortest electrical path between a load and generation is through another zone or utility. When this occurs, such as when a generator in Zone A supplies electricity to a load in Zone A via a line in Zone B, utilities describe the power flow as a loop flow [49]. Similarly, when a transfer between two utilities flows through additional systems, utilities describe this special case of a loop flow as wheeling [15], [50]. Fig. 3.1 represents summarizes these loop flow interactions in side-by-side diagrams comparing

contracted and loop flows.

3.2.1 Impact of Loop Flows

Before the deregulation or liberalizing of the electrical grid in both Europe and North America, electric utilities were primarily vertically integrated with limited transactions between utilities. As electrical demand outpaced the development of new generation, utilities began to rely on interconnection transactions to bolster in-area generation. This change in interactions between utilities began to highlight loop flows on the electrical grid, especially within the Eastern interconnection which has both high reliability and many parallel paths. In the mid-1980s Pennsylvania-New Jersey-Maryland (PJM) noticed that the New York Power Pool (NYPP) was importing large amounts of hydro-energy from Canada's Ontario Hydro. Instead of flowing entirely through the expected direct connection between Ontario and NYPP, around 50% of NYPP's requested energy flowed through a parallel path through Ontario, Michigan, Ohio, and Pennsylvania. As a result of these loop flows PJM was unable to source energy from coal power plants in the west. Similar events including American Electric Power and Allegheny Power System further highlighted the parallel paths that energy could take in the Eastern interconnection [48].

Due to the nature of meshed electrical grids at the transmission level, any interconnected utility should expect to experience some amount of loop flows. Loop flows become an issue when they affect the ability of a utility to provide reliable

service to its customers, to operate transmission lines with acceptable reliability margins, or to operate economically [15]. Specifically, loop flows in the same direction as regular power flows increase system losses and production costs, increase short-circuit current at interconnections potentially exceeding circuit breaker ratings, and affect the ability to operate lines with the reliability margin needed to avoid transmission line overloads [14]. To avoid these impacts utilities reduce loop flows by either implementing new pricing strategies to discourage transfers causing loop flows or adding power flow controlling equipment to stop loop flows such as phase-shifting transformers or FACTS devices [51], [52].

Loop flows can be split into major and minor loop flows. Minor loop flows occur between utilities where as major loop flows can flow through an entire interconnect. Depending on the location of the utility, minor loop flows can have just as detrimental effects as major loop flows. The Western interconnection in the US is very susceptible to major loop flows which circle through several states. The large geographic area with few major load centers combined with remote generation sources leads to long transmission lines which make the interconnection especially susceptible to loop flows. Additionally the dynamic changes in hydro power scheduling caused by water availability also increases the potential for loop flows [15].

Increased penetrations of renewable energy, particularly wind, has had considerable effects on the loop flows in the Central European grid. Wind power located on the northern side of Germany must reach industrial load centers in southern Germany. As a result of inadequate transmission resources, much of this

energy takes parallel paths through Austria and other central-European countries. Studies have shown that increased transmission capabilities between the renewable resource and the bulk load reduced cross-border flows [16], [17].

3.2.2 Determining Loop Flow Contribution

In the 1990s, both North America and Europe moved towards a deregulated grid and increased interconnection. As a result, separate operators can now control the generation, transmission, and distribution of energy. This led to the creation of independent system operators (ISOs) who ensure the reliability of their own zones. These ISOs have detailed representations of their own internal grid; but, all components outside of their area are typically represented as an equivalent circuit. These equivalences make it hard for a single ISO to determine the effects of their power flow on neighboring utilities. Despite these restrictions the Federal Energy Regulatory Commission requires that all parties have fair access to transmission which requires looking at the transmission losses due to loop flows [52]. In response, utilities and researchers developed several methods for calculating ownership of loop effects.

One way to calculate a specific generator's contribution to a loop flow is to use the the Power Transfer Distribution Factor (PTDF). PTDFs are sensitivities that can be used with a linearized power flow to determine the percent flow in any branch or group of branches based on a specific generator [48]. The PTDF can be found as follows:

$$PTDF = \frac{\text{flow during transfer} - \text{base case flow}}{\text{transfer test level}} \tag{3.1}$$

Other research on analyzing loop flows include the use of Margin Participation algorithms to extend the PTDF [53], power flow decomposition (PFD) [49], mesh-to-tree graph analysis [50], flow-based market coupling [54], and using least-squares estimation [55].

3.3 Ocean Wave Energy Converters

Earth's oceans have an immense amount of power that could be used to meet increasing energy demand, making marine renewable energy (MRE) an advantageous contributor to powering the grid with carbon-free generation. The density of power in a 1-meter plane perpendicular to the wave direction of the ocean can exceed 50 kW. A high-quality solar panel, comparatively produces 500 W. This illustrates the significant potential in harnessing power from the ocean to replace existing fossil-fuel generators [7]. For the US specifically, marine renewable energy technology could recover 1,170 TWh/year or approximately 30% of the annual US energy demand. Despite these advantages, MRE is still a developing generation resource that requires more research to remove barriers. One of these barriers is MRE's economic competitiveness with other generation sources. Levelized Cost of Energy (LCOE) compares the total capital and lifetime operational cost of a generator to the amount of energy generated over its lifetime. A lower LCOE indicates a more economically competitive source. For MRE to be economically

viable its LCOE needs to be lower than \$0.30/kWh, which few designs are able to meet [56]. In addition to economic concerns MRE designs must be able to weather harsh ocean conditions [57].

While supplying the electrical grid with generation is often a goal of Wave Energy Converter (WEC) development, a review [12] of the design process for WECs found that grid integration is one of the least considered factors in WEC design. Considering the grid connection early in the design can allow a developer to site a device such that wave direction and sea state have minimal detrimental effect on the grid. Grid integration is a specific area for improvement in WEC design as no common design or evaluation methods exist currently. Additionally, common evaluation methods of WEC designs such as LCOE ignore the additional benefits that a WEC could have on the electrical grid, such as the temporal benefits relative to other renewable sources.

The ocean's magnitude of power combined with the variability of renewable sources impact both the reliability of the transmission system. There have been several studies considering the effects of WECs on the electrical grid and these studies can be split into three groups: those that consider temporal characteristics of a WEC, those evaluating the effects of WEC interconnections on the transmission or distribution steady-state models and those that focus on the dynamic power quality effects at the point of connection. The next subsections explore temporal and steady-state studies.

3.3.1 WEC Temporal Characterization

Since the power available in waves is variable at several timescales, including second-to-second, temporal studies are a natural first step to look at how WECs affect the electrical grid. The unique properties of wave power is such that when wave energy may be present while solar or wind energy experiences natural lows. Existing research looks at the timing value of wave energy compared to existing renewable sources. One way to quantify the benefits of a variable resource is to look at its availability and persistence. Resource Availability is when the resource is above a given threshold and as a result available for energy production for the given time step. Similarly, Resource Persistence measures how persistently a resource is available for a given window width [58]–[62].

The capacity factor of a WEC remains one of the most common metrics across research to describe a WEC's impact on the power grid. Capacity factor compares the actual energy output of a generator over a given time frame to its maximum designed power output. For WECs, the capacity factor captures the effect of a WEC's variability with a generation profile. As an important metric to determine financial viability [61], capacity factor can be a useful way to compare different resources or mixes of generation types [60], [63]. Capacity factor's prevalence in reporting has allowed for metrics which extend the applicability of capacity factor to effective load carrying capacity [59] annual energy penetration [11], and operational risk posed by a WEC [64].

Since MRE includes both offshore wind and wave energy solutions, several

researchers have explored how the two types of MRE might complement each other when connected to the electrical grid. A study [65] looking at the variability of both resources off the coast of California concluded that co-located wind and wave farms have less variability and provide more suitable energy for base load generation. A similar study [66] found less energy curtailment and a higher farm-to-grid efficiency when compared to only wind generation. The relative ease of forecasting wave energy, especially tidal energy complements both solar and wind whose power outputs are harder to forecast with accuracy [67]. For the larger grid, a study by Halamay et al. [62] found that mixing wind, solar and wave energy sources allowed for greater penetrations of all three resources without negative impacts on the system reserve requirements.

The spacing of wave farms is an important consideration in MRE variability. Just as co-siting wind and wave helped to improve generation stability, spreading out wave farms can improve the ability to forecast wave energy by smoothing out noise [67]. Similarly when considering grid impacts, spacing out WECs reduces the idle time and step changes in the power supply leading to less negative impact on the electrical grid [68].

Energy storage can reduce the variability of a renewable resource and several studies have looked at the effect of energy storage on the interconnection of WECs. One study [66] found that in general as the fraction of wave energy compared to wind energy increased for a given penetration of renewable energy, the energy storage capacity decreased. A parametric study [13] looking at wind, solar, tidal, and wave power found that MRE helped reduce storage capacity and costs in

general; but, cautioned that the location, profiles of other renewable resources, load profile, and MRE characteristics could limit that benefit. This study looked at the generation and load mismatch, the required energy storage profile, the energy storage capacity, and avoided or incurred storage costs.

3.3.2 WEC-to-Grid Power Flow Studies

The temporal studies above while helpful in determining the effects of WECs on the electrical grid still require additional modeling that incorporates grid-specific details [13]. Tools such as power flow analysis include grid topology and transmission line models which better model the grid's response. The integration of WECs into the grid affects the network's reliability, reserve power requirements, voltage profiles, branch loading, and stability.

A study [69] investigating the combination of wave energy with wind and solar looked at the impact of various combinations of renewable energy penetrations on the probability of failure of the power flow. This study modeled WECs using the method in [70] and used the 179 bus WSCC/WECC power flow case as the electrical grid model. This study defined failures as non-convergence of the power flow and branches exceeding line limits.

A study by Khan et al. [8] modeled the effects of a WEC on both the WECC interconnection and the Korean electricity system on three different scales: Steady-state, time-domain, and small-signal. The steady-state analysis uses the power-flow to look at voltage deviation, branch overloads, and voltage stability margin.

Time-domain analysis looks at transient stability and transient voltage dips. For the WECC, transmission line overloading is the primary limiting factor on WEC integration, requiring several upgrades near the point of connection. For the Korean system the primary limiting factor is the voltage stability of the system with the fault of a major transmission line; otherwise, the addition of WECs did not cause issues with voltage violations.

To evaluate the impact of connecting WECs for testing at the Pacific Marine Energy Center Wave Farm in Newport, Oregon, [9] equivalenced a 17,000 bus Western Electricity Coordinating Council (WECC) model and studied the effects at the connections with the larger interconnection for four different seasonal transmission system states. Adding a WEC farm at this point had a minimal effect on the voltage magnitude and consistently decreased transmission line loading.

A study by Johnson and Cotilla-Sanchez [10] looked at the reliability of the grid with a significant WEC penetration using a well-being approach coupled with a Monte Carlo method of state generation. This study looked at the probability, duration, and frequency at which the grid was in healthy, marginal, or at-risk states with the addition of WEC power. The study used data from three sites on the western coast of the US and mapped those sites to three generators in the 73-bus IEEE RTS test case. Johnson and Cotilla-Sanchez found that wave energy has a small, negative effect on the hourly reliability, but only increases the probability of marginal status rather than additional failure statuses. The marginal system states could be mitigated by adding a small increase in controllable generation system-wide.

While most transmission-level studies consider systems with a high degree of interconnection, [11] considers adding 500 MW of MRE to Vancouver island which has only two connections to the continent. Moazzen et al. find that although adding ten WECs to the small grid requires a new bulk transmission line from northern to southern Vancouver island, the solution helps the primarily hydro generation supply and reduces reliance on the transmission line connecting it with the continent.

The previous studies looked at applying a WEC to a transmission grid, yet a small WEC could be found as a distributed energy resource on a distribution grid. Distribution analysis removes the assumption that all three phases are balanced and adds more detail, often while reducing the network complexity under analysis. Mendonica et al. [71] proposes a strategy to mitigate voltage fluctuations on the distribution power flow by controlling the grid-side converter. The proposed control eliminated WEC voltage fluctuations with the balanced three-phase power from the WEC contributing to more balanced phase voltages. Another distribution study [72] finds that two WECs can help ensure voltage stability on Adriatic Islands, looking specifically at total losses and voltage violations.

3.4 Synthetic Power Flow Cases

Due to the high reliability requirements of the power grid, experiments evaluating new generation or components must use models of the power grid rather than physically modify the electrical grid. To do so, power system engineers use power

flow models. A power flow model contains information on transmission, generation and load configurations along with voltage and loading settings. The power grid synthetic power flow cases are one tool this paper uses to look at WEC interconnection. To understand the need for synthetic cases, one must first understand how utilities use load-flow cases. System operators must carry out load flow studies of the grid on both the entire interconnection as a whole and for each utility to ensure that the system will remain stable and within limits. As a result, most existing power flow cases are of entire electrical grid or utility sub-sections. In particular grid operators use these load flows for a variety of purposes including long- and short-term planning and near-real-time operation analysis [73].

Planning cases cases represent a generalized version of a utilities expected generation, demand, and topology. Long-term planning cases have loading representing the peak, average, or minimum load for a future season, often a couple years out. Planners use these cases to evaluate potential upgrades, asset retirements, or changes in loading. Operational planning cases cover a range from an hour to a year ahead of real time. These cases let planners determine the actual state of the transmission grid and the generation and topology needed [73]. Several assessments of WEC grid interconnection use planning or base cases [8], [9]. A select number of historical planning cases have been published and modified for general use with research. These cases allow researchers to perform analysis on real-world cases that can be freely shared and compared by other researchers.

In order to ensure continued reliability of a grid, utility systems often use real-time data to construct power flow cases that model a specific snapshot of the grid

for contingency analysis. These snapshots are modifications of a general grid with updates based on device status, generator outputs, demand and voltage levels [73]. Due to the specific nature of their construction these cases have limited application, but can construct a quasi-steady-state look at a system.

3.4.1 Relevance of Synthetic Cases

Both planning and near-real time cases are essential for researchers to apply their experiments to real-world grids. In order to safeguard infrastructure, countries, such as the United States, label power flow models as critical energy infrastructure information (CEII) and restrict access to existing models through non-disclosure agreements [74]. Peer reproducible work is a key component to further research. While some historical planning cases exist for open access, they are often limited in size and scope of models covered. For a power flow case to be broadly applicable for research it needs to represent the complexities of the modern electrical grid with adequate complexity, grid characteristics, and size [75].

In response to the gap in open-access broadly-applicable power flow cases researchers developed synthetic power-flow cases which avoid CEII restrictions with a fictitious and still resemble real-world electrical grids. Synthetic power flow cases span existing geography and are statistically similar to existing electrical characteristics of the area, but contain entirely fictitious information. The siting and sizing of load and generation matches the statistics present in publicly accessible data such as the U.S. Census and the Energy Information Administration, with

load and generation clustered together to create individual buses. Transmission line lengths and voltage levels follow conventional standards while not specifically following existing infrastructure. To provide sufficient grid complexity, synthetic grids contain phase shifting transformers, transformer impedance correction tables, remote tap-changing, bus voltage regulation, and switched-shunt reactive power compensation. Researchers test these cases against real-world structural characteristics [18], [75]. While initial power-flow cases included only a single base case, Li et al. added load modeling and distributed energy resource (DER) generation to create steady-state scenarios for an entire year [74].

3.5 Experimental Setup

In order to model a WEC's effect on loop flows, the author extended the ACTIVSg2000 case to include varying renewable energy and demand based on historical generation and load. The authors start with modeling WEC variability for use with a power flow.

3.5.1 WEC Modeling

Wave energy is notable for its temporal characteristics as WEC generation is much easier to forecast [67], thus reducing the error between expected and actual generation. Additionally, WECs score highly for both resource availability and resource persistence which means that WECs are often present even when other renewable

generation is unavailable [60]. Still, on an hourly-basis WECs exhibit significant variability in the power they produce. To model this variability, this dissertation begins with hourly wave resource data from the National Data Buoy Center [76]. This limits the temporal study resolution to an hourly basis.

There are many different ways to construct a WEC, for this dissertation we use a floating point absorber. A point absorber WEC is combination of a floating structure interacting with surface waves and a PTO system connected to the float and moored to the sea-bed. Incident waves induce a heave motion of the structure, $z(t)$, that is damped by an electric generator. The linear equation of motion for one degree of freedom in heave-only operation from [77]:

$$m\ddot{z} = f_e + f_r + f_h + f_{\text{PTO}} \tag{3.2}$$

where:

- m is the device's mass,
- $\ddot{z}$ is the heave acceleration of the body,
- f_e is the wave excitation force,
- f_r is the radiation force,
- f_h is the hydrostatic restoring force acting on the body (buoyancy),
- f_{PTO} is the reaction force exerted by the PTO on the the body.

Point absorbers, like many WEC types produces power by damping the incoming waves by applying a force via its power take-off (PTO). This PTO produces power proportional to the potential energy in the ocean within its designed frequencies. Equation (3.3) gives the power from a point absorber:

$$P_{\mathrm{PTO}} = -F_{\mathrm{PTO}}\dot{z} \tag{3.3}$$

where:

- P_{PTO} is the WEC's power output,
- $\dot{z}$ is the heave velocity of the float.

For many WECs, wave lengths between 8 to 12 seconds produce the most power.

The excitation force from the waves can be calculated using the water surface elevation, found in the harmonic content of the waves [70]. For this research, the author starts with power spectral density (PSD) from NDBC, finds a PSD mass function from the binned data, and then integrates the mass function to determine the total power in the wave at the desired frequency range for the given snapshot, shown in (3.4).

$$P_{\text{wave},i} = \sum \text{PSD}(f \cdot i) \cdot \Delta f \tag{3.4}$$

where:

- P_{wave} is the wave power in bin i,
- PSD is the power spectral density mass function,
- f is the frequency,

3.5.2 Creating Hourly Quasi-Steady-State Scenarios

In power systems, quasi-steady-state scenarios (QSS) are power flow solutions that represent a snapshot of the power system. Each scenario contains regular power flow information such as generator outputs, load at buses, transmission line and transformer parameters and element statuses. These models can be adapted for use in long- and short-term planning as well as near-real-time operation analysis. Utility planners use QSS scenarios for contingency analysis, reliability assessment, voltage stability studies and generator commitment [74]. In QSS analysis, power engineers analyze sequential scenarios on the system over time, assuming that the power system transients are able to converge over the in-between times.

The PSD data given by NDBC records changes on an hourly basis. This hour length forms the base time-step between each scenario developed for this experiment. Since the PSD changes every hour, the WEC power from (3.4) will also change hourly. To evaluate seasonal variations in WEC power, the scenarios for this study cover an entire calendar year, from January 1, 2016 through December

31, 2016.

The ACTIVSg2000 (Texas 2000) case contains a single steady-state solution for the ERCOT interconnection. To adequately model the complexity of the ERCOT interconnection, the case 2000 buses, 2345 transmission lines, 861 transformers and 1125 demand nodes. This complexity makes the Texas 2000 model a great starting point for examining the effects of large-scale WEC farms on the grid. Additionally, the southeastern side of Texas lies along the Gulf of Mexico, which has NDBC wave data buoys. This will allow the author to add a variable WECs that match the geographic area.

To create a series of QSS scenarios to model the interactions of WECs, the ACTIVSg2000 case must be expanded as the base-case only represents a single point in time. The author took inspiration from [78] to extend the synthetic case and make the required changes to both active and reactive demand as well as variable generation such as wind and solar generation. For this study, the author simplified the model to exclude device outages and contingencies. Fig. 3.2 represents this process in a high-level flow chart.

3.5.2.1 Demand Modification

Since ACTIVSg2000 represents a planning case where loads are representative rather than real time, the author needed a year's worth of hourly load data for each bus to extend the Texas 2000 case to the desired length and detail. Birchfield et al. [18] used ERCOT load data archives from the year 2016 to create the repre-

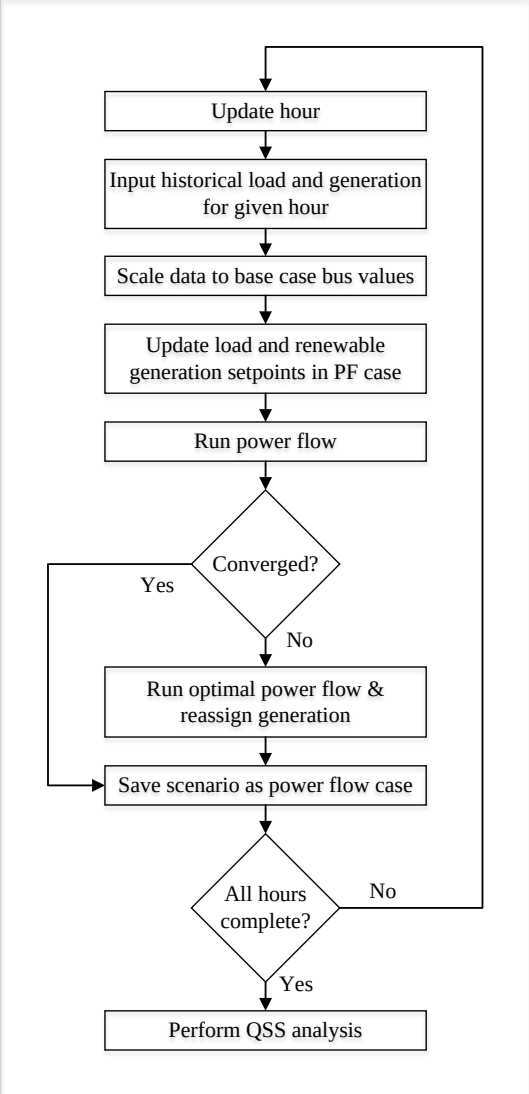

Figure 3.2: Flow chart outlining the high-level quasi-steady-state scenario creation with historical load and generation.

sentative load at each of the buses in the ACTIVSg2000 case, so the author used the same load data from ERCOT to create hourly demand [79]. Due to the large size of Texas and the variety of demand profiles contained, the load information

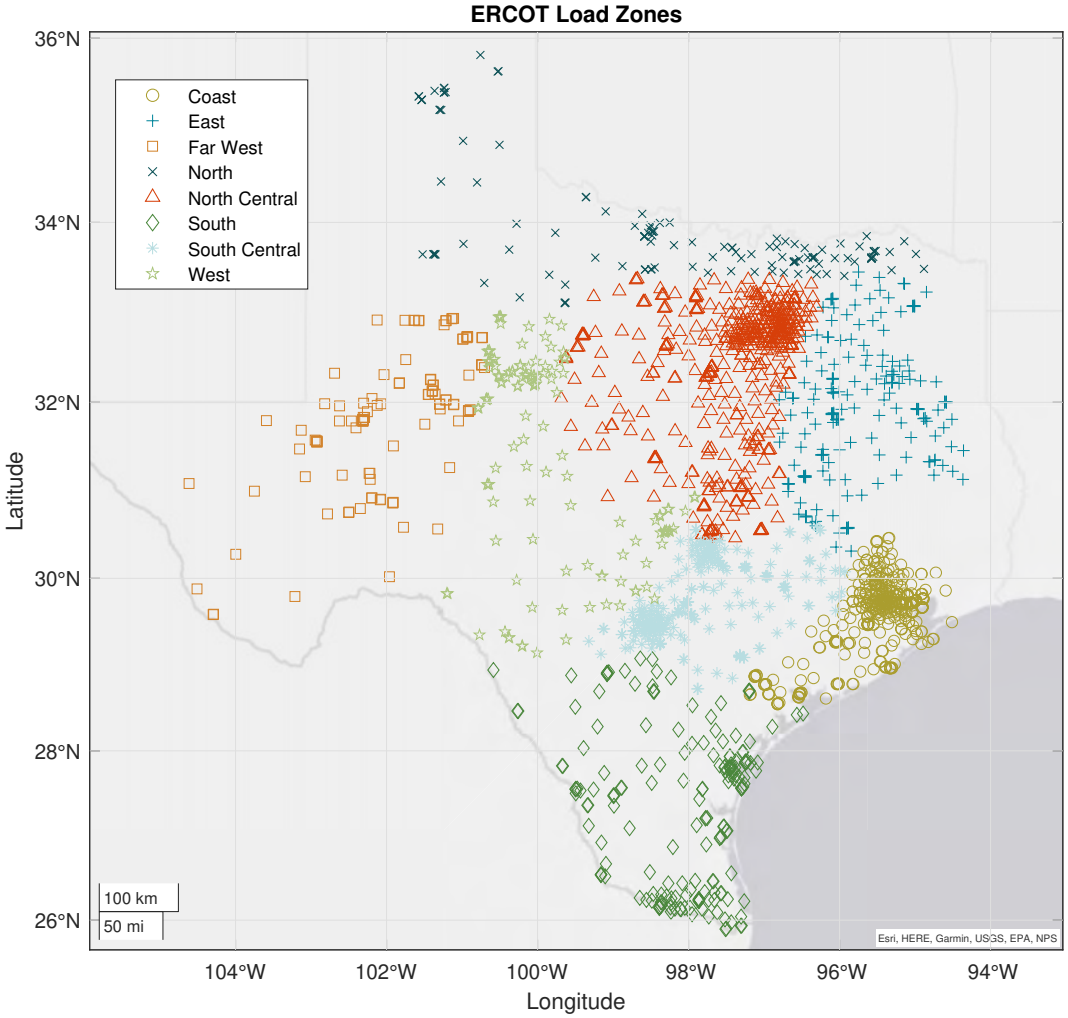

Figure 3.3: The load zones defined by ERCOT. Each symbol represents a bus in the ACTIVSg2000 synthetic case.

from ERCOT has eight sub-areas based on geography and weather. Although the buses in Texas 2000 are fictitious, each bus has geographic coordinates which can be mapped to ERCOT's load zones. Fig. 3.3 shows the eight load-zones as defined by ERCOT mapped to the 2000 buses of ACTIVSg2000.

Despite ERCOT's load data only giving eight general values for demand at each hour, each individual bus in the Texas 2000 case has a unique load value. To preserve these individual values, the QSS scenario's loads need to be based off of the load at each individual bus. These individual load values can be preserved in a new time step by scaling all loads in a given area using a demand factor based on the recorded hourly load for that zone. The demand scalar (3.5) is a relative loading factor that represents the load value at a given time step relative to the maximum load in a given ERCOT area:

$$D_{t,z} = \frac{P_{D_{t,z}}}{\max(\mathbf{P_{D_z}})} \tag{3.5}$$

where:

- $D_{t,z}$ is the demand scalar used to determine the current load for a given ERCOT zone z and time step t,
- $P_{D_{t,z}}$ is the active power demand for ERCOT zone z and time step t,
- $\mathbf{P_{D_z}}$ is the set of active power demands for the ERCOT zone z for all time steps.

One can find the new active power demand values for each time step by using the demand scalar, $D_{t,z}$, by making two assumptions: 1) the load values in ACTIVSg2000 represent peak load values and 2) each ERCOT load zone, the fraction of load consumed by an individual bus remains constant for all time periods. The first assumption allows the author to match up the peak load in each ERCOT

load zone with the load shown in the Texas 2000 base case with the second assumption allowing the author to create a simple proportional relationship between each bus's base-case active power demand and its QSS scenario loading using the bus's ERCOT load zone, shown in (3.6):

$$P_{D_{i,t}} = D_{t,z} \cdot P_{D_{i,0}} \tag{3.6}$$

where:

- $P_{D_{i,t}}$ is the QSS active power at bus i for time step t,
- $P_{D_{i,0}}$ is the active power at bus i for the synthetic base-case ($t = 0$).

Reactive power demand, just like active power demand varies based on time of day and season, thus the reactive power demand must also vary with each time step [78]. Although ERCOT data only provides active power demand, the author uses the same demand scalar, $D_{t,z}$, to model changes in reactive power demand. Similar to (3.6) the reactive power demand for the given QSS scenario is proportional to the synthetic base-case reactive load:

$$Q_{D_{i,t}} = D_{t,z} \cdot Q_{D_{i,0}} \tag{3.7}$$

where:

- $Q_{D_{i,t}}$ is the reactive power at bus i for time step t,
- $Q_{D_{i,0}}$ is the reactive power at bus i for the synthetic base case.

3.5.2.2 Renewable Generation Modification

The active and reactive power demand is not the only change on the electrical grid for the set of yearly QSS scenarios. The Texas interconnection has a large wind and solar resource which the ACTIVSg2000 case models with significant wind and solar resources. For accurate QSS snapshots, the wind and solar generation must vary hour-to-hour. Solar generation will correspond for the most part with daylight hours while wind generation is strongest in the evening. ERCOT records its fuel mix with actual generation values for each fuel type in 15-minute intervals [80].

To make this data consistent with the hourly time step, the author averaged the four, 15-minute active power values to produce a single value for each hour. Similar to the load data from ERCOT, the generation fuel mix data included only one value for an entire hour. As each renewable site's power production varies based on location, direction, and generation capabilities, the fuel mix needed to be individualized for each site. To link the synthetic case with the fuel mix, the author made two assumptions necessary to reduce the complexity: 1) the generator set points for renewable generators in the base-case represent average production capacity (ie. when ERCOT reports an average amount of wind generation, the base case represents this level of power production for wind) and 2) renewable generation amounts scale linearly based off of the average production as the author does not model stochastic variations due to other variables such as resource availability for a single generator. To create a generation scalar to linearly change the renewable generation levels, the author divided the active renewable generation from ERCOT

by the average renewable generation output, accounting for type of fuel (ie. wind or solar).

$$G_{t,k} = \frac{P_{G_{t,k}}}{\frac{\sum \mathbf{P_{G_k}}}{n_k}} \tag{3.8}$$

where:

- $G_{t,k}$ is the variable generation scalar for time step t and generation type k,
- $P_{G_{t,k}}$ is the reported power generated at time step t by fuel type k,
- $\mathbf{P_{G_k}}$ is the set of reported power generation for all time steps and fuel type k,
- n_k is the number of generators with fuel type k.

The renewable generator set-points change based on this generation scalar. To ensure that the power-flow treats the renewable generation source as a fixed input rather than a generator with varying set-points, active power maximums and minimums equal the given active power set-point for a each time step. While the power-flow does not have a set reactive-power set-point, when a user enforces reactive limits, the power flow keeps reactive generation within maximum and minimum values. Similar to demand, reactive power maximum and minimum set points vary based on the generation scalar. Equations (3.9)-(3.13) give the new

power set points for renewable generation:

$$P_{G_{i,t}} = G_{t,k} \cdot P_{G_{i,0}} \tag{3.9}$$

$$P_{max_{i,t}} = G_{t,k} \cdot P_{G_{i,0}} \tag{3.10}$$

$$P_{min_{i,t}} = G_{t,k} \cdot P_{G_{i,0}} \tag{3.11}$$

$$Q_{max_{i,t}} = G_{t,k} \cdot Q_{max_{i,0}} \tag{3.12}$$

$$Q_{min_{i,t}} = G_{t,k} \cdot Q_{min_{i,0}} \tag{3.13}$$

where:

- $P_{G_{i,t}}$ is the active power set-point for generator i at time step t with a fuel type of k,
- $P_{G_{i,0}}$ is the active power set-point for generator i in the synthetic base-case,
- $P_{max_{i,t}}$ is the maximum active power set-point for generator i at time step t,
- $P_{min_{i,t}}$ is the minimum active power set-point for generator i at time step t,
- $Q_{max_{i,t}}$ is the maximum reactive power set-point for generator i at time step t,
- $Q_{max_{i,0}}$ is the maximum reactive power set-point for generator i in the synthetic base-case,
- $Q_{min_{i,t}}$ is the minimum reactive power set-point for generator i at time step t,

- $Q_{min_{i,0}}$ is the minimum reactive power set-point for generator i in the synthetic base-case.

3.5.2.3 Case Convergence

The addition of variable demand and generation allow the ACTVISg2000 case to extend to cover hourly QSS analysis for a year. To begin QSS analysis, these cases must converge. In order for the power-flow method to converge to a solution, the method must start with relatively-close approximations for voltage magnitude and angle, as well as active and reactive power at each bus. With both generation and load changing from the initial base-case, a single power-flow solution is not guaranteed to converge. In many cases the combination of an increase or decrease in generation combined with an increase or decrease in load may throw off the balance of generation and demand such that the QSS scenario requires new generator set-points for its dispatchable generation. In this case the author uses an optimal power flow to adjust the active power set-points such that the case converges.

3.5.3 Adding WEC Generation

For each QSS scenario, the author models WEC generation similar to renewables such as wind and solar and fixed the active power set-points such that the WEC applied power to the grid without the ability for dispatch. Equation (3.4) gives power available in the waves to the WEC. The author computes this value for

all hourly intervals for the entire year and finds the average wave power. Hourly sea state information for 2016 comes from NOAA buoy 42019 off the coast of Texas [76].

In practice, WEC developers design WECs for a maximum power output under specific conditions. As a developing generation source WEC conversion efficiency is still low due to the large amount of power present in the natural waves. For this experiment, the author assumes that the WEC is designed to capture energy from waves with wavelengths of 8-12 seconds, with maximum rated power occurring when the wave resource peaks based on those wavelengths.

To evaluate the effects of WEC placement on the grid, the author considers two types of WEC farm implementation: 1) The centralized case is where all wave penetration on the grid comes from a single 500 MW farm located at one of four buses on the coast of Texas, while 2) the distributed case is where the wave penetration on the grid comes from four equally-sized farms of 125 MW located at each of the four buses. These two types make up five cases of WEC integration. The farms reach full reactive power capacity when the wave resource peaks for the year along with a very low reactive power generation capacity of 5.0% of active power generation. Active and reactive generation set points use a WEC generation scalar, W_t based on the available wave power relative to the peak wave power (3.14)

$$W_t = \frac{P_{\text{wave},t}}{\max(\mathbf{P}_{\text{wave}})} \tag{3.14}$$

where:

- W_t is the WEC generation scalar for time step t,
- $P_{\text{wave},t}$ is the wave resource power for time step, t,
- $\mathbf{P}_{\text{wave}}$ is the set of all wave resource power values for the given year.

The WEC generation scalar then linearly effects the output of the WEC farm via the generation set points:

$$P_{G_{i,t}} = W_t \cdot P_{\text{rated}} \tag{3.15}$$

$$P_{max_{i,t}} = W_t \cdot P_{\text{rated}} \tag{3.16}$$

$$P_{min_{i,t}} = W_t \cdot -P_{\text{rated}} \tag{3.17}$$

$$Q_{max_{i,t}} = W_t \cdot Q_{\%} \cdot P_{\text{rated}} \tag{3.18}$$

$$Q_{min_{i,t}} = W_t \cdot Q_{\%} \cdot -P_{\text{rated}} \tag{3.19}$$

where:

- $P_{G_{i,t}}$ is the active power set-point for WEC farm i at time step t,
- P_{rated} is the rated active power set-point for the WEC farm i (either 500 MW or 125 MW),
- $P_{max_{i,t}}$ is the maximum active power set-point for WEC farm i at time step t,

- $P_{min_{i,t}}$ is the minimum active power set-point for WEC farm i at time step t,
- $Q_{max_{i,t}}$ is the maximum reactive power set-point for WEC farm i at time step t,
- $Q_{\%}$ is the ratio of reactive power to active power for the WEC farm i,
- $Q_{min_{i,t}}$ is the minimum reactive power set-point for WEC farm i at time step t.

3.5.4 VCAs and Loop Flows

Due to their dynamic scheduling caused by natural variations in generation, renewable generators such as WECs can easily increase loop flows within a system. A well-sited WEC should increase the available generation within a system while also causing minimal negative impact to existing systems. As such, from a grid integration perspective, WECs should minimize their effect on loop flows.

To calculate loop flows, one must have separate areas or zones. As this experiment uses a synthetic case without historical partitioning of buses, the author must use another way to group buses. VCAs serve as the zones for loop flow calculation with the advantage of well-clustered VCAs having low inter-area flows. There are many ways to calculate or trace flows within a power system, however, for this experiment the author primarily uses a method published by PJM and the Midwestern ISO (MISO) [81].

The loop flow methodology starts by calculating the generation and demand within each zone, using the VCA zones as the zone assignments for each bus. Like most loop flow methods, this method only considers active power flows:

$$P_{D_z} = \sum_{i \in B_z} P_{D_i} \tag{3.20}$$

$$P_{G_z} = \sum_{i \in B_z} P_{G_i} \tag{3.21}$$

where:

- P_{D_z} is the active power demand in zone z,
- B_z is the set of buses in zone z, P_{D_i} is the active power for bus i,
- P_{G_z} is the active power generation in zone z,
- P_{G_i} is the active power generation at bus i.

This method calculates the flows between zones by aggregating the active power flows on each branch going in or out of a zone. Negative flows or flows into the zone are imports while positive flows or flows out of a zone are exports. These values must be calculated separately, otherwise the loop flow would be canceled out and only a net import or export would remain. The active power import and exports are:

$$P_{in_z} = \sum_{j \in Bin_z} P_{in_j} \tag{3.22}$$

$$P_{out_z} = \sum_{j \in Bout_z} P_{out_j} \tag{3.23}$$

where:

- P_{in_z} is the active power imports into the zone z,
- Bin_z are the branches with imports into the zone z,
- P_{in_j} is the active power import on branch j,
- P_{out_z} is the active power exports from the zone z,
- $Bout_z$ are the branches with exports from the zone z,
- P_{in_j} is the active power export on branch j.

The calculation of loop flows depends on if the generation in the zone is greater than the demand. In this case, the loop flow in the zone is equal to the imports, otherwise the loop flow is the sum of generation and imports minus the demand in the zone as in (3.24):

$$\text{Loop Flow}_z = \begin{cases} P_{in_z} & P_{G_z} > P_{D_z} \\ P_{G_z} + P_{in_z} - P_{D_z} & P_{G_z} \leq P_{D_z} \end{cases} \tag{3.24}$$

where:

- Loop Flow$_z$ is the loop flow in zone z,
- P_{G_z} is the active power generation in zone z,
- P_{D_z} is the active power demand in zone z,
- P_{in_z} is the active power imports into the zone z.

3.6 Results

This section presents the QSS scenario results with various WEC placements considered. Subsection 3.6.1 presents sample results from the completed QSS scenarios, showing the varying demand and generation for each season. A WEC is added in subsection 3.6.2 and loop flow changes created by the WEC are analyzed in subsection 3.6.3.

3.6.1 QSS Scenarios for ACTIVSg2000

The process of creating QSS scenarios for Texas 2000 starts with mapping historical ERCOT load onto individual buses in the base-case. As previously shown in Fig. 3.3, the author separated the synthetic buses based on geographic coordi-

nates into eight load-zones based on existing boundaries given by ERCOT. Using the ERCOT load-zones and the given historical demand, the author created new demand for each day, shown in Fig. 3.4 as total load for all buses on a selection of sample days (24-hour periods) in each of the four seasons. The sample days all represent week-days near the midpoint of each season, specifically February 3, May 6, August 4, and November 2. As expected, demand on the electrical grid peaks in summer due to Texas's warmer climate and the heavy loading caused by AC units. The load curve for winter peaks around 9:00 in the morning, which is unusual compared to normal load curves which peak in early evening; however, the curve is repsentative of loads in that time of year.

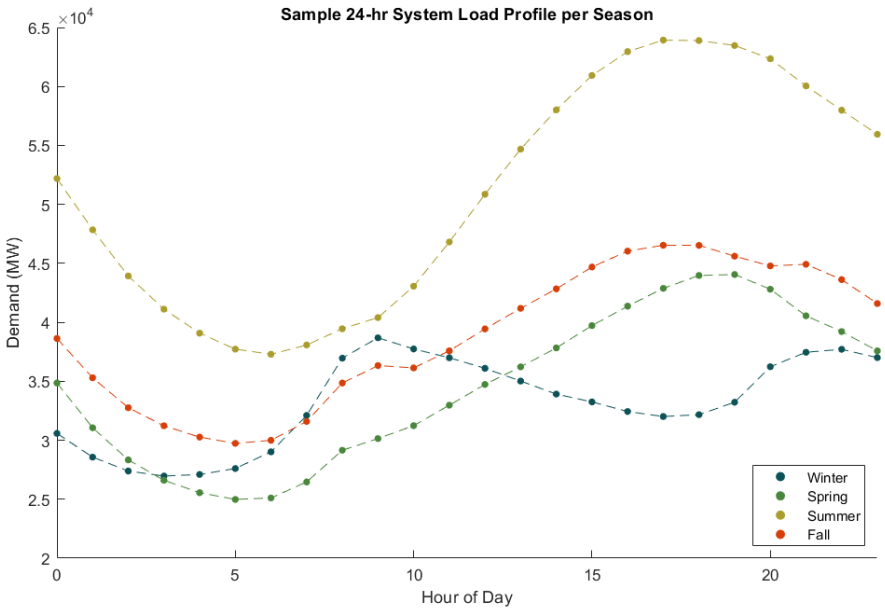

Figure 3.4: The total load for four sampled days in each season.

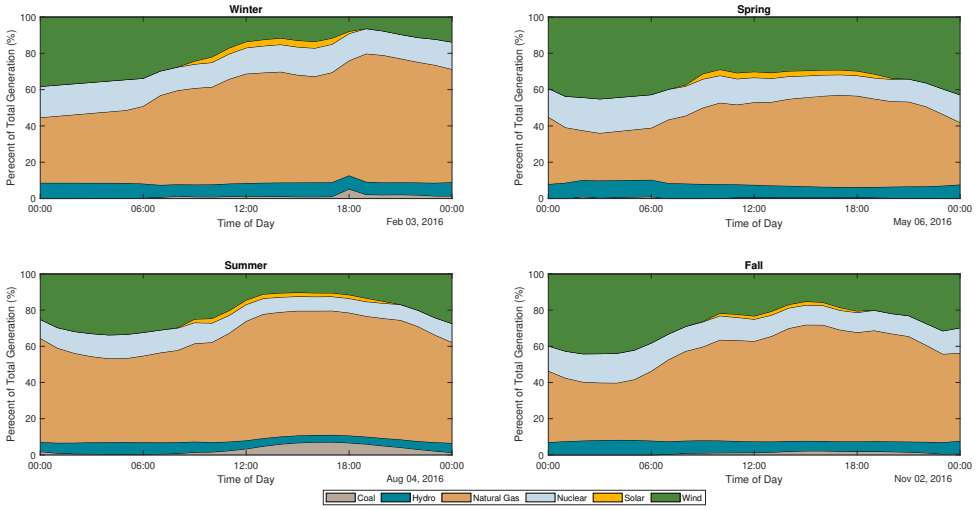

Figure 3.5: Generation profile for each season. Each subplot show the share a given resource makes up out of the entire generation - based off of scheduled MW.

With demand profiles for each bus created, the author then introduced variable generation in the form of variable wind and solar inputs. Both wind and solar have seasonal, daily, and hourly variations that can be seen in the sample generation fuel mixture for four sample days, Fig. 3.5. Note that wind generation is generally greater at night, but can be incredible variable based on day, where as solar is only available in the daytime. This variation in both load and generation caused imbalances in the balance between load and generation, requiring the author to run an optimal power flow (OPF) to adjust the active and reactive power set points for the fossil-fuel generation. This OPF then adjusted generators running on natural-gas, coal, and nuclear to allow for varying penetrations of wind and solar generation based on the generator costs included with the ACTIVSg200 case. Fig. 3.5 shows

the large variation in primarily natural gas generation output caused by changing amounts of wind and solar through out the day.

As a synthetic case, the Texas 2000 case lacks adequate reactive resources for an entire year. In order to help balance the system in times with high wind generation, the author allowed all generation sources to be lowered to zero active power output to allow the case to converge. Without this relaxation in modeling only a few days out of the year could be created using the historical data.

3.6.2 Adding WEC Generation

To model the effects of WEC generation on loop flows, the author evaluated potential buses based on their proximity to the geographic coast and their proximity to the boundary between VCA zones. For this experiment, the VCA zones stay the same as in Section 2.5.1, shown in Fig. 2.3. Two of these zones are located on the coast, specifically Zones 1 and 5. Fig. 3.6 shows the proposed buses for connection to WEC farms, buses 4017, 4108, 4170 and 4180. These sites are both close to the coast and close to the boundary buses between Zones 1 and 5 (shown in Fig. 3.7) making them ideal candidates for looking at loop flows.

Fig. 3.8 shows the output of the 500 MW WEC farm for four different days (24-hour periods), one for each season of the year. The generation varies greatly based on both season and time-of-day. This variability has potential to influcence flows on the power system. This sample shows the WEC resource is high during fall and winter, while spring and summer have relatively less available wave resource.

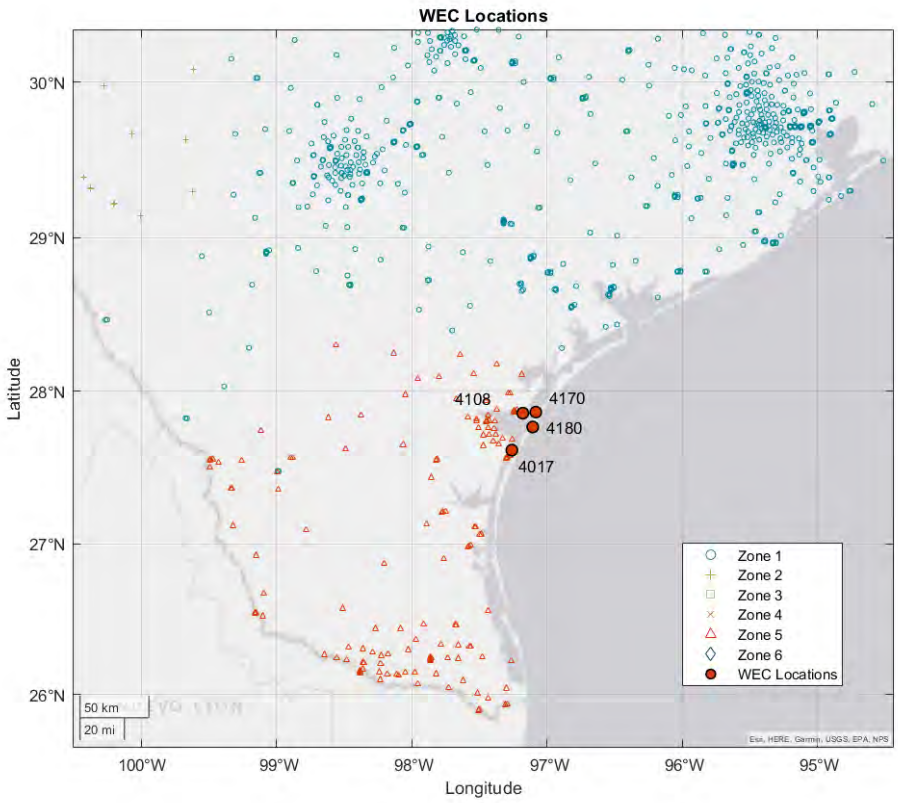

Figure 3.6: Locations of the proposed WEC sites in the ACTIVSg2000 case. All WECs are located close to the intertie for maximum effect on loop flows.

The average WEC power output per season in Fig. 3.9 confirms that the based on the 2016 historical data, this wave resource is largest in the fall season followed by winter. Spring season has lower wave resource with the summer season having the lowest wave resource. This is especially important to note when considering the results from loop flows as fall and winter seasons will have higher penetrations of WEC power than spring and summer.

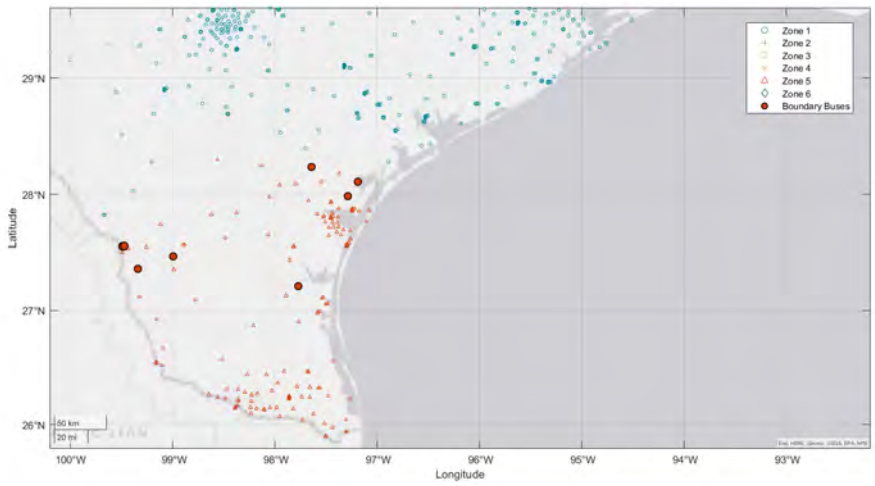

Figure 3.7: Boundary buses located within Zone 5 that connect Zone 5 with Zone 1 and the rest of the ACTIVSg2000 system.

3.6.3 Loop Flows

For this subsection, the author begins by stepping through the loop flow calculation for a single day, December 18, 2016. This day represents a high WEC resource, which leads to greater loop flow impacts at each potential point. The loop flow calculation begins by calculating the balance of load and generation, shown in Fig. 3.10 for the sample day, without WEC generation. This can be found by following (3.20) and (3.21). Since a VCA is not guaranteed to have generation, some zones such as Zone 4 may lack generation entirely. For this case, Zones 1, 2, 3, and 6 on average generate more power than demand, while Zone 5 has less generation than needed to meet demand. A direct balance does not account for system losses, which requires a zone to have excess generation in order to meet

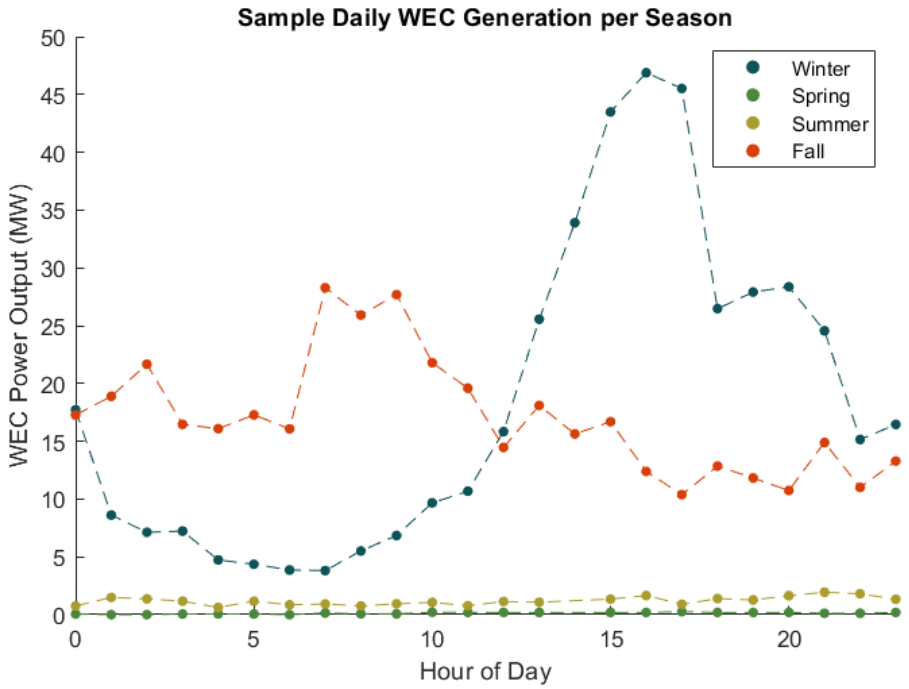

Figure 3.8: Profile of WEC farm generation per season. Note the variability and power difference based on times of year.

demand within its zone after accounting for losses in transmission. From these plots in Fig 3.10, the author expects to find imports into Zones 4 and 5 from their connected zones.

In addition to calculating the balance between load and generation, loop flow calculations also require the aggregation of power that is either imported or exported from each zone. Fig. 3.11 shows the power each zone imports as well as the zone providing the power imported into the zone. Respectively, Fig. 3.12 shows power each zone exports as well as the zone receiving the exported power. Both exports and imports are average power values for the entire sample day of Decem-

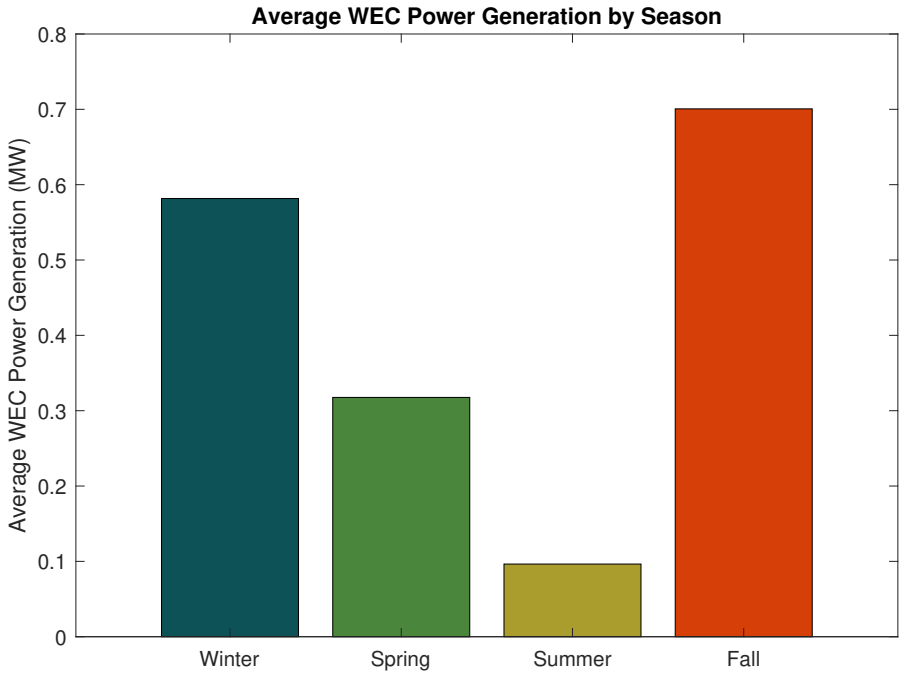

Figure 3.9: Average generation of WEC farm per season.

ber 18, 2016. Similar to the power balance, these imports and exports are without the addition of a WEC. Imports and exports are summed according to (3.22) and (3.23) respectively.

The physical branches between networks limit the options a zone has for importing and exporting power. For example, Zone 5 only has connections to Zone 1. With limited options, Zone 5 imports power from Zone 1 while also exporting a small amount of power back to Zone 1. Some loop flows are already evident when comparing the plots of imports and exports, as Zone 1 both imports and exports power to Zone 5. While a researcher can calculate loop flows occurring

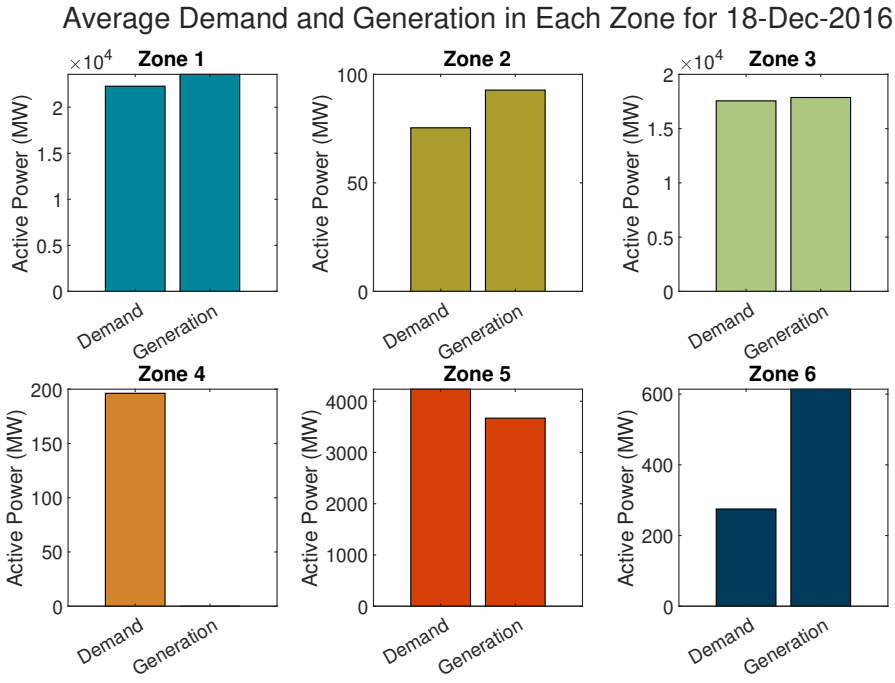

Figure 3.10: Average daily balance of generation and load for each zone on December 18, 2016.

during transfer of power within a single zone from these plots, the method needs additional data to calculate loop flows which occur during wheeling transactions.

The wheeling loop flows can be determined based on the balance of generation and load in each area, as in (3.24). Loop flows results for the sample case from December 18, 2016 without WEC power appear in Fig. 3.13. For cases where generation exceeds load, all imports become loop flow, such as in Zones 1, 2, 3 and 6 which all report their imported power as loop flows. For areas where demand is greater than generation, then the loop flow becomes the difference between the combination of imported and generated power and the demand within an area.

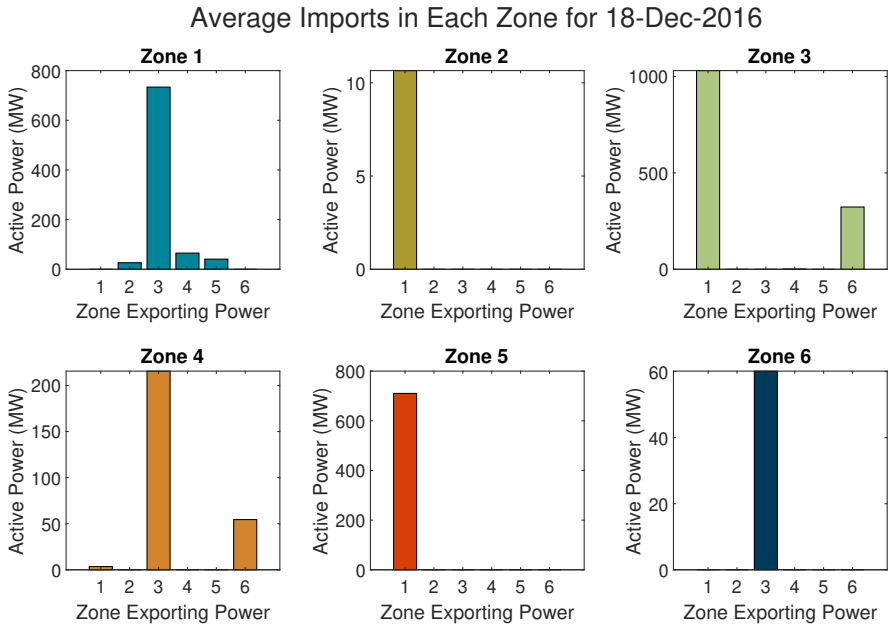

Figure 3.11: Average daily imports into each zone on December 18, 2016.

For this Fig. 3.13, the loop flows in Zones 4 and 5 occur due to an excess of imported power compared to the balance of generation and demand. In this case, Zones 1 and 3 experience the largest loop flows compared to other zones, which corresponds with the size of the clusters as both zones contain the majority of the system's buses.

Up to this point, this section has not yet considered the effects of WEC placements on loop flows. Building on the previous examples of computing average loop flows for a single day, the author now looks at how WEC placement affects average loop flows. For this study there are five potential cases for WEC farm placement including four distinct 500 MW WEC farm cases and a single case considering 125

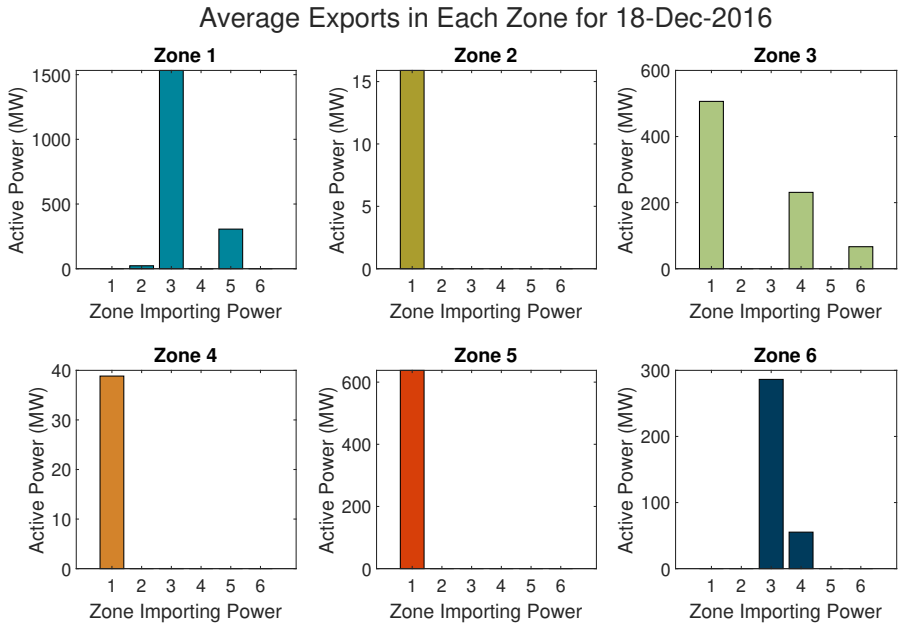

Figure 3.12: Average daily exports from each zone on December 18, 2016.

MW WEC farms distributed to all four potential sites. Fig. 3.14 shows the average difference in loop flows due to WEC placement. A positive change indicates that adding a WEC at the given site increased loop flows for that zone, where as a negative change indicates reduced loop flows in that zone for the given WEC location. For this system, adding a WEC had very little change on Zones 2, 4, and 6 which have limited buses and less power transfers with Zone 5 where the WECs are located. As the closest neighbor to Zone 5, the addition of a WEC adds substantial loop flows to Zone 1, mirroring loop flow increases in Zone 5, although with considerably less imports and exports, the loop flow increases are less in Zone 5. Despite the additional WEC generation, Zone 5 still requires additional imports

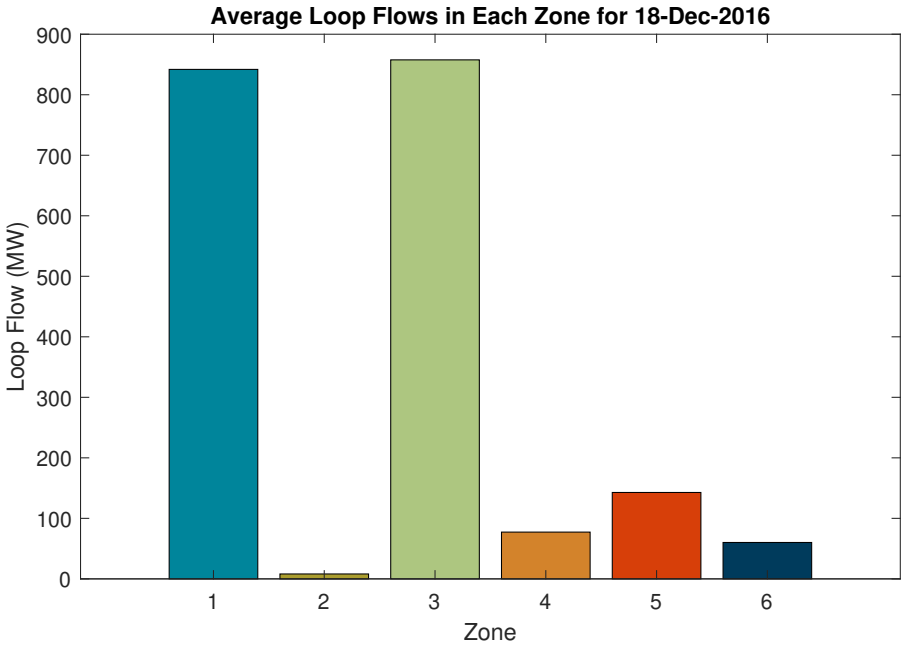

Figure 3.13: Average loop flows for each zone on December 18, 2016.

to meet demand and both imports and exports rise, causing increased loop flows. Zone 3 exhibits small decreases in loop flow due to the addition of WEC farms in Zone 5, but does not appear to have drastic changes, especially when compared to its original loop flow values.

The average change in loop flows caused by adding a WEC are summarized in Fig. 3.15. For this figure, a positive average change means that on average the WEC increased loop flows within the zone, where as a negative average change means that on average a WEC decreased loop flows. Adding a WEC consistently increased loop flows within the WEC's own zone (Zone 5); however, flows in the remaining zones were almost always reduced or negligible. This is seen in winter, fall, and

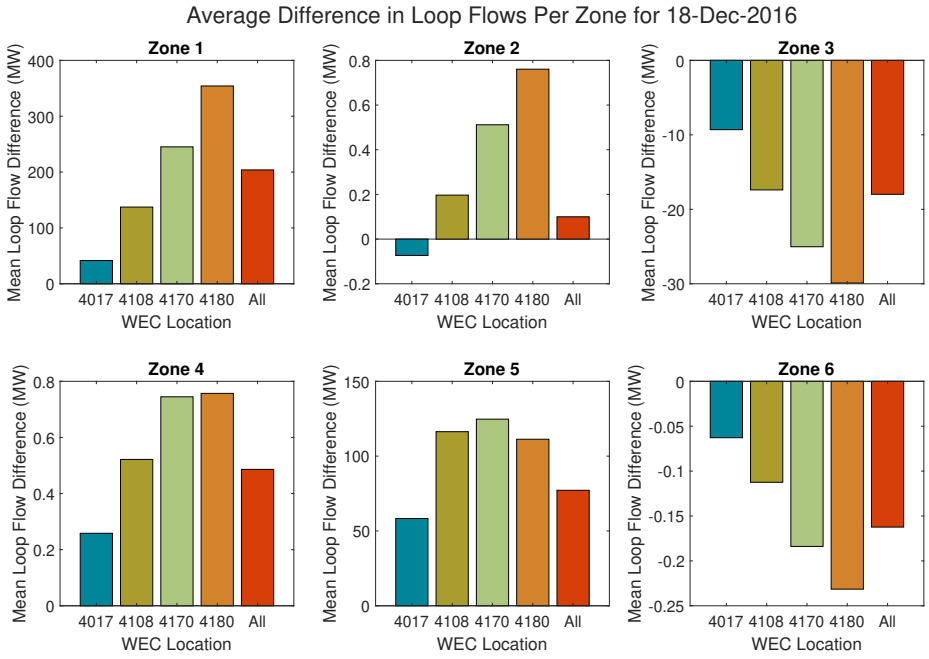

Figure 3.14: Average loop flows for each zone compared with the bus location of the WEC.

spring with summer having higher Zone 5 loop flows without much reduction in loop flows elsewhere.

The location of a WEC on the electrical grid has significant effects on loop flow changes, with Bus 4017 and the distributed option creating the least amount of changes to existing loop flows. In times with lower wave power, such as spring and summer, the distributed option caused the least amount of loop flow. During high wave resource times, fall and winter, Bus 4017 outperformed the other WEC placements. This is expected as bus 4017 is located the furthest geographically from the zone boundary and due to the close proximity of all test buses, the

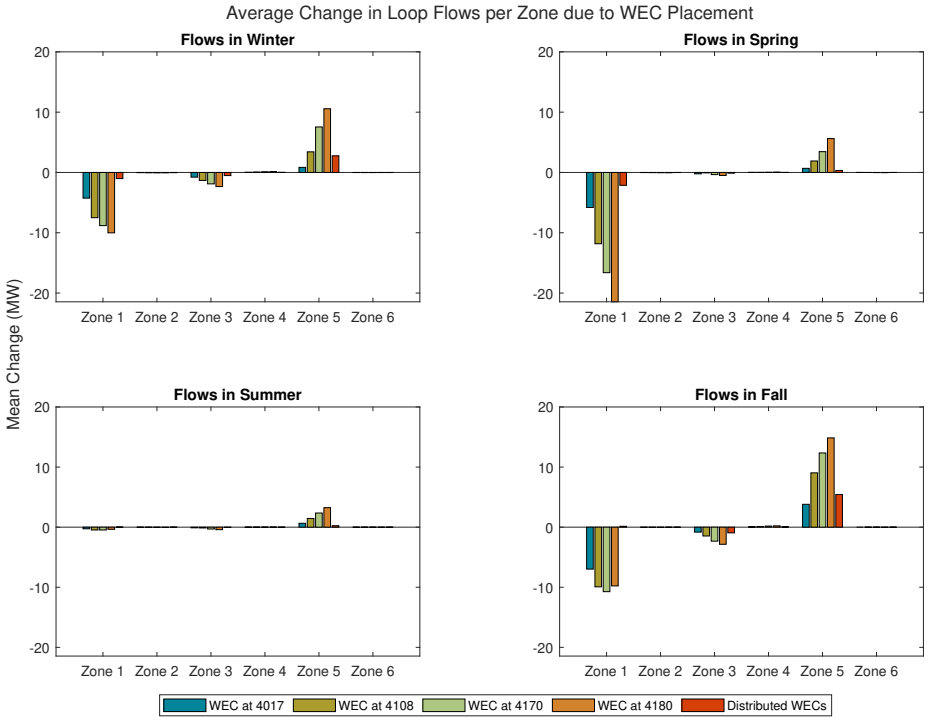

Figure 3.15: Average loop flows in each zone by season and compared with the bus location of the WEC.

geographic location approximates the electrical distance. The bus with the furthest electrical distance from the zone boundary should have the least effect on the loop flows through the boundary. Bus 4180 was the most sensitive to loop flows, as the addition of a WEC caused relatively significant changes, both positive and negative.

3.7 Conclusion

Utilities look to minimize loop flows due to their detrimental effects on transmission capacity, reliability, and protection. As a variable renewable resource, WECs also cause loop flow affects on the transmission grid, similar to wind and hydro generation. This chapter considers the temporal effects of WECs by developing hourly quasi-steady-state scenarios for an entire year. The author bases the QSS scenarios off of the ACTIVSg2000 synthetic power flow case which has sufficient electrical and topological properties that it may be used to evaluate larger transmission effects of WECs without requiring critical energy infrastructure information. To extend the Texas 2000 case, the author modifies both the load and renewable generation resources to match available load and generation data for Texas in 2016.

The analysis of loop flows uses VCA zones to mark the boundaries at which the author calculates loop flows. This study considers multiple placements of WEC farms including both a single larger farm and smaller farms. Average loop flows changed most significantly with the WEC farm large located close to the interconnection between zones while locations further away had less effect on loop flows. For periods of less WEC generation, the distributed smaller farms caused the least impact to the existing loop flows.

There is still significant research to be done to determine the effects of larger-scale WEC generation on the transmission grid. Future work could look at optimizing WEC placement for loop flow effects, implementing additional loop flow tracing, or expanding the locations to include higher wave resource areas such as

the Western United States.

Chapter 4: Hybrid Simulation of an Wave Energy Converter Power Take Off for Flicker and Power Quality Studies

4.1 Introduction

One of the most pressing issues for grid-interconnection of Wave Energy Converters (WECs) is the mitigation of power-quality issues. Although predictable on larger timescales, at the seconds timescale, wave energy is vary variable. This variablity causes the voltage and current output of a WEC to produce power with sub-standard power quality [19]. As discussed in the introduction 4.3, a single WEC generator usually has poor power quality which may be caused by the type of device, the control scheme, the sea-state, and the strength of the connected grid [9], [82]. This may be rectified in multiple ways including adding energy storage to smooth out voltages spikes, aggregating the voltage outputs from multiple WEC devices to smooth out aggregated voltage, and implementing PTO control schemes.

Despite decades of research, WEC technology is still a developing field, with many challenges for developers looking to generate energy from ocean waves. Harsh ocean conditions combined with wave resonance effects make developing grid-connected WEC prototypes complex and expensive [83]. In addition to these existing constraints, WEC developers must also focus on the quality of power they produce with the measurement of flicker playing an important role in creating grid-

scale prototypes [84]. To determine a prototype WEC's performance, developers turn to simulated and scaled physical models.

Both simulation and scaled physical models present limitations when developers apply their results to full-scale grid-connected testing. Real-time hybrid simulation, which originates from the field of seismic civil engineering looks to ease these issues by splitting testing into a computer-based numerical model and a connected physical system, using appropriate testing techniques for each portion. Borner and Alamfound [20] applied hybrid-simulation to evaluate complex wave fluid dynamics coupled with the power takeoff (PTO) of a WEC. Previous research done with Oregon State University's Wallace Energy Systems and Renewables Facility (WESRF) hybrid-simulation testbed has examined the numerical modeling of a WEC with a physical grid-connected generator [21].

This chapter looks to combine the advantages of a numerically modeled WEC with physical, grid-connected energy generation to measure a WEC's power quality, specifically its flicker and current harmonic outputs. With hybrid-simulation the author can measure power quality on a physical generator connected to a representative weak grid without the extra time and expense necessary to develop a physical WEC prototype. This allows the author to measure power quality metrics directly from physical components without requiring the abstractions made to model electrical devices.

Section 4.4 describes the experimental setup for the hybrid-simulated WEC including the numerical WEC model, physical devices, representative weak grid, and data processing. The power quality results from the experiment are found in

Section 4.5 with Section 4.6 offering concluding thoughts and next steps.

4.2 Interconnection Power Quality

There are many aspects to electrical power quality, including voltage fluctuations, current harmonics and high-frequency components. One way to measure the power quality with respect to voltage fluctuations is to look at flicker [85]. Flicker is a human-centered metric that refers to a person's perception of the variation in light intensity caused by voltage variations. The perception of light flicker depends on two factors, the magnitude of the voltage dip along with the frequency of the dips. Frequent, larger dips in voltage will cause variations in light that can cause irritation. Standards such as IEC 61000-4-15 [86] and IEEE 1453 define flicker and its measurement using a flickermeter [87]. From a histogram of the instantaneous flicker level, a probability density function and an overall cumulative distribution function can be created to predict the probability that the flicker will not exceed a certain value. These values are called short- and long-term flicker severity [87].

In addition to voltage fluctuations, changes in current harmonics can change the fundamental sinusoidal-nature of three-phase power. Arc-furnaces and power electronic converters such as inverters and rectifiers all increase harmonic currents in power systems. In particular converters using pulse-width modulation (PWM) increase harmonic current in a system. Harmonic currents interfere with communication circuits and can also cause increased heating and losses in electromagnetic motors and transformers [88].

4.3 WEC Power Quality Studies

At the point of interconnection, WECs have significant dynamic effects on the power quality of the grid, especially flicker. Flicker refers to the visual change in brightness of an electrical lighting source observed by the human eye due to a combination of frequent and/or large voltage fluctuations. WECs create fluctuations in voltage on the grid due to their large changes in output power due to the wave resource [19]. These fluctuations are within the range of flicker measurement [89]. The flicker induced on the grid depends on the type of WEC device, the control scheme applied to the WEC, and the sea-state [82]. Flicker also depends on the strength of the connected grid. Coastal grids are often weak grids with low short-circuit capacity and grid impedance which causes higher flicker[9].

Both IEEE and IEC have standards relating specifically to the power quality in WECs including flicker, current harmonics, and low-voltage-ride-through. As a distributed energy resource, IEEE 1547 [90] gives minimum flicker emission standards that grid-connected WECs must adhere to. In addition to flicker standards, IEEE 1547 places limits on harmonics and current distortion for inverter-based connections. IEC standard 62600-30 standard gives specific guidelines for measuring flicker and current harmonic outputs of marine renewable energy [85].

As a medium- or low-voltage connected device, a WEC must maintain a short-term flicker severity (P_{st}) of less than 0.35, although some jurisdictions may have less stringent flicker requirements [90], as high as 1.0 for the flicker severity [91]. The IEC recommends measuring P_{st} at the point of connection, ignoring switching

events such as start-up or switching between generators. Additionally, up to 15 short-term flicker measurements may be needed to account for variations in wave conditions [85].

Current harmonics must be measured and reported up to 50 times the fundamental frequency. At least three different tests for all phases must be performed for each 10% bin of WEC power rating. IEC 62600-30 also requires WEC developers to report interharmonics and higher-frequency harmonics [85]. IEEE 1547 gives limits for current harmonics based on even or odd multiples of the harmonic frequency, with the most stringent limit requiring less than 0.3% of rated current [90].

Several publications have explored simulating the flicker output of both one and several devices, with particular focus on mitigating flicker. While the power quality of a single WEC may fail to meet the flicker standards for grid connection, the aggregation of multiple devices smooths the power output from the wave farm and reduces the flicker emissions [9], [84], [92]. In addition, the layout of a WEC farm can further reduce flicker by spacing WECs such that there is no coherence between power outputs of nearby WECs [93].

Introducing an energy storage system can be critical to smooth WEC voltage fluctuations, especially during some powerful sea states. A study [82] compares the life-cycle costs of centralized versus decentralized storage for a WEC with the goal of reducing the flicker severity to $P_{st} = 0.25$. While centralized energy storage systems reduce the life cycle costs, they increase the power fluctuations at the device-level. Another study [94] sizes an energy storage system for a single 700 kW point-absorber WEC using rainflow counting to determine flicker. They

find a significant increase in energy storage capacity to keep voltage variations at 1%, from 0.69 kW at 99% of the time to 1.2 kW at 100% of the time.

Experimental tests of grid-connected WECs are rare, which limits the availability of experimental flicker results [9]. In order to continue testing, researchers have created several wave-to-wire models of WECs which model the entire process from waves to the point of common connection (PCC) with the grid [92]. WEC types considered include the SEAREV pendulum-generator [91] and a permanent-magnet linear generator [95]. Blavette et al. [96] uses the sea-state energy period, complex maximum and minimum output power levels, and a storage time constant to estimate the flicker output of a WEC.

A few studies have considered other power-quality aspects such as harmonics. A study of the propsed integration of a WEC test site in Oregon, United States found that the total harmonic (THD) distortion from a WEC was below the 5% requirement, after a back-to-back converter with STATCOM at the PCC. Another study found current THD for a WEC to be up to 1.01% of the fundamental frequency. Parwal et al. [97] implemented an LCL-filter with a VSC to reduce current harmonics when connecting to the grid. Grid-side control of a WEC can also reduce the reactive consumption of a WEC [98].

4.4 Experimental Setup

The central component of the author's testing is WESRF's hybrid simulation testbed. As an application of hybrid-simulation, this experiment contains both

numerical and physical models. The numerical model represents the waves and power take-off (PTO) effects while they physical component contains an induction machine, a modeled weak grid, and measuring devices. The first subsection, 4.4.1, describes the numerical model of a heaving point absorber WEC following with a description of the physical testbed that reproduces the power output of the WEC and measures power quality.

4.4.1 WEC Dynamics and Modelling

This study models the numerically models the WEC as a point absorber. Compered to the different WEC technologies (see [99]), the point absorber device is one of the simplest WEC concepts. It is easy to manufacture and install, reliable to operate and economical to maintain [100]. The PA considered in this study is a floating structure interacting with surface waves, connected to a PTO system, and moored to the sea-bed. In particular, incident waves induce a heave motion of the structure, $z(t)$, that is damped by an electric generator for power absorption. In contrast to base-load generation, the power output of WECs include the variability of the wave resource causing variable power output on small time scales.

As referenced in Chapter 3.5, (3.2) gives the linear hydrodynamic model of a point absorber. For this study, the Pierson-Moskowitz spectrum generates the input wave [77]. The hydrostatic restoring force acts proportional to the heave motion, $f_h = -s_h z$, where s_h is the hydrostatic stiffness coefficient. Cummins'

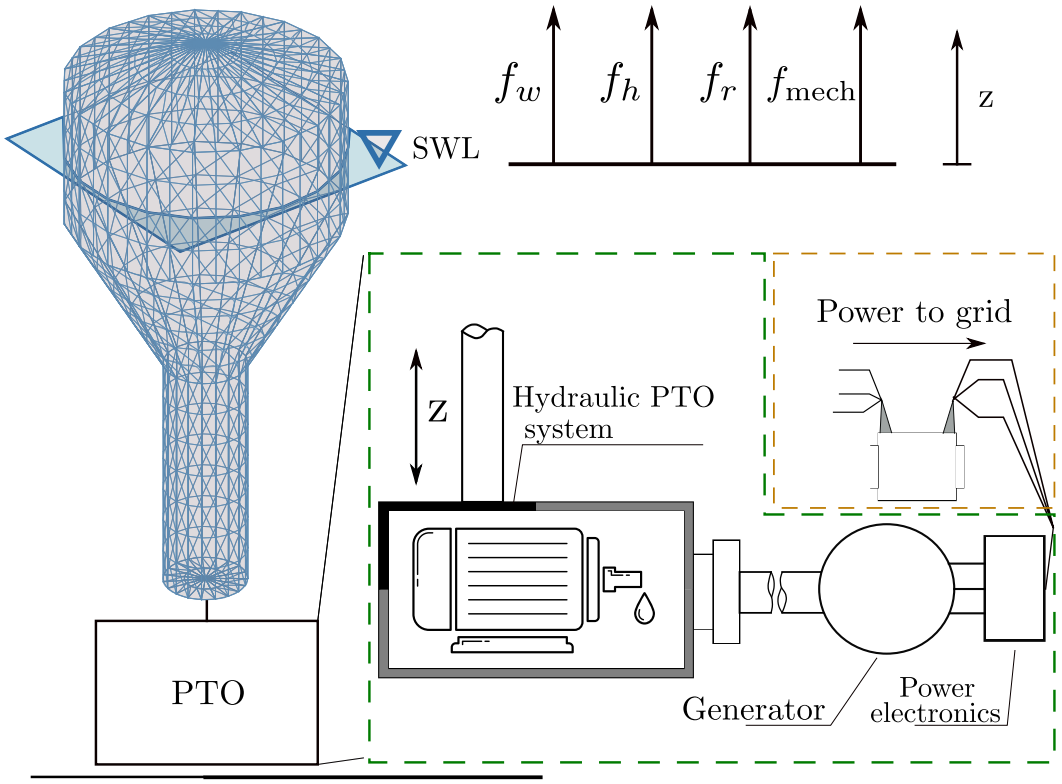

Figure 4.1: Schematic representation of Falnes point absorber power conversion process [77].

equation models the radiation force f_r,

$$f_r(t) = -\left(A_r\ddot{z}(t) + \int h_r(t-\tau)\dot{z}(\tau)\mathrm{d}\tau\right), \tag{4.1}$$

where:

- $\ddot{z}$ corresponds to an inertial increase due to the displacement of the water surrounding the floater, proportional to the floater acceleration in heave,

- A_r is the added-mass coefficient,
- $\dot{z}$ is the floater velocity,
- $h_r(t)$ is the radiation impulse response function.

Boundary element modeling, such as NEMOH or WAMIT, computes the hydrodynamic parameters [101]. These equations combined with (3.3) and (3.2) give the power output for the WEC related to its input wave. Fig 4.1 shows several of the mechanical stages the force on the PTO will go through to rectify the motion such that the that the direction of the motor rotation and torque is always the same [102].

4.4.2 Real-Time Hybrid-Simulation Testbed

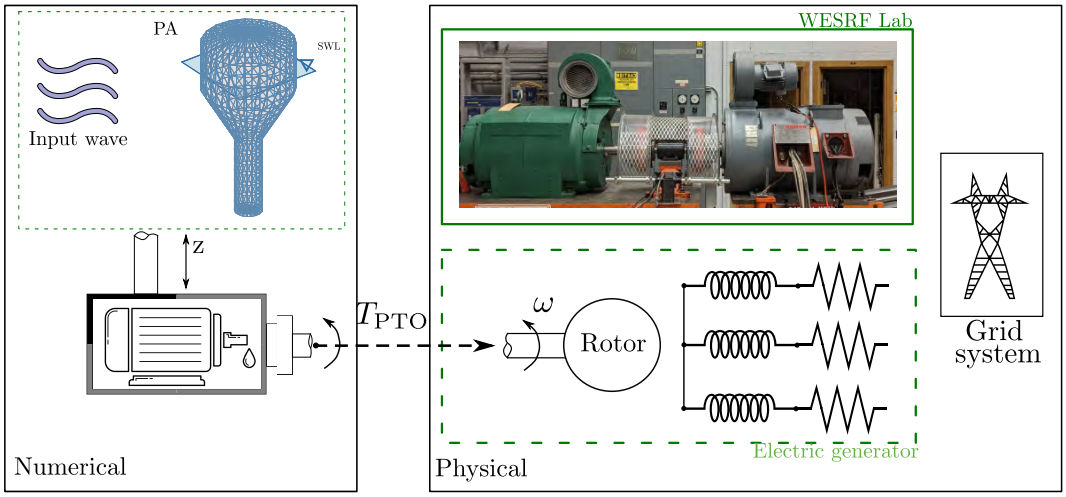

Figure 4.2: Hybrid simulation block diagram: numerical block communicating with the physical testbed in WESRF.

The author couples the numerical model of the point absorber with a physical generator to create the real-time hybrid-simulation testbed. Fig. 4.2 shows the two types of models included in the testbed: 1) The numerical simulation which calculates the torque of the PTO system using the hydrodynamic forces as inputs and 2) the physical motor-generator where the dynomometer (green machine in Fig. 4.2), actuates PTO torque from the numerical model and the electric generator (see gray machine in Fig. 4.2) which turns the mechanical torque into electrical power on the representative weak grid.

For this experiment, a 80 kW, six-pole, squirrel-cage induction machine serves as the three-phase generator. The generator's stator windings connect to a representative weak grid consisting a group of reactors with a total reactance of $X_L = j0.7163\ \Omega$, or 25 % per-unit. These reactors connect to the grid through a motor starter and three 480-V autotransformers, which can be set to different voltage values at 60 Hz.

A three phase inverter duty induction motor whose shaft is mechanically coupled to the grey generator's output shaft emulates PTO output from the point absorber by applying torque to the grey machine. The ASD-300 Kenetech drive ensures that the green motor applies the requested speed or torque at its output. A user can give the Kenetech drive speed or torque commands via RS-232 protocol. In addition to applying torque or speed to the physical testbed, the ASD-300 also receives torque, speed, and power information from the dynamometer and relays it to the target computer, acting as the interface between the numerical and physical components in Fig. 4.2.

The numerical modeling as well as data acquisition and control of the equipment occurs in Matlab Simulink Real-Time and runs on a Speedgoat Real-Time Performance Target Machine. Three differential voltage probes and three current probes provide respective line-to-neutral voltage and line current measurements for the target machine to read and synchronize with the numerical model. In addition, Speedgoat target machine sends torque commands to the ASD-300 based on the output of the WEC numerical model.

4.5 Results

4.5.1 WEC Power

This study uses modeled waves from three different sea states as inputs to the WEC. Significant wave heights range from 0.3 to 2.1 meters and wave periods span 5.5 to 7.5 seconds. These ranges represent the range of significant wave heights and wave periods measured by NOAA buoy 42019. The ASD-300 drive commanded the induction motor to apply 10.5 minutes worth of torque values to the PTO generator. The physical testbed setup is shown in Fig. 4.3 including labels for each component. Table 4.1 gives the maximum and average values of the applied torque for each sea state. IEC 62600-30 requires five tests per sea-state, which change based on the specific wave spectrum applied. This table reports maximum and average torque values for each of the five tests.

In general, while maximum torque values change based on the specific applied

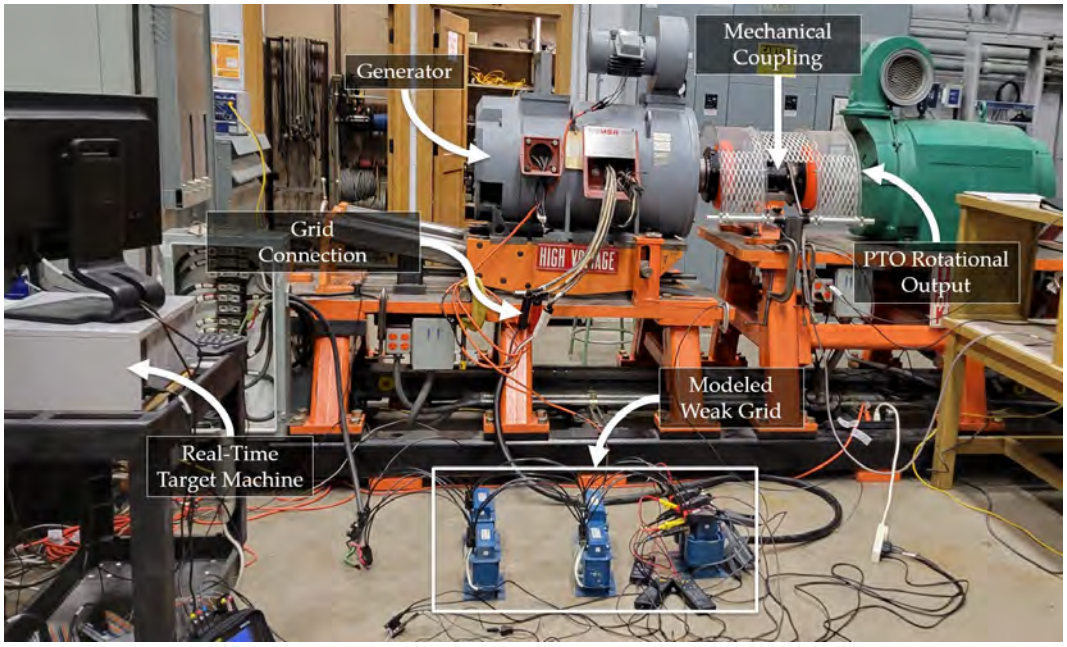

Figure 4.3: WESRF Hybrid Simulation Test Bed configured for flicker and current harmonic measurement. The Speedgoat Real-Time Target Machine simulates the numerical system and interfaces with the physical control and sensors.

Table 4.1: Maximum and Average Input PTO Torque for Given Sea States

Sea State:	2.1 m, 7.5 s		1.0 m, 6.4 s		0.3 m, 5.5 s	
Test #	$\mathbf{T_{max}}$ (N)	$\mathbf{T_{avg}}$ (N)	$\mathbf{T_{max}}$ (N)	$\mathbf{T_{avg}}$ (N)	$\mathbf{T_{max}}$ (N)	$\mathbf{T_{avg}}$ (N)
1	192.3	46.71	192.2	47.10	192.5	37.72
2	192.2	42.76	136.7	32.98	172.9	37.42
3	148.4	40.61	170.4	35.27	162.5	35.37
4	167.7	39.22	154.6	32.66	160.7	36.77
5	167.5	41.30	151.2	31.27	169.5	39.91

wave spectrum, higher-energy sea states with higher significant wave heights and longer wave periods result in higher average torque applied to the PTO, which follows expected ocean trends.

Table 4.2: Max and Mean Electrical Power Generation for Given Sea States

Sea State:	2.1 m, 7.5 s		1.0 m, 6.4 s		0.3 m, 5.5 s	
Test #	$\mathbf{P_{max}}$ (kW)	$\mathbf{P_{avg}}$ (kW)	$\mathbf{P_{max}}$ (kW)	$\mathbf{P_{avg}}$ (kW)	$\mathbf{P_{max}}$ (kW)	$\mathbf{P_{avg}}$ (kW)
1	28.50	6.524	27.93	6.258	28.22	4.848
2	28.89	5.837	19.82	3.996	25.12	4.650
3	21.92	5.356	24.53	4.296	23.15	4.292
4	24.79	5.043	22.25	3.866	23.18	4.465
5	23.99	5.281	21.77	3.597	24.67	4.912

Running at a constant, rated 1200 RPM, the induction generator produced power by damping the applied torque shown in Table 4.1. The author calculates the electrical power at the point of connection with the modeled weak grid based on the sum of the line-to-neutral voltage and current readings from probes at the interconnection between the generator and the reactors modeling the weak grid for each phase. Equation (4.2) gives the calculation for three-phase instantaneous power:

$$P_{inst} = \sum_{p=A,B,C} V_p \cdot I_p \tag{4.2}$$

where:

- P_{inst} is the instantaneous power,
- V_p is the line-to-neutral voltage for phase p,
- I_p is the current for phase p.

Table 4.2 gives the maximum and average power generated by the PTO for each give sea state. Similar to the torque, higher-energy sea-states produce higher values for average power.

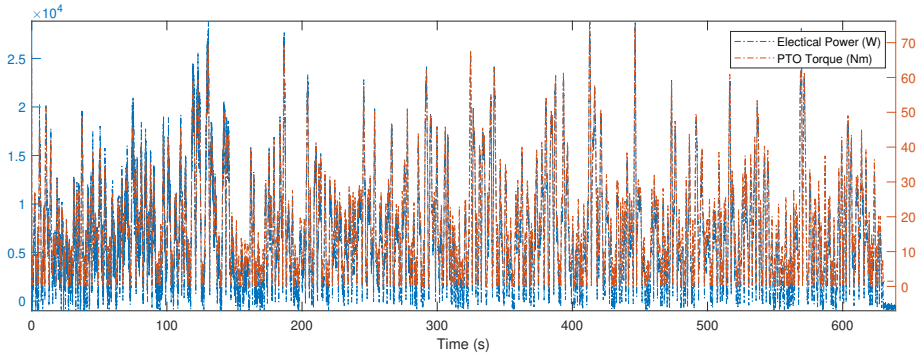

Figure 4.4: Commanded PTO torque (right axis) and electrical power generated from the given mechanical torque (left axis).

For a more in-depth look at the power and torque, Fig. 4.4 shows the full 10.5 minutes of the hybrid simulation for the 2.1 m, 7.5 s sea state. In general, peak torque values correspond to peak generation, with both torque and power following the variable wave resource which changes on the order of seconds. To give a clearer picture of the the torque and power of the system, Fig. 4.5 shows

a 100 second sample of the data in Fig. 4.4, from 250 to 350 seconds into the simulation. Some of the apparent variation in power is caused by measurement noise as the applied torque is a reference value and the electrical power comes from physical measurements. These large fluctuations in output power can cause variations in the power quality at the point of connection to the grid.

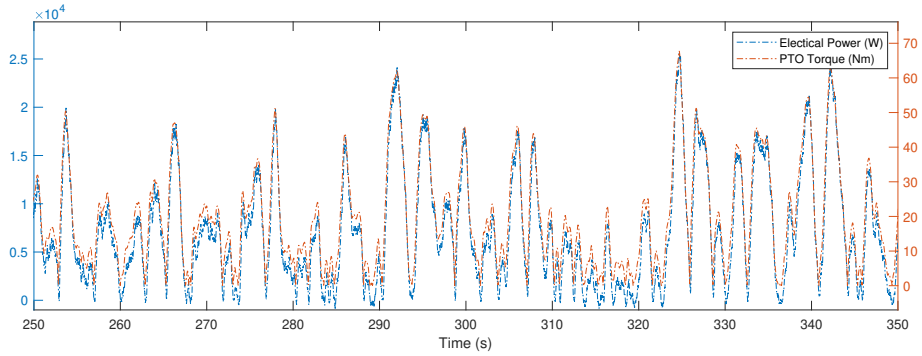

Figure 4.5: A sample of PTO torque and electrical power for 100 seconds of simulation time, from 250-350 seconds.

4.5.2 Flicker

Starting with the power quality metric of flicker, the large changes in power generation can affect the output voltage at the point of connection. For example, the voltage can vary from 231.4 V to 252.1 V RMS, line-to-neutral in the sample power results shown in Fig. 4.4 with a 2.1 m, 7.5 s sea state. These frequent voltage fluctuations cause the flicker severity to increase. Figure 4.6 shows the instantaneous flicker values for each phase for the entire duration of this specific case. Matlab Simulink's Digital Fickermeter block set at a sample time of 100 μs and the mea-

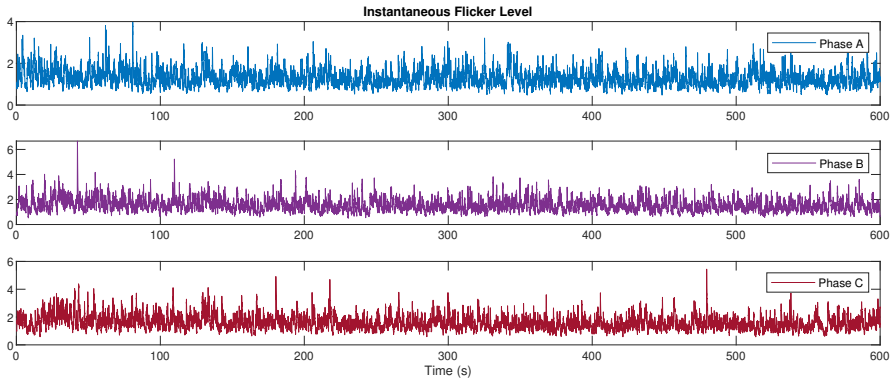

Figure 4.6: Instantaneous flicker measurements for each of the three phase connections to the weak grid with a 2.1 m, 7.5 s sea state.

sured RMS voltage value for each phase produced these intensity results based on the voltage measurements.

Table 4.3: Maximum Short-term Flicker Severity Per Phase and Sea State

Sea State	0.3 m, 5.5 s	1.0 m, 6.4 s	2.1 m, 7.5 s
Phase		**P_{st}**	
A	1.0539	1.0779	1.0902
B	1.2432	1.2375	1.2300
C	1.2353	1.2262	1.2586

Matlab's *power_flicker* function computes the flicker severity based on the instantaneous flicker such as the sample shown in Fig. 4.6. Table 4.3 shows the maximum short-term flicker severity values for each phase and sea-state. As expected for connecting a single WEC to a weak grid, the flicker measurement is above even the most lenient flicker requirements which require P_{st} to be under 1.0. These results are similar to previously reported values for individual WEC devices. Armstrong, Cotilla-Sanchez, and Kovaltchouk [9] report P_{st} values ranging from

1.3042 to 1.8207, Nambiar et al. [93] also estimates flicker values from 0.93 to 1.42 for a single WEC in non-optimal conditions, Blavette et al. [19] finds a maximum P_{st} of 0.87 and Rasool et al. [95] calculates flicker values as high as 1.0924 for a linear generator on a weak grid. These flicker severity values can be reduced by either adding energy storage or by aggregating multiple WECs together to smooth out the power output.

4.5.3 Current Harmonics, Interharmonics and Higher Harmonics

In addition to requiring limited variation in the voltage at the point of connection, a grid connection with good power quality also requires voltage and current waveforms to be purely sinusoidal with no higher harmonic components adjusting the shape of the waveform. Harmonic issues are most common when the grid connection involves switching or power-electronics, as might occur in a controllable WEC. For this study's case the WEC is an uncontrollable output directly applied to the electrical grid. In this case, the induction generator's output is less susceptible to harmonic violations. Additionally, the generator and power electronics will have a greater effect on current harmonics than the variable power output.

To get the harmonic information from the instantaneous current measurements, the author applies the Fast Fourier transform (FFT) function in Matlab to the measurements. The FFT transforms measured signals from the time-domain to the frequency-domain. In the frequency domain it is possible to visualize other frequency components that could distort the sinusoidal nature of AC current and

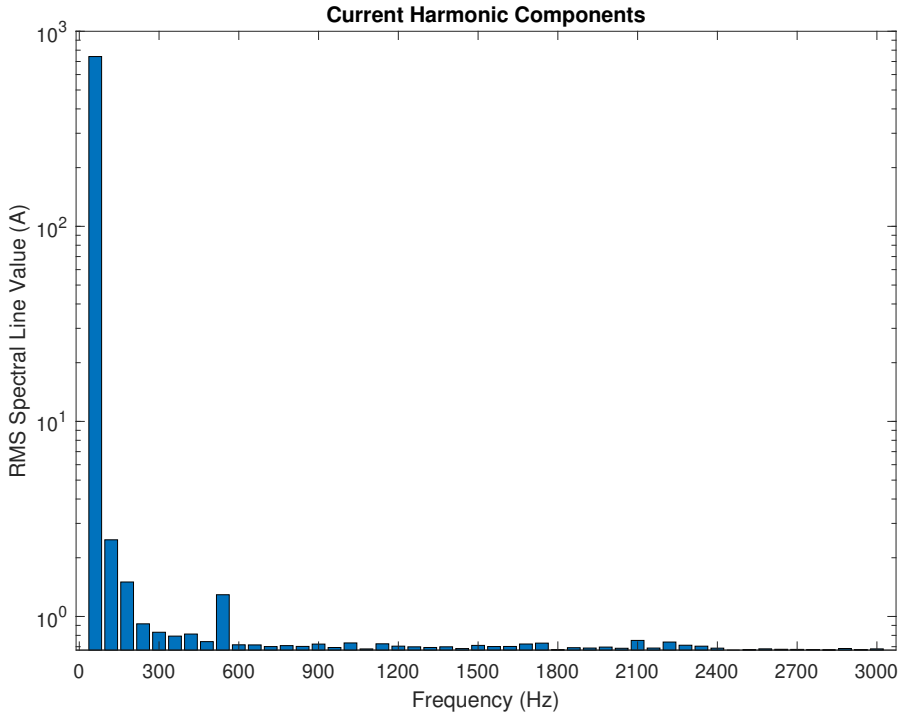

Figure 4.7: Individual harmonic components of the current at the point of connection with the WEC for 95% of rated power and a sea state of 2.1 m, 7.5 s.

voltage. For this study, the author used the IEC 61000-4-7 standard to bin the frequency components. Fig. 4.7 shows the harmonic components of the WEC's current output at the point of connection for a test with 95% rated power and a sea state of 2.1 m, 7.5 s. Note that for Fig. 4.7 the y-axis is logarithmic, as the higher-frequency components are considerably smaller than the primary harmonic value at 60 Hz. This trend carries over into the remaining tests for varying sea-states and power levels.

IEEE standard 1547 suggests limits based on the order of the harmonics, which are split into odd and even harmonics. For the purpose of this study we will compare the acceptability of WEC power quality based on IEEE 1547. Table 4.4 lists the maximum odd harmonic components in percentage of rated current. The most stringent requirement for odd harmonics is that harmonics 35-50 must be lower than 0.30%, although earlier harmonics such as 1-11 may be as high as 4.0%. In this case all odd harmonics are lower than the most stringent case.

IEEE 1547 gives similar requirements for even harmonics as percentages of rated current. For the even harmonics, the second harmonic must be under 1.0%, the fourth under 2.0% and the sixth under 3.0%; otherwise the same harmonic restrictions apply. In this case all harmonics after the second harmonic are less than the most stringent requirement of 0.30% with the second order harmonic still below the required 1.0%.

IEC Standard 61000-4-7 and IEC 62600-30 use total harmonic current distortion (THC) to summarize the frequency information into a single metric. THC compares the value of each higher order harmonic with the fundamental harmonic

Table 4.4: Maximum Odd Current Harmonic in Percent of Rated Current for Sampled Sea States

Sea State	0.3 m, 5.5 s	1.0 m, 6.4 s	2.1 m, 7.5 s
Harmonic	**Current Harmonic of Rated Current (%)**		
3	0.2689	0.2590	0.2562
5	0.1528	0.1506	0.1460
7	0.1426	0.1436	0.1426
9	0.2391	0.2254	0.2226
11	0.1329	0.1353	0.1320
13	0.1311	0.1283	0.1382
15	0.1358	0.1330	0.1263
17	0.1263	0.1299	0.1298
19	0.1284	0.1282	0.1271
21	0.1269	0.1264	0.1314
23	0.1266	0.1281	0.1299
25	0.1290	0.1297	0.1296
27	0.1755	0.1395	0.1793
29	0.1286	0.1309	0.1298
31	0.1243	0.1270	0.1283
33	0.1227	0.1244	0.1244
35	0.1262	0.1334	0.1286
37	0.1292	0.1362	0.1320
39	0.1257	0.1263	0.1278
41	0.1243	0.1244	0.1295
43	0.1295	0.1265	0.1265
45	0.1241	0.1220	0.1270
47	0.1263	0.1283	0.1223
49	0.1226	0.1231	0.1265

Table 4.5: Maximum Even Current Harmonic in Percent of Rated Current for Sampled Sea States

Sea State	0.3 m, 5.5 s	1.0 m, 6.4 s	2.1 m, 7.5 s
Harmonic	**Current Harmonic of Rated Current (%)**		
2	0.3658	0.3676	0.3699
4	0.1540	0.1537	0.1645
6	0.1372	0.1372	0.1341
8	0.1307	0.1317	0.1303
10	0.1310	0.1322	0.1310
12	0.1242	0.1242	0.1328
14	0.1290	0.1288	0.1296
16	0.1248	0.1230	0.1325
18	0.1259	0.1222	0.1297
20	0.1226	0.1218	0.1277
22	0.1235	0.1214	0.1265
24	0.1278	0.1331	0.1357
26	0.1258	0.1253	0.1272
28	0.1471	0.1564	0.1480
30	0.1252	0.1233	0.1287
32	0.1258	0.1263	0.1232
34	0.1270	0.1218	0.1324
36	0.1318	0.1248	0.1362
38	0.1245	0.1224	0.1300
40	0.1215	0.1218	0.1253
42	0.1240	0.1226	0.1279
44	0.1247	0.1212	0.1240
46	0.1238	0.1229	0.1239
48	0.1198	0.1225	0.1256
50	0.1202	0.1204	0.1233

Table 4.6: Maximum Total Harmonic Current Distortion for Sea States and Operating Power

Sea State	0.3 m, 5.5 s	1.0 m, 6.4 s	2.1 m, 7.5 s
% $\mathbf{P_{rated}}$		**THC (%)**	
95	0.9044	0.8993	0.8691
85	0.8827	0.8240	0.8953
75	0.9248	0.8622	0.9201
65	0.9398	0.8893	0.9337
55	0.9570	0.9303	0.9446
45	0.9719	0.9577	0.9797
35	0.9840	0.9808	1.0028
25	0.9947	0.9831	0.9945
15	0.9899	1.0000	1.0109
5	1.00895	0.9920	1.0008

of 60 Hz and sums together the resulting values, as shown in (4.3)

$$\text{THC} = \frac{\sqrt{\sum_{h=2}^{50} I_h^2}}{I_r} \times 100 \tag{4.3}$$

where:

- I_h is the subgrouped RMS current harmonic of harmonic order h,
- I_r is the rated current of the WEC.

Table 4.6 reports the maximum THC values for each bin of rated power operation and the three sea states. In general, THC increases as the WEC power decreases; however, all THC values are below the threshold of 5.0% THC given by IEEE 1547. These THC values match similarly reported maximum THC values

Table 4.7: Maximum Total Harmonic Voltage Distortion for Sea States and Operating Power

Sea State	0.3 m, 5.5 s	1.0 m, 6.4 s	2.1 m, 7.5 s
% $\mathbf{P_{rated}}$		**THD (%)**	
95	0.09115	0.09013	0.08849
85	0.09105	0.09096	0.09152
75	0.09098	0.09126	0.09156
65	0.09117	0.09109	0.09162
55	0.09130	0.09093	0.09154
45	0.09123	0.09094	0.09132
35	0.09120	0.09083	0.09128
25	0.09106	0.09065	0.09133
15	0.09119	0.09056	0.09085
5	0.091146	0.09046	0.09025

of 1.8% or 0.91% by [9] and [95]. The total harmonic distortion of voltage (THD) can also be found using a formula similar to (4.3):

$$\text{THD} = \frac{\sqrt{\sum_{h=2}^{50} V_h^2}}{V_r} \times 100 \tag{4.4}$$

where:

- V_h is the subgrouped RMS voltage harmonic of harmonic order h,
- V_r is the rated voltage of the WEC.

The THD results for each bin of rated power operation and the three sea states are shown in Table 4.7. In contrast to the current results, these sine waves are even more ideal with very limited additional harmonics.

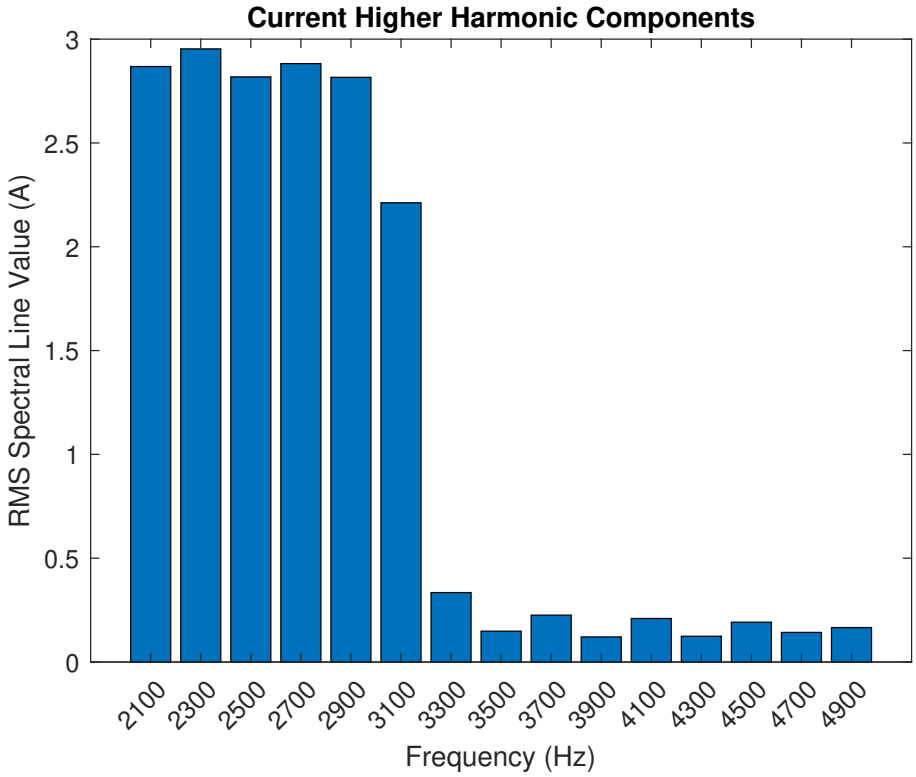

Figure 4.8: Individual higher harmonic components (2.1-4.9 kHz) of the current at the point of connection with the WEC for 95% of rated power and a sea state of 2.1 m, 7.5 s.

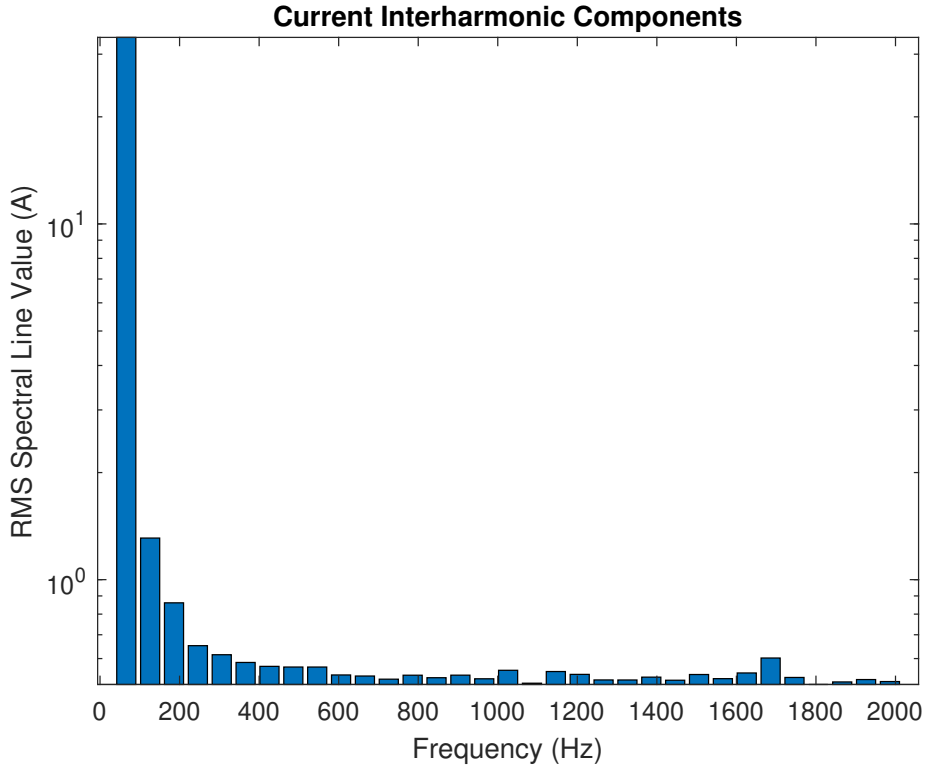

Figure 4.9: Interharmonic components up to 2 kHz of the current at the point of connection with the WEC for 95% of rated power and a sea state of 2.1 m, 7.5 s.

In addition to the summary metric of total harmonic distortion, IEC 61000-4-7 also requires one to measure higher-order harmonics defined as harmonics between 2 kHz and 9 kHz. Similar to the current harmonic components, higher harmonics is grouped into bands of 200 Hz with a center frequencies from 2.1 kHz to 8.9 kHz. Fig. 4.8 shows the higher harmonic components for the WEC operating at 95% of rated power and an input sea state of 2.1 m, 7.5 s. For this case, the components higher than 5 kHz were too small to report. For the uncontrolled WEC, the lack of switching or power electronics kept higher-order frequency components to a minimum.

While current harmonics, higher harmonics and THC look at specific harmonic frequency components, several additional frequency components fall in between these discrete harmonic frequencies, known as interharmonics. IEC 61000-4-7 sums these values and reports the sum between each discrete harmonic. Fig. 4.9 displays the interharmonic components for the WEC operating at 95% of rated power and an input sea state of 2.1 m, 7.5 s. Note that for Fig. 4.7 the y-axis is logarithmic, as the higher-frequency interharmonics are considerably smaller than those between the first four harmonics.

4.5.4 Voltage Drop Response

As a grid-connected generation source, the WEC will be subject to voltage deviations at the electrical grid. In the case of a voltage drop, the WEC will need to ride-through the voltage drop and continue to produce usable power for the

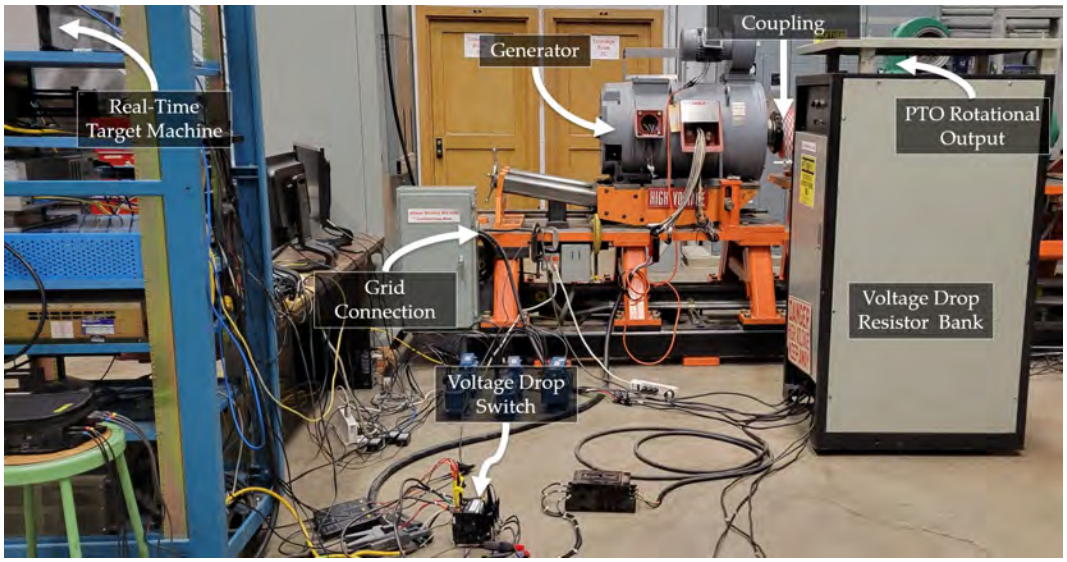

Figure 4.10: WESRF Hybrid Simulation Test Bed configured for grid voltage drop connection tests. The Speedgoat Real-Time Target Machine simulates the numerical system and interfaces with the physical control and sensors.

electrical grid. For this study, the author implemented a 0.18 p.u. voltage drop, dropping the 480.0 V usually seen at the point of connection to the WEC to 393.6 V. A voltage divider consisting of a 1.09 Ω resistor in series with the generator and a shunt resistance of 5.06 Ω. To control the switching of the shunt resistance such that the voltage drop happens with the 0.5 second timing specified by IEC 62600-30, a relay operated by the Speedgoat real-time target machine synchronizes the WEC testing and voltage drops. The setup for this test is shown in Fig. 4.10 For this experiment, the author applied a sea-state of 2.1 m, 7.5 s at rated power. Voltage drops of 0.18 p.u. occurred 10 seconds and 30 seconds into the simulation.

Fig. 4.11 shows the voltage response of the grid-connected WEC to the 0.18 p.u. voltage drops. Fig. 4.12 and Fig. 4.13 show the current and power respective

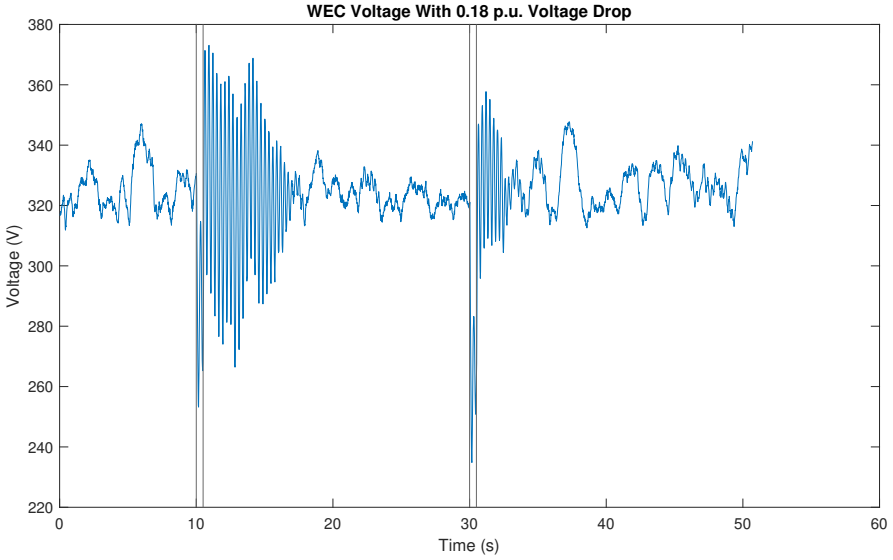

Figure 4.11: WEC voltage with two 0.18 p.u. voltage drops at T=10s and T=30s. Vertical lines mark the start and stop of the voltage drops. WEC is at rated power with a sea state of 2.1m, 7.5s.

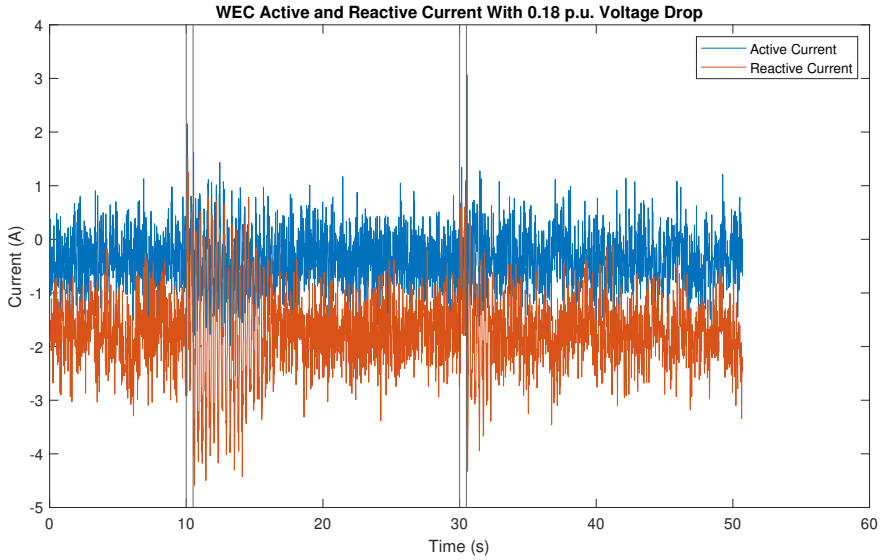

Figure 4.12: WEC active and reactive current with two 0.18 p.u. voltage drops at T=10s and T=30s. Vertical lines mark the start and stop of the voltage drops. WEC is at rated power with a sea state of 2.1m, 7.5s.

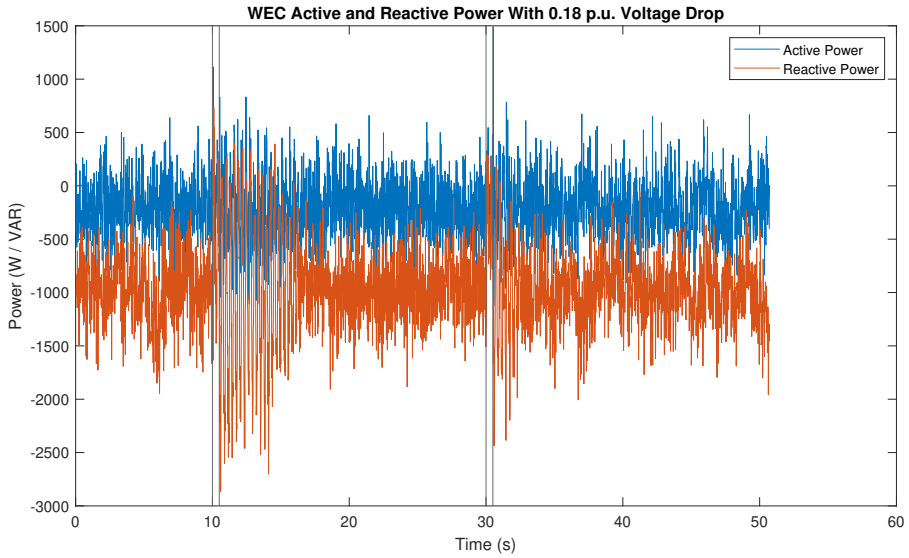

Figure 4.13: WEC active and reactive power with two 0.18 p.u. voltage drops at T=10s and T=30s. Vertical lines mark the start and stop of the voltage drops. WEC is at rated power with a sea state of 2.1m, 7.5s.

responses to the voltage drops. While the duration of the two voltage drops is identical, the torque on the PTO generator changed due to the variable wave input. The first drop coincided with a large decrease in wave power, followed by a sharp increase in wave power as the voltage drop subsided. This combination caused longer oscillations than the second voltage drop, which occurred during less volatile wave conditions.

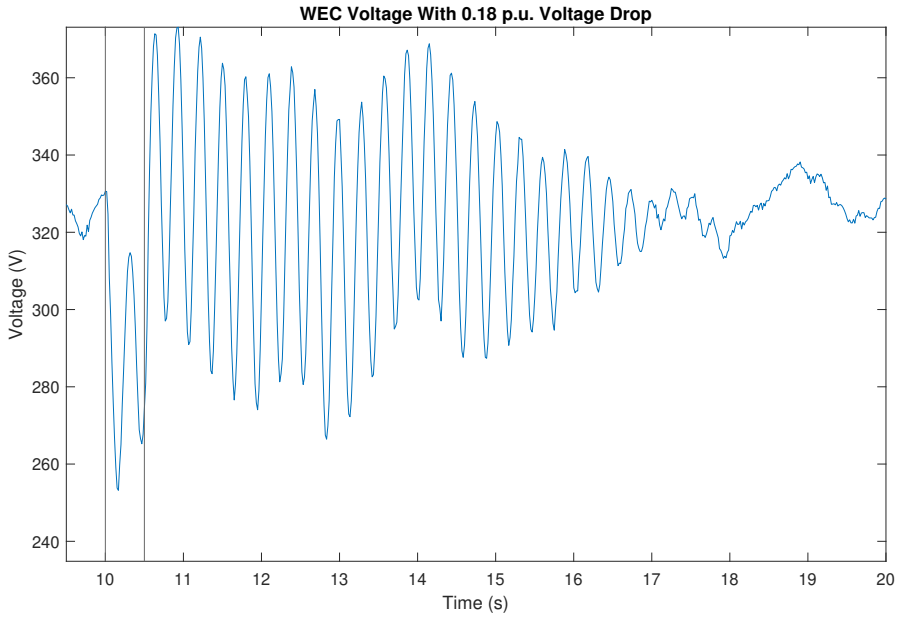

Figure 4.14: Sub-plot of WEC voltage with a 0.18 p.u. voltage drops at T=10s. Vertical lines mark the start and stop of the voltage drop. WEC is at rated power with a sea state of 2.1m, 7.5s.

Fig. 4.14 shows the voltage response of the grid-connected WEC to the first 0.18 p.u. voltage drop at 10 seconds. Fig. 4.15 and Fig. 4.16 show the current and power respective responses to the voltage drop. The combination of large changes

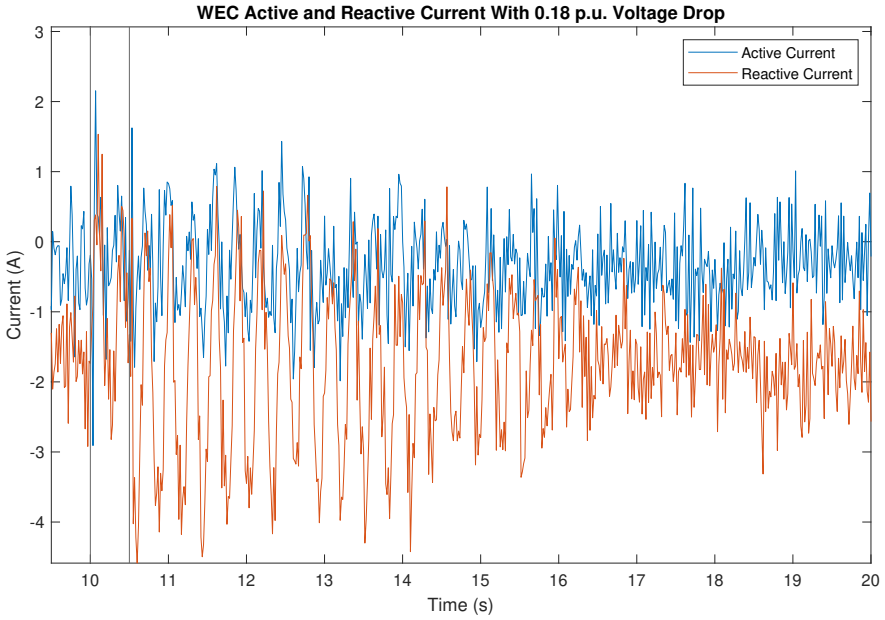

Figure 4.15: Sub-plot of WEC active and reactive current with a 0.18 p.u. voltage drops at T=10s. Vertical lines mark the start and stop of the voltage drop. WEC is at rated power with a sea state of 2.1m, 7.5s.

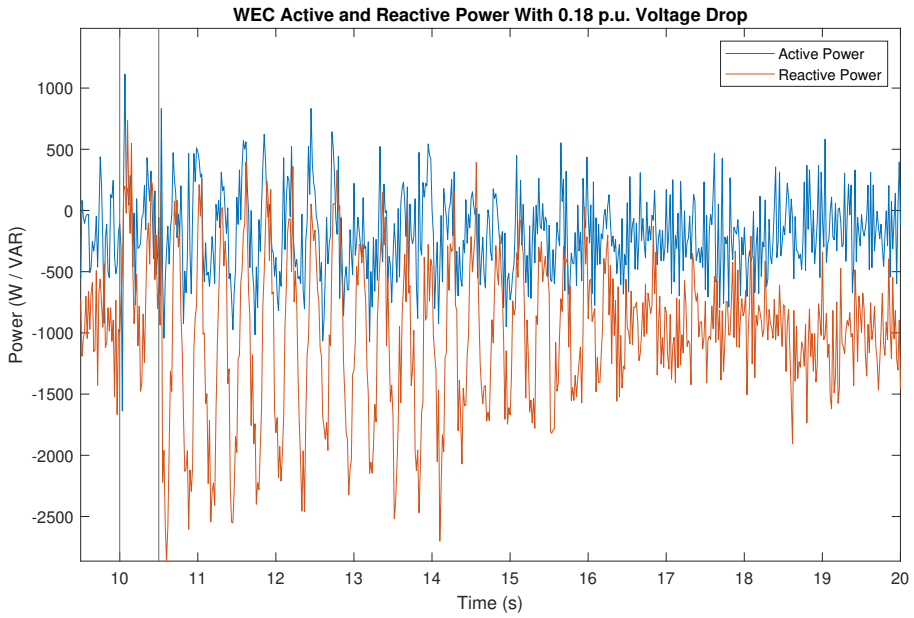

Figure 4.16: Sub-plot of WEC active and reactive power with a 0.18 p.u. voltage drops at T=10s. Vertical lines mark the start and stop of the voltage drop. WEC is at rated power with a sea state of 2.1m, 7.5s.

in wave conditions with the voltage drop causes significant oscillations which last from 10.5 seconds to 16.9 seconds. While causing a significant disturbance to the voltage, the generator did continue to operate through the voltage depression.

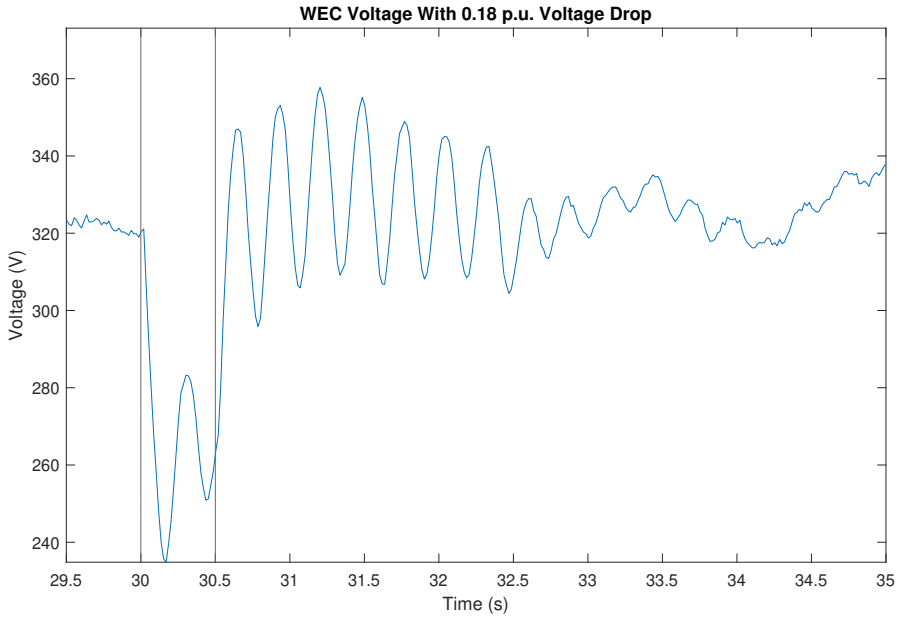

Figure 4.17: Sub-plot of WEC voltage with a 0.18 p.u. voltage drops at T=30s. Vertical lines mark the start and stop of the voltage drop. WEC is at rated power with a sea state of 2.1m, 7.5s.

The voltage response for the grid-connected WEC to the second 0.18 p.u. voltage drop at 30 seconds, shown in Fig. 4.14 has considerably less oscillations and recovers quicker. Fig. 4.15 and Fig. 4.16 show the current and power respective responses to the voltage drop. In this case, compared to the first voltage drop, the oscillations only last a few seconds from 30.5 seconds to 32.5 seconds. In both cases the added series resistance of the voltage divider needed to create the given

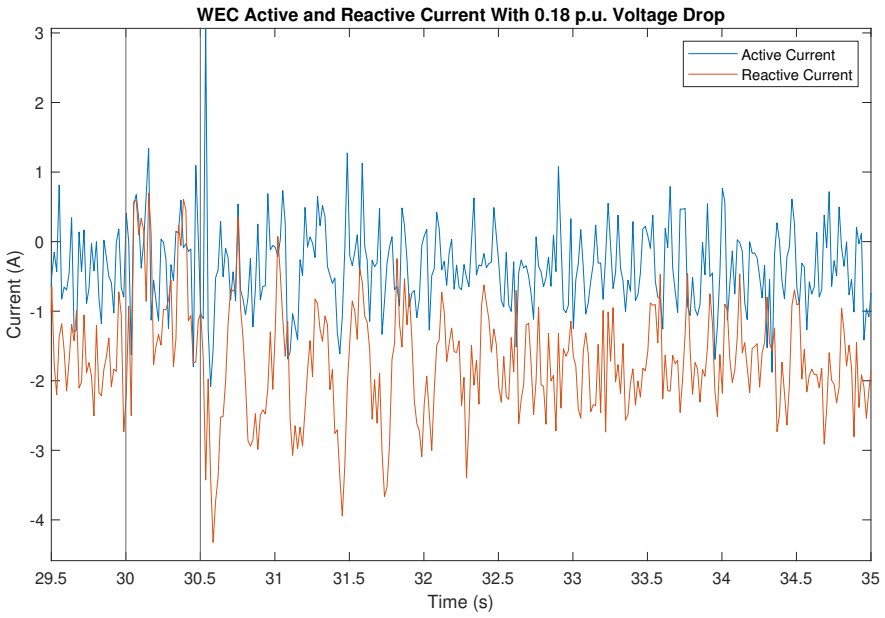

Figure 4.18: Sub-plot of WEC active and reactive current with a 0.18 p.u. voltage drops at T=30s. Vertical lines mark the start and stop of the voltage drop. WEC is at rated power with a sea state of 2.1m, 7.5s.

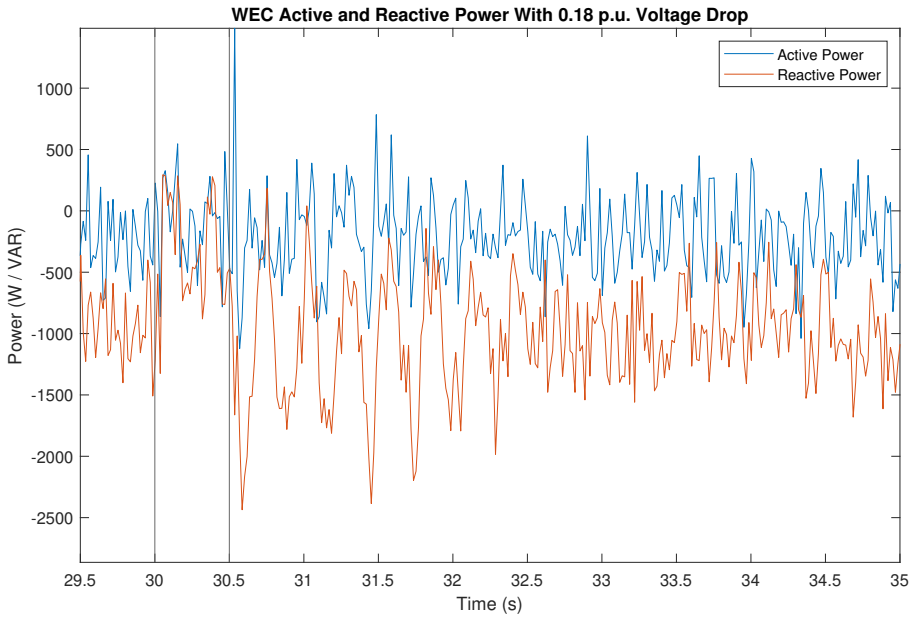

Figure 4.19: Sub-plot of WEC active and reactive power with a 0.18 p.u. voltage drops at T=30s. Vertical lines mark the start and stop of the voltage drop. WEC is at rated power with a sea state of 2.1m, 7.5s.

voltage drop decreased the generator's voltage such that the generator primarily acted as a motor rather than a generator. However, when the switching of the shunt resistor created additional drops in grid voltage, the generator consistently provided power to the grid rather than motoring in an attempt to increase the voltage.

4.6 Conclusion

This chapter demonstrated an application of the real-time hybrid-simulation testbed described in [21] to the measurement of power quality from a WEC device. In addition to examining the average power from a WEC, we also used the voltage signals to compute the flicker of an individual, uncontrolled WEC device. The short-term flicker severity values exceeded the most lenient standards for grid-connection. With these flicker values, grid power quality standards prohibit the WEC in this study to be connected to the electrical grid. Still, this matches other reported flicker values a single grid-connected WEC and highlights the need for storage or aggregation to smooth out the WEC's flicker.

In examining the current harmonics, interharmonics and higher harmonics, the author noted that WEC generation does not appear to have a detrimental effect on the harmonics at the point of connection. For all cases, the current harmonics were below the values required by IEEE standards. Since this study used an uncontrolled WEC, the induction generator serving as the WEC's PTO was directly connected to the grid. As induction generators naturally produce sinusoidal cur-

rents, the author expected this WEC to produce currents with limited harmonics. Controlling the WEC's PTO with a AC-AC converter introduces power-electronics, switching and PWM. Adding control will significantly increase the current harmonics produced by the WEC. This chapter also demonstrated the effect a voltage drop in the electrical grid has on a WEC. The WEC stayed connected to the electrical grid, but did introduce oscillations as it re-synchronized after the voltage drop.

Future work looks to address the smoothing of power and reduction of flicker through combining multiple WEC devices before the point of connection as well as adding a second variable-frequency drive to control the generator of the testbed to investigate the effects on the power grid of various PTO-control strategies.

Chapter 5: Conclusion

This dissertation examined multiple ways for utility operators to analyze the electrical grid to ensure system reliability and quality. By combining reactive reserve assessment with Voltage Control Areas the author quickly and accurately determined the VQ-margin at critical buses. This method of finding an optimal VCA clustering solution for a given case was also applied to determine loop flows from a connected Wave Energy Converter farm. The variability of WECs causes changes in the transmission system's loop flows as shown by the analysis of a year-long collection of hourly quasi-steady-state scenarios developed for the ACTIVSg2000 synthetic case. Smaller, distributed WEC farms created less effects on loop flows than single, large WEC farms. Additionally, the connection of a WEC even within a small geographic area could greatly affect increase the loop flows on the transmission system. Future work in VCAs and loop flows could consider expanding the locations from Texas to the Western US for better wave resources.

Moving from the transmission-level to the device level, this dissertation also examined the power quality of a grid-connected WEC using WESRF's hybrid-simulation testbed. Testing confirmed that as expected, the high short-term flicker severity values would cause power quality issues and require mitigation methods. Still, the results matched previously simulated results, highlighting the usefulness of hybrid-simulation for validating modeled results. This dissertation also presents

the results from current harmonic and voltage drop testing, expanding the available data for experimental WEC power quality data. Adding control of the WEC's PTO generation through a variable-frequency drive would allow for greater grid-integration testing and validation of existing control techniques.

Bibliography

[1] J. Modarresi, E. Gholipour, and A. Khodabakhshian, "A comprehensive review of the voltage stability indices," *Renewable and Sustainable Energy Reviews*, vol. 63, pp. 1–12, Sep. 2016. DOI: 10.1016/j.rser.2016.05.010.

[2] P. Kessel and H. Glavitsch, "Estimating the voltage stability of a power system," *IEEE Power Engineering Review*, vol. PER-6, no. 7, pp. 72–72, 1986. DOI: 10.1109/MPER.1986.5527889.

[3] P. Guimarães, U. Fernandez, T. Ocariz, F. W. Mohn, and A. C. Z. de Souza, "Qv and pv curves as a planning tool of analysis," in *2011 4th International Conference on Electric Utility Deregulation and Restructuring and Power Technologies (DRPT)*, 2011, pp. 1601–1606. DOI: 10.1109/DRPT.2011.5994153.

[4] S. D. Naik, M. K. Khedkar, and S. S. Bhat, "On critical mode of bifurcation point and loadability in shunt compensated multi-bus power system," in *2011 International Conference on Power and Energy Systems*, 2011, pp. 1–6. DOI: 10.1109/ICPES.2011.6156653.

[5] Manjaree Pandit, Laxmi Srivastava, and Vijay Singh, "Identification and ranking of weak buses using modified counterpropagation neural network,"

in *2006 IEEE Power India Conference*, 2006, 7 pp.-. DOI: 10.1109/POWERI.2006.1632531.

[6] H. H. Happ, "Diakoptics—the solution of system problems by tearing," *Proceedings of the IEEE*, vol. 62, no. 7, pp. 930–940, Jul. 1974. DOI: 10.1109/PROC.1974.9545.

[7] R. G. Coe, S. Ahn, V. S. Neary, P. H. Kobos, and G. Bacelli, "Maybe less is more: Considering capacity factor, saturation, variability, and filtering effects of wave energy devices," *Applied Energy*, vol. 291, p. 116 763, 2021, ISSN: 0306-2619. DOI: https://doi.org/10.1016/j.apenergy.2021.116763. [Online]. Available: https://www.sciencedirect.com/science/article/pii/S0306261921002701.

[8] J. Khan, D. Leon, A. Moshref, S. Arabi, and G. Bhuyan, "Network security assessments for integrating large-scale tidal current and ocean wave resources into future electrical grids," *Proceedings of the IEEE*, vol. 101, no. 4, pp. 956–977, 2013. DOI: 10.1109/JPROC.2013.2238491.

[9] S. Armstrong, E. Cotilla-Sanchez, and T. Kovaltchouk, "Assessing the impact of the grid-connected pacific marine energy center wave farm," *IEEE Journal of Emerging and Selected Topics in Power Electronics*, vol. 3, no. 4, pp. 1011–1020, 2015. DOI: 10.1109/JESTPE.2015.2429577.

[10] B. Johnson and E. Cotilla-Sanchez, "Estimating the impact of ocean wave energy on power system reliability with a well-being approach," *IET Re-*

newable Power Generation, vol. 14, Dec. 2019. DOI: 10.1049/iet-rpg.2019.0567.

[11] I. Moazzen, B. Robertson, P. Wild, A. Rowe, and B. Buckham, "Impacts of large-scale wave integration into a transmission-constrained grid," *Renewable Energy*, vol. 88, pp. 408–417, 2016, ISSN: 0960-1481. DOI: https://doi.org/10.1016/j.renene.2015.11.049. [Online]. Available: https://www.sciencedirect.com/science/article/pii/S0960148115304705.

[12] A. Trueworthy and B. DuPont, "The wave energy converter design process: Methods applied in industry and shortcomings of current practices," *Journal of Marine Science and Engineering*, vol. 8, no. 11, 2020, ISSN: 2077-1312. [Online]. Available: https://www.mdpi.com/2077-1312/8/11/932.

[13] S. Hanif, S. Bhattacharya, V. Chalishazar, *et al.*, "Storage requirements for grid integration of marine renewable energy - a parametric study," in *2021 IEEE Power and Energy Society Innovative Smart Grid Technologies Conference (ISGT)*, 2021, pp. 01–05. DOI: 10.1109/ISGT49243.2021.9372165.

[14] W. Wu and C. Wong, "Facts applications in preventing loop flows in interconnected systems," in *2003 IEEE Power Engineering Society General Meeting (IEEE Cat. No.03CH37491)*, vol. 1, 2003, 170–174 Vol. 1. DOI: 10.1109/PES.2003.1267161.

[15] "Operating problems with parallel flows," *IEEE Transactions on Power Systems*, vol. 6, no. 3, pp. 1024–1034, 1991. DOI: 10.1109/59.119242.

[16] A. Singh, T. Frei, N. Chokani, and R. S. Abhari, "Impact of unplanned power flows in interconnected transmission systems – case study of central eastern european region," *Energy Policy*, vol. 91, pp. 287–303, 2016, ISSN: 0301-4215. DOI: https://doi.org/10.1016/j.enpol.2016.01.006. [Online]. Available: https://www.sciencedirect.com/science/article/pii/S0301421516300064.

[17] P. Eser, A. Singh, N. Chokani, and R. S. Abhari, "High resolution simulations of increased renewable penetration on central european transmission grid," in *2015 IEEE Power and Energy Society General Meeting*, 2015, pp. 1–5. DOI: 10.1109/PESGM.2015.7285991.

[18] A. B. Birchfield, T. Xu, K. M. Gegner, K. S. Shetye, and T. J. Overbye, "Grid structural characteristics as validation criteria for synthetic networks," *IEEE Transactions on Power Systems*, vol. 32, no. 4, pp. 3258–3265, 2017. DOI: 10.1109/TPWRS.2016.2616385.

[19] A. Blavette, D. L. O'Sullivan, A. W. Lewis, and M. G. Egan, "Impact of a wave farm on its local grid: Voltage limits, flicker level and power fluctuations," in *2012 Oceans - Yeosu*, 2012, pp. 1–9. DOI: 10.1109/OCEANS-Yeosu.2012.6263552.

[20] T. Börner and M.-R. Alam, "Real time hybrid modeling for ocean wave energy converters," *Renewable and Sustainable Energy Reviews*, vol. 43, pp. 784–795, 2015.

[21] J. Harris, M. Boller, T. Brekken, M. Magaña, and D. Gaebele, "Development of a hybrid simulation for an ocean wave energy converter," in *2021 IEEE Power Energy Society General Meeting (PESGM)*, 2021, pp. 1–5. DOI: 10.1109/PESGM46819.2021.9638187.

[22] E. Cotilla-Sanchez, P. D. H. Hines, C. Barrows, S. Blumsack, and M. Patel, "Multi-attribute partitioning of power networks based on electrical distance," *IEEE Transactions on Power Systems*, vol. 28, no. 4, pp. 4979–4987, Nov. 2013. DOI: 10.1109/TPWRS.2013.2263886.

[23] B. Leonardi and V. Ajjarapu, "Investigation of various generator reactive power reserve (grpr) definitions for online voltage stability/security assessment," in *2008 IEEE Power and Energy Society General Meeting - Conversion and Delivery of Electrical Energy in the 21st Century*, Jul. 2008, pp. 1–7. DOI: 10.1109/PES.2008.4596235.

[24] C. W. Taylor, *Power System Voltage Stability*. New York: McGraw-Hill, 1994.

[25] N. Savvopoulos, C. Y. Evrenosoglu, A. Marinakis, A. Oudalov, and N. Hatziargyriou, "A long-term reactive power planning framework for transmission grids with high shares of variable renewable generation," in *2019 IEEE Milan PowerTech*, Jun. 2019, pp. 1–6. DOI: 10.1109/PTC.2019.8810680.

[26] I. Dobson, T. Van Cutsem, C. Vournas, *et al.*, "Voltage stability assessment: Concepts, practices and tools," *IEEE Power Engineering Society, Power*

System Stability Subcommittee Special Publication, vol. 11, pp. 21–22, Jan. 2002.

[27] T. V. Cutsem, *Voltage Stability of Electric Power Systems*. Boston: Kluwer Academic Publishers, 1998, ISBN: 9780792381396.

[28] S. S. Ladhani, C. Quist, J. Seabrook, and C. Thomas, "Guide to wecc/nerc planning standards i.d: Voltage support and reactive power," Western Electricity Coordinating Council, Tech. Rep., Mar. 2006.

[29] B. H. Chowdhury and C. W. Taylor, "Voltage stability analysis: V-q power flow simulation versus dynamic simulation," *IEEE Transactions on Power Systems*, vol. 15, no. 4, pp. 1354–1359, Nov. 2000. DOI: 10.1109/59.898112.

[30] K. Chakraborty and A. Chakrabarti, *Soft Computing Techniques in Voltage Security Analysis*. India: Springer, Jan. 2015. DOI: 10.1007/978-81-322-2307-8.

[31] R. A. Schlueter, "A voltage stability security assessment method," *IEEE Transactions on Power Systems*, vol. 13, no. 4, pp. 1423–1438, Nov. 1998. DOI: 10.1109/59.736286.

[32] P. Pourbeik, R. J. Koessler, W. Quaintance, and W. Wong, "Performing comprehensive voltage stability studies for the determination of optimal location, size and type of reactive compensation," in *2006 IEEE Power Engineering Society General Meeting*, Jun. 2006, 6 pp.-. DOI: 10.1109/PES.2006.1709294.

[33] Y. H. Choi, S. Seo, S. Kang, and B. Lee, "Justification of effective reactive power reserves with respect to a particular bus using linear sensitivity," *IEEE Transactions on Power Systems*, vol. 26, no. 4, pp. 2118–2124, Nov. 2011. DOI: 10.1109/TPWRS.2011.2151212.

[34] R. A. Schlueter, Shu-Zhen Liu, and K. Ben-Kilani, "Justification of the voltage stability security assessment and diagnostic procedure using a bifurcation subsystem method," *IEEE Transactions on Power Systems*, vol. 15, no. 3, pp. 1105–1111, Aug. 2000. DOI: 10.1109/59.871740.

[35] Hang Liu, A. Bose, and V. Venkatasubramanian, "A fast voltage security assessment method using adaptive bounding," *IEEE Transactions on Power Systems*, vol. 15, no. 3, pp. 1137–1141, Aug. 2000. DOI: 10.1109/59.871745.

[36] Feng Dong, B. H. Chowdhury, M. L. Crow, and L. Acar, "Improving voltage stability by reactive power reserve management," *IEEE Transactions on Power Systems*, vol. 20, no. 1, pp. 338–345, Feb. 2005. DOI: 10.1109/TPWRS.2004.841241.

[37] C. Huo and E. Cotilla-Sanchez, "A power-balanced clustering algorithm to improve electrical infrastructure resiliency," in *2018 Power Systems Computation Conference (PSCC)*, Jun. 2018, pp. 1–8. DOI: 10.23919/PSCC.2018.8442565.

[38] U. von Luxburg, "A tutorial on spectral clustering," *Statistics and Computing*, vol. 17, no. 4, pp. 395–416, Dec. 2007, ISSN: 1573-1375. DOI: 10.

1007/s11222-007-9033-z. [Online]. Available: https://doi.org/10.1007/s11222-007-9033-z.

[39] R. J. Sánchez-García, M. Fennelly, S. Norris, *et al.*, "Hierarchical spectral clustering of power grids," *IEEE Transactions on Power Systems*, vol. 29, no. 5, pp. 2229–2237, Sep. 2014, ISSN: 0885-8950. DOI: 10.1109/TPWRS.2014.2306756.

[40] M. Goubko and V. Ginz, "Improved spectral clustering for multi-objective controlled islanding of power grid," *Energy Systems*, vol. 10, May 2017. DOI: 10.1007/s12667-017-0240-1.

[41] E. Hogan, E. Cotilla-Sanchez, M. Halappanavar, *et al.*, "Comparative studies of clustering techniques for real-time dynamic model reduction," *Statistical Analysis and Data Mining: The ASA Data Science Journal*, Jan. 2015. DOI: 10.1002/sam.11352.

[42] "Identification of voltage control areas and reactive power reserves adequacy: Vca studio software," Electric Power Research Institute, Palo Alto, CA, USA, Technical Update 3002016170, Dec. 2019.

[43] "Identification of voltage control areas and reactive power reserves: Mathematical formulations and preliminary results," Electric Power Research Institute, Palo Alto, CA, USA, Technical Update 3002010722, Nov. 2017.

[44] "Methodology and software tool for identifying voltage control areas and computing reactive power reserve," Electric Power Research Institute, Palo Alto, CA, USA, Technical Update 3002013861, Dec. 2018.

[45] T. Ibrahim, K. Dowling, T. Tinoco De Rubira, A. Del Rosso, M. Patel, and A. Mohamd, "Voltage stability contingency screening and ranking for voltage control areas," in *CIGRE US National Committee 2019 Grid of the Future Symposium*, 2019.

[46] R. Korab, *Case2383wp power flow data for polish system - winter 1999-2000 peak.* 2000 (Accessed May 3, 2023). [Online]. Available: https://matpower.org/docs/ref/matpower5.0/case2383wp.html.

[47] T. Ibrahim, A. Del Rosso, S. Guggilam, K. Dowling, and M. Patel, "Eprivca: Optimal reactive power dispatch tool," in *2022 IEEE Power and Energy Society General Meeting (PESGM)*, 2022, pp. 1–5. DOI: 10.1109/PESGM48719.2022.9917236.

[48] J. Kavicky and S. Shahidehpour, "Parallel path aspects of transmission modeling," *IEEE Transactions on Power Systems*, vol. 11, no. 3, pp. 1180–1190, 1996. DOI: 10.1109/59.535589.

[49] M. Schneider, H. Barrios, and A. Schnettler, "Evaluation of unscheduled power flows in the european transmission system," in *2018 IEEE International Energy Conference (ENERGYCON)*, 2018, pp. 1–6. DOI: 10.1109/ENERGYCON.2018.8398820.

[50] S. Cvijić and M. D. Ilić, "Part i: A new framework for modeling and tracing of bilateral transactions and the corresponding loop flows in multi-control area power networks," *IEEE Transactions on Power Systems*, vol. 29, no. 6, pp. 2706–2714, 2014. DOI: 10.1109/TPWRS.2014.2312376.

[51] G. Granelli, M. Montagna, F. Zanellini, P. Bresesti, and R. Vailati, "A genetic algorithm-based procedure to optimize system topology against parallel flows," *IEEE Transactions on Power Systems*, vol. 21, no. 1, pp. 333–340, 2006. DOI: 10.1109/TPWRS.2005.860921.

[52] S. Cvijić and M. D. Ilić, "Part ii: Par flow control based on the framework for modeling and tracing of bilateral transactions and corresponding loop flows," *IEEE Transactions on Power Systems*, vol. 29, no. 6, pp. 2715–2722, 2014. DOI: 10.1109/TPWRS.2014.2312372.

[53] T. Brown, "Transmission network loading in europe with high shares of renewables," *IET Renewable Power Generation*, vol. 9, no. 1, pp. 57–65, 2015. DOI: https://doi.org/10.1049/iet-rpg.2014.0114. [Online]. Available: https://ietresearch.onlinelibrary.wiley.com/doi/abs/10.1049/iet-rpg.2014.0114.

[54] P. Henneaux, P. Lamprinakos, G. de Maere d'Aertrycke, and K. Karoui, "Impact assessment of a minimum threshold on cross-zonal capacity in a flow-based market," *Electric Power Systems Research*, vol. 190, p. 106 693, 2021, ISSN: 0378-7796. DOI: https://doi.org/10.1016/j.epsr.2020.106693. [Online]. Available: https://www.sciencedirect.com/science/article/pii/S037877962030496X.

[55] S. Suryanarayanan, R. Farmer, G. Heydt, and S. Chakka, "Estimation of unscheduled flows and contribution factors based on l/sub p/ norms," *IEEE*

Transactions on Power Systems, vol. 19, no. 2, pp. 1245–1246, 2004. DOI: 10.1109/TPWRS.2003.821630.

[56] G. Chang, C. A. Jones, J. D. Roberts, and V. S. Neary, "A comprehensive evaluation of factors affecting the levelized cost of wave energy conversion projects," *Renewable Energy*, vol. 127, pp. 344–354, 2018, ISSN: 0960-1481. DOI: https://doi.org/10.1016/j.renene.2018.04.071. [Online]. Available: https://www.sciencedirect.com/science/article/pii/S0960148118304798.

[57] M. Lehmann, F. Karimpour, C. A. Goudey, P. T. Jacobson, and M.-R. Alam, "Ocean wave energy in the united states: Current status and future perspectives," *Renewable and Sustainable Energy Reviews*, vol. 74, pp. 1300–1313, 2017, ISSN: 1364-0321. DOI: https://doi.org/10.1016/j.rser.2016.11.101. [Online]. Available: https://www.sciencedirect.com/science/article/pii/S1364032116308164.

[58] S. Bhattacharya, D. Bhatnagar, D. Preziuso, M. J. E. Alam, and R. O'Neil, "Grid value propositions for tidal based generation resources - a temporal analysis," in *OCEANS 2019 MTS/IEEE SEATTLE*, 2019, pp. 1–5. DOI: 10.23919/OCEANS40490.2019.8962857.

[59] S. Bhattacharya, S. Pennock, B. Robertson, *et al.*, "Timing value of marine renewable energy resources for potential grid applications," *Applied Energy*, vol. 299, p. 117 281, 2021, ISSN: 0306-2619. DOI: https://doi.

org/10.1016/j.apenergy.2021.117281. [Online]. Available: https://www.sciencedirect.com/science/article/pii/S030626192100698X.

[60] S. Pennock, D. Coles, A. Angeloudis, S. Bhattacharya, and H. Jeffrey, "Temporal complementarity of marine renewables with wind and solar generation: Implications for gb system benefits," *Applied Energy*, vol. 319, p. 119 276, 2022, ISSN: 0306-2619. DOI: https://doi.org/10.1016/j.apenergy.2022.119276. [Online]. Available: https://www.sciencedirect.com/science/article/pii/S030626192200633X.

[61] P. Coker, J. Barlow, T. Cockerill, and D. Shipworth, "Measuring significant variability characteristics: An assessment of three uk renewables," *Renewable Energy*, vol. 53, pp. 111–120, 2013, ISSN: 0960-1481. DOI: https://doi.org/10.1016/j.renene.2012.11.013. [Online]. Available: https://www.sciencedirect.com/science/article/pii/S0960148112007161.

[62] D. A. Halamay, T. K. A. Brekken, A. Simmons, and S. McArthur, "Reserve requirement impacts of large-scale integration of wind, solar, and ocean wave power generation," *IEEE Transactions on Sustainable Energy*, vol. 2, no. 3, pp. 321–328, 2011. DOI: 10.1109/TSTE.2011.2114902.

[63] D. Coles, B. Wray, R. Stevens, S. Crawford, S. Pennock, and J. Miles, "Impacts of tidal stream power on energy system security: An isle of wight case study," *Applied Energy*, vol. 334, p. 120 686, 2023, ISSN: 0306-2619. DOI: https://doi.org/10.1016/j.apenergy.2023.120686. [Online].

Available: https://www.sciencedirect.com/science/article/pii/S0306261923000508.

[64] V. Chalishazar, S. Bhattacharya, S. Hanif, *et al.*, "Data-driven reliability assessment for marine renewable energy enabled island power systems," in *2021 IEEE Power and Energy Society General Meeting (PESGM)*, 2021, pp. 1–5. DOI: 10.1109/PESGM46819.2021.9637995.

[65] E. D. Stoutenburg, N. Jenkins, and M. Z. Jacobson, "Power output variations of co-located offshore wind turbines and wave energy converters in california," *Renewable Energy*, vol. 35, no. 12, pp. 2781–2791, 2010, ISSN: 0960-1481. DOI: https://doi.org/10.1016/j.renene.2010.04.033. [Online]. Available: https://www.sciencedirect.com/science/article/pii/S0960148110002004.

[66] J. M. Kluger, M. N. Haji, and A. H. Slocum, "The power balancing benefits of wave energy converters in offshore wind-wave farms with energy storage," *Applied Energy*, vol. 331, p. 120 389, 2023, ISSN: 0306-2619. DOI: https://doi.org/10.1016/j.apenergy.2022.120389. [Online]. Available: https://www.sciencedirect.com/science/article/pii/S0306261922016464.

[67] G. Reikard, B. Robertson, and J.-R. Bidlot, "Combining wave energy with wind and solar: Short-term forecasting," *Renewable Energy*, vol. 81, pp. 442–456, 2015, ISSN: 0960-1481. DOI: https://doi.org/10.1016/j.renene.2015.03.032. [Online]. Available: https://www.sciencedirect.com/science/article/pii/S0960148115002141.

[68] I. Fairley, H. Smith, B. Robertson, M. Abusara, and I. Masters, "Spatio-temporal variation in wave power and implications for electricity supply," *Renewable Energy*, vol. 114, pp. 154–165, 2017, Wave and Tidal Resource Characterization, ISSN: 0960-1481. DOI: https://doi.org/10.1016/j.renene.2017.03.075. [Online]. Available: https://www.sciencedirect.com/science/article/pii/S0960148117302653.

[69] D. A. Halamay and T. K. Brekken, "Monte carlo analysis of the impacts of high renewable power penetration," in *2011 IEEE Energy Conversion Congress and Exposition*, 2011, pp. 3059–3066. DOI: 10.1109/ECCE.2011.6064181.

[70] T. K. A. Brekken, H. T. Ozkan-Haller, and A. Simmons, "A methodology for large-scale ocean wave power time-series generation," *IEEE Journal of Oceanic Engineering*, vol. 37, no. 2, pp. 294–300, 2012. DOI: 10.1109/JOE.2012.2187393.

[71] H. Mendonça, R. M. De Castro, S. Martínez, and D. Montalbán, "Voltage impact of a wave energy converter on an unbalanced distribution grid and corrective actions," *Sustainability*, vol. 9, no. 10, 2017, ISSN: 2071-1050. DOI: 10.3390/su9101844. [Online]. Available: https://www.mdpi.com/2071-1050/9/10/1844.

[72] D. Šljivac, I. Temiz, B. Nakomčić-Smaragdakis, and M. Žnidarec, "Integration of wave power farms into power systems of the adriatic islands: Technical possibilities and cross-cutting aspects," *Water*, vol. 13, no. 1, 2021,

ISSN: 2073-4441. DOI: 10.3390/w13010013. [Online]. Available: https://www.mdpi.com/2073-4441/13/1/13.

[73] "Power flow modeling reference document," North American Transmission Forum, Charlotte, NC, USA, Tech. Rep., Jun. 2013. [Online]. Available: https://www.natf.net/docs/natf/documents/resources/planning-and-modeling/natf-power-flow-modeling-reference-document-v-1-1-1-06-13-open.pdf.

[74] H. Li, J. H. Yeo, J. L. Wert, and T. J. Overbye, "Steady-state scenario development for synthetic transmission systems," in *2020 IEEE Texas Power and Energy Conference (TPEC)*, 2020, pp. 1–6. DOI: 10.1109/TPEC48276.2020.9042493.

[75] K. M. Gegner, A. B. Birchfield, T. Xu, K. S. Shetye, and T. J. Overbye, "A methodology for the creation of geographically realistic synthetic power flow models," in *2016 IEEE Power and Energy Conference at Illinois (PECI)*, 2016, pp. 1–6. DOI: 10.1109/PECI.2016.7459256.

[76] National Data Buoy Center, *National data bouy center*, May 2023 (Accessed May 3, 2023). [Online]. Available: https://www.ndbc.noaa.gov/.

[77] J. Falnes, *Ocean Waves and Oscillating Systems*. Cambridge University Press, Mar. 2002, ISBN: 9780521782111. DOI: 10.1017/CBO9780511754630.

[78] A. Mate and E. Cotilla-Sanchez, "Rapid method for generation prioritization during system restoration with renewable resources," in *2019 IEEE/IAS*

55th Industrial and Commercial Power Systems Technical Conference (I&CPS), 2019, pp. 1–8. DOI: 10.1109/ICPS.2019.8733358.

[79] Electric Reliability Council of Texas, Inc., *Hourly load data archives*, 2016 (Accessed May 3, 2023). [Online]. Available: https://www.ercot.com/files/docs/2017/01/10/native%5C_Load%5C_2016.zip.

[80] Electric Reliability Council of Texas, Inc., *Fuel mix*, Mar. 2017 (Accessed May 3, 2023). [Online]. Available: https://www.ercot.com/files/docs/2021/03/10/FuelMixReport%5C_PreviousYears.zip.

[81] PJM Interconnection and Midwestern ISO, "Investigation of loop flows across combined midwest iso and pjm footprint phase ii," Norristown, PA, USA, Tech. Rep., Nov. 2008. [Online]. Available: https://www.miso-pjm.com/$%5Csim$/$%5Csim$/media/6A3A3B32A0E54EED877E5EFBE9846DA4.ashx.

[82] T. Kovaltchouk, A. Blavette, J. Aubry, H. B. Ahmed, and B. Multon, "Comparison between centralized and decentralized storage energy management for direct wave energy converter farm," *IEEE Transactions on Energy Conversion*, vol. 31, no. 3, pp. 1051–1058, 2016. DOI: 10.1109/TEC.2016.2547462.

[83] A. F. de O. Falcão, "Wave energy utilization: A review of the technologies," *Renewable and Sustainable Energy Reviews*, vol. 14, no. 3, pp. 899–918, 2010, ISSN: 1364-0321. DOI: https://doi.org/10.1016/j.rser.2009.

11.003. [Online]. Available: https://www.sciencedirect.com/science/article/pii/S1364032109002652.

[84] M. Göteman, M. Giassi, J. Engström, and J. Isberg, "Advances and challenges in wave energy park optimization—a review," *Frontiers in Energy Research*, vol. 8, 2020, ISSN: 2296-598X. DOI: 10.3389/fenrg.2020.00026. [Online]. Available: https://www.frontiersin.org/article/10.3389/fenrg.2020.00026.

[85] *Marine energy - Wave, tidal and other water current converters - Part 30: Electrical power quality requirements*. IEC TS 62600-30, 2018.

[86] *Electromagnetic compatibility (emc) - part 4-15: Testing and measurement techniques - flickermeter - functional and design specifications*, 2010.

[87] *Ieee recommended practice for the analysis of fluctuating installations on power systems*, 2015.

[88] "Ieee standard for harmonic control in electric power systems," *IEEE Std 519-2022 (Revision of IEEE Std 519-2014)*, pp. 1–31, 2022. DOI: 10.1109/IEEESTD.2022.9848440.

[89] F. Sharkey, J. MacEnri, E. Bannon, M. Conlon, and K. Gaughan, "Resource-induced voltage flicker for wave energy converters – assessment tools," *IET Renewable Power Generation*, vol. 7, no. 6, pp. 623–630, 2013. DOI: https://doi.org/10.1049/iet-rpg.2012.0367. eprint: https://ietresearch.onlinelibrary.wiley.com/doi/pdf/10.1049/iet-rpg.2012.0367. [On-

line]. Available: https://ietresearch.onlinelibrary.wiley.com/doi/abs/10.1049/iet-rpg.2012.0367.

[90] *Ieee standard for interconnection and interoperability of distributed energy resources with associated electric power systems interfaces*, 2018.

[91] H. Clémot, A. Babarit, F. Dupriez-Robin, and T. Q. Tran, "Development of a wave-to-wire model to calculate flicker caused by wave energy converters and study power quality," in *2017 IEEE Manchester PowerTech*, 2017, pp. 1–6. DOI: 10.1109/PTC.2017.7981020.

[92] L. Trilla, T. Thiringer, S. Sahlin, and T. Andersson, "Wave energy park power quality impact and collection grid economic assessment," *IET Renewable Power Generation*, vol. 9, no. 4, pp. 368–378, 2015. DOI: https://doi.org/10.1049/iet-rpg.2014.0139. eprint: https://ietresearch.onlinelibrary.wiley.com/doi/pdf/10.1049/iet-rpg.2014.0139. [Online]. Available: https://ietresearch.onlinelibrary.wiley.com/doi/abs/10.1049/iet-rpg.2014.0139.

[93] A. J. Nambiar, D. Forehand, A. E. Kiprakis, and A. R. Wallace, "Effects of spacing in wave energy converter arrays on voltage flicker," in *5th IET International Conference on Renewable Power Generation (RPG) 2016*, 2016, pp. 1–6. DOI: 10.1049/cp.2016.0533.

[94] A. S. Haider, L. G. Zadeh, and T. K. Brekken, "Wave energy converter energy storage system sizing for flicker considerations," in *2021 IEEE Power*

and Energy Society General Meeting (PESGM), 2021, pp. 01–05. DOI: 10.1109/PESGM46819.2021.9637950.

[95] S. Rasool, K. M. Muttaqi, and D. Sutanto, "Modelling of a wave-to-wire system for a wave farm and its response analysis against power quality and grid codes," *Renewable Energy*, vol. 162, pp. 2041–2055, 2020, ISSN: 0960-1481. DOI: https://doi.org/10.1016/j.renene.2020.10.035. [Online]. Available: https://www.sciencedirect.com/science/article/pii/S0960148120316025.

[96] A. Blavette, D. L. O'Sullivan, R. Alcorn, M. G. Egan, and T. W. Lewis, "Simplified estimation of the flicker level induced by wave energy farms," *IEEE Transactions on Sustainable Energy*, vol. 7, no. 3, pp. 1216–1223, 2016. DOI: 10.1109/TSTE.2016.2535327.

[97] A. Parwal, M. Fregelius, J. Leijon, *et al.*, "Experimental test of grid connected vsc to improve the power quality in a wave power system," in *2018 5th International Conference on Electric Power and Energy Conversion Systems (EPECS)*, 2018, pp. 1–7. DOI: 10.1109/EPECS.2018.8443488.

[98] E. Tedeschi and M. Santos-Mugica, "Modeling and control of a wave energy farm including energy storage for power quality enhancement: The bimep case study," *IEEE Transactions on Power Systems*, vol. 29, no. 3, pp. 1489–1497, 2014. DOI: 10.1109/TPWRS.2013.2282213.

[99] B. Guo and J. V. Ringwood, "A review of wave energy technology from a research and commercial perspective," *IET Renewable Power Generation*,

vol. 15, no. 14, pp. 3065–3090, Oct. 2021, ISSN: 1752-1416. DOI: 10.1049/rpg2.12302.

[100] B. Guo, T. Wang, S. Jin, S. Duan, K. Yang, and Y. Zhao, "A review of point absorber wave energy converters," *Journal of Marine Science and Engineering*, vol. 10, no. 10, 2022, ISSN: 2077-1312. DOI: 10.3390/jmse10101534. [Online]. Available: https://www.mdpi.com/2077-1312/10/10/1534.

[101] M. Penalba, T. Kelly, and J. V. Ringwood, "Using NEMOH for Modelling Wave Energy Converters: A Comparative Study with WAMIT," in *12th European Wave and Tidal Energy Conference*, Cork, Ireland, 2017.

[102] M. Penalba, N. P. Sell, A. J. Hillis, and J. V. Ringwood, "Validating a wave-to-wire model for a wave energy converter—part i: The hydraulic transmission system," *Energies*, vol. 10, no. 7, 2017, ISSN: 1996-1073. DOI: 10.3390/en10070977. [Online]. Available: https://www.mdpi.com/1996-1073/10/7/977.